Atmospheric dispersion of a heavy gas release from an elevated source

Cristina Vidali

N° d'ordre NNT: 2021LYSEC17

THÈSE de DOCTORAT DE L'UNIVERSITÉ DE LYON
opérée au sein de l'École Centrale de Lyon

École Doctorale N° 162
Mécanique Énergétique Génie Civil Acoustique

Spécialité de doctorat : Mécanique

Soutenue publiquement le 12.05.2021, par

Cristina Vidali

Atmospheric dispersion of a heavy gas release from an elevated source

---

Devant le jury composé de

Carpentieri, Matteo	Professeur	University of Surrey	Rapporteur
Bonometti, Thomas	Maître de conférencse	IMFT	Rapporteur
Soulhac, Lionel	Professeur	INSA - LMFA	Président du jury
Amielh, Muriel	Chercheuse	CNRS - IRPHE	Examinatrice
Vyazmina, Elena	Ingénieur	ICP - Air Liquide R&D	Invitée
Salizzoni, Pietro	Professeur	ECL - LMFA	Directeur de thèse
Gostiaux, Louis	Chercheur	CNRS - LMFA	Co-encadrant

ÉCOLE CENTRALE DE LYON

Abstract

École Doctorale N°162 Mécanique Énergétique Génie Civil Acoustique
Laboratoire de Mécanique des Fluides et d'Acoustique (LMFA)

Atmospheric dispersion of a heavy gas release from an elevated source

by Cristina VIDALI

Understanding the physics of the atmospheric dispersion of heavy gases is essential to the assessment and management of risks associated to accidental releases of airborne pollutants. The release of gases heavier than air may produce favourable conditions to asphyxia, explosions and fires. The consequences of these releases are today further enhanced by the proximity of urban areas to industrial sites. The density difference between the heavy release and the surrounding air induces buoyancy and stratification effects that have a major impact on the dispersion of these gases. Once released, the heavy gas ends up spreading to the ground, producing a stable stratified flow configuration, that inhibits the dilution of the heavy gas with the ambient air. Consequently, the hazard threshold concentration limits (related to asphyxia, toxicity, explosiveness, flammability) can be locally exceeded by peaks of concentration, increasing the risk for workers, people and structures.

The aims of this work is to investigate the turbulent dispersion dynamics of an elevated heavy gas release by means of wind tunnel experiments, enlightening its main differences compared to that of a passive scalar, and to test the ability of operational dispersion models in simulating this phenomena. The risk assessment of heavy gas release requires to correctly estimate the intensity of the concentration fluctuations and their interactions with the velocity fluctuations. For this reason, we employ a coupled system, composed of a Flame Ionization Detector and a Hot-Wire Anemometry, to characterise the pollutant plumes downwind the source by measuring simultaneously the concentration and velocity field. This experimental technique is sensitive to the density gradients within the plume and a specific calibration procedure is defined (Chapter 2). The scenario of interest is defined with the industrial partner Air Liquide as the emission from an Air Separation Units (ASU) that releases O_2 at a temperature of -40°C in the atmospheric boundary layer. We simulate it with a scale model in our wind tunnel facility, where the inflow condition has been set to reproduce a fully developed turbulent boundary layer over a rough surface in neutral condition. From an elevated source we release a dense mixture of carbon dioxide and ethane, the latter used as a tracer in concentration measurements. Under the same flow and emission set-up we reproduce a passive scalar release, employing a mixture of air and ethane, comparing the dataset with the heavy gas one. In the data analysis (Chapter 3), focus

is set on the mean concentration field and its higher-order moments, the concentration probability distribution and the turbulent mass fluxes, characterising the spectra, the turbulent kinetic energy exchange, the mixing on large and small scale, as well as the temporal structure of the signal. Finally, the data collected during the experiments on the heavy gas release is used to test and validate two operational dispersion models (Chapter 4). To that purpose we consider an integral model (Ventjet, Miller et al., 2021), developed by Air Product and Air Liquide, and a Lagrangian model (SLAM, Vendel et al., 2011), developed by the team AIR of the École Centrale de Lyon. We complete the study by investigating the structure of the concentration time series, estimating the crossing time and rate of a concentration threshold by means of analytic models.

The wind tunnel experiments proved that the trajectory of the heavy gas plume, emitted from an elevated source, was affected by buoyancy effects, whereas its turbulent dispersion was unaltered compared to the passive scalar. For this reason, operational models, validated to simulate passive scalar release, have been employed with success to model the elevated heavy gas releases. These models considered the gravitational effect on the vertical displacement on the plume centreline reproducing with good agreement the trajectory, the mean concentration and the higher order moments of the wind tunnel experiments.

Key word: Heavy gas, Atmospheric dispersion, Wind tunnel, Coupled measurements, Integral and Lagrangian models.

ÉCOLE CENTRALE DE LYON

Résumé

École Doctorale N°162 Mécanique Énergétique Génie Civil Acoustique
Laboratoire de Mécanique des Fluides et d'Acoustique (LMFA)

Dispersion atmosphérique d'un rejet de gaz lourd depuis une source élevée

by Cristina VIDALI

La compréhension physique de la dispersion atmosphérique des gaz lourds est fondamentale pour améliorer l'évaluation et la gestion des risques liés à des rejets accidentels. La dispersion d'un gaz lourd est caractérisée par des effets de flottabilité et de stratification, qui peuvent générer des conditions favorables à l'asphyxie, l'explosion et l'incendie. La proximité du milieu urbain et industriel amplifie l'impact potentiel des rejets accidentels sur les personnes et les structures alentours. Le panache d'un gaz plus dense que l'air s'étale au sol en produisant un écoulement stable et stratifié qui réduit sa dilution dans l'air. En conséquence, la valeur seuil, relative aux conditions d'asphyxie, de toxicité, d'explosion et d'inflammabilité, peut être localement dépassée par des pics de concentration.

Le principal objectif scientifique du projet est d'améliorer la modélisation de la dynamique des rejets de gaz lourds au moyen d'expériences en soufflerie. Les expériences sont conçues pour mettre en évidence les différences avec un rejet de scalaire passif. L'évaluation des risques lors de rejets de gaz lourds nécessite une estimation précise des intensités de fluctuation de concentration, ainsi que la prise en compte de leur interaction avec les fluctuations de vitesse. Pour cette raison, la caractérisation du panache est effectuée au moyen d'un système de mesure couplé, qui permet de mesurer simultanément la concentration et la vitesse du fluide, en combinant deux techniques expérimentales, le détecteur par ionisation de flamme et l'anémomètre à fil chaud. Cette technique expérimentale est sensible aux gradients de densité dans le panache et une procédure de calibration spécifique est établie dans le cas de gaz lourds (Chapitre 2). Le scénario d'étude a été défini en collaboration avec le partenaire industriel Air Liquide et il correspond à l'émission depuis une grande unité de séparation d'air (ASU), qui émet du O_2 à une température de -40 °C dans la couche limite atmosphérique. Nous avons reproduit en soufflerie cette configuration à l'échelle, en générant une couche limite neutre développée sur une surface rugueuse. Les rejets de gaz lourds sont simulés expérimentalement par l'émission d'un mélange de dioxyde de carbone, d'air et d'éthane, le dernier étant utilisé comme traceur dans les mesures de concentration. Pour comparer l'expérience avec le rejet d'un scalaire passif, nous avons aussi utilisé un mélange d'air et d'éthane, dans les mêmes conditions. L'analyse

des données expérimentales (Chapitre 3) est focalisée sur la caractérisation du champ de vitesse et concentration, en analysant la moyenne et les moments d'ordre supérieur ; on a égalementestimé les lois de distribution de la concentration, les flux turbulents de masse, les échanges d'énergie cinétique turbulente et les temps de mélange à grande et petite échelles. Les paramètres obtenus par l'analyse de données expérimentales sont utilisés pour la validation de deux modèles opérationnels (Chapitre 4) : un modèle intégral (Ventjet, Miller et al., 2021), développé par Air Product et Air Liquide et un modèle Lagrangien (SLAM, Vendel et al., 2011), développé par l'équipe AIR de l'École Centrale de Lyon. L'étude est complétée par l'investigation de la structure de la série temporelle de la concentration, en estimant le temps et la fréquence de dépassement du seuil de concentration à travers un modèle analytique.

Les expériences en soufflerie ont montré que la trajectoire du panache de gaz lourd émis depuis une source élevée est affectée par les effets de flottabilité, alors que la dispersion turbulente n'est pas modifiée par rapport au cas d'un scalaire passif. Pour cette raison, les modèles opérationnels, précédemment validés pour un rejet de scalaire passif, reproduisent avec succès la dispersion atmosphérique d'un gaz lourd depuis une source élevée. Ces modèles prennent en compte les effets gravitationnels dans le déplacement vertical du centre du panache en reproduisant, avec une bonne précision, la trajectoire, la concentration moyenne et les moments d'ordre supérieur obtenus dans les expériences en soufflerie.

Mots clés: Gaz lourds, Dispersion atmosphérique, Soufflerie, Mesures couplées, Modèle Intégral, Modèle Lagrangien.

Acknowledgements

This project would not have been possible without the support of many people.

First of all my advisor Pietro Salizzoni for his guidance, patience and support and all that he taught me throughout this journey. I am grateful to Louis Gostiaux, for always encouraging me and believing in me, for the patience answering all my questions and, more important, for teaching me how to search for the answer myself.

Thank you to committee members Matteo Carpentieri, Thomas Bonometti and Muriel Amielh for they valuable comments and suggestions.

I would like to acknowledge Air Liquide for the precious opportunity of the thèse CIFRE. Thank you to the Air Liquide team, especially to Elena Vyazmina and Deborah Houssin for their guidance and support throughout this thesis. Thanks also to Simon Jallais for starting this project and collaboration.

This project wouldn't be possible without the help of Massimo Marro: his knowledge, kindness and calm helped me get trough the experiments and so much more. A special thank you also to Horacio Correia, whose help and knowledge in the realization of the wind tunnel experiments was essential. It was a pleasure working with you.

Thank you to all and each member of the Équipe AIR and the LMFA and all the co-workers and friends for sharing the joy and the struggling of the research. Special thanks to Lionel Sohulac, for sharing his knowledge with kindness and wisdom. Many thanks to Andrea Maffioli whose advices really helped me with both science and life and for being a part of my second family in Lyon along with Jheyson Brayam Mejia Estrada and Sofia Fellini. Thanks to all my friends in Lyon and all over the world. I wouldn't make it without you.

Thanks to my dad, my sister and Lorenzo, their strength and love nourished my life and work. Thanks to my mum, who made me who I am.

Contents

List of Figures

List of Tables

List of Abbreviations

ASU	**A**ir **S**eparation **U**nits
BL	**B**oundary **L**ayer
CFD	**C**omputational **F**luid **D**ynamics
DNS	**D**irect **N**umerical **S**imulation
FID	**F**lame **I**onisation **D**etector
HWA	**H**ot **W**ire **A**nemometry
IEM	**I**nteraction by **E**xchange with the **M**ean
IECM	**I**nteraction by **E**xchange with the **C**onditional **M**ean
LES	**L**arge **E**ddy **S**imulations
LDA	**L**aser **D**oppler **A**nemometry
LNG	**L**iquefied **N**atural **G**as
LPG	**L**iquefied **P**propane **G**as
PDF	**P**robability **D**ensity **F**unction
PID	**P**hoto **I**onization **D**etector
PSD	**P**ower **S**pectral **D**ensity
RANS	**R**eynolds **A**veraged **N**avier **S**tokes
SLAM	**S**afety **L**agrangian **A**tmospheric **M**odel
TKE	**T**urublent **K**inetic **E**nergy
CO_2	Carbon dioxide
C_2H_6	Ethane
H_2	Hydrogen
N_2	Nitrogen
O_2	Oxygen

Physical Constants

D_{CO_2}	molecular diffusion coefficient in air for CO_2 at 20°	$= 1.16 \cdot 10^{-4} \mathrm{m}^2\,\mathrm{s}^{-1}$
$D_{C_2H_6}$	molecular diffusion coefficient in air for C_2H_6 at 20°	$= 1.48 \cdot 10^{-4} \mathrm{m}^2\,\mathrm{s}^{-1}$
C_0	Kolmogorov constant	$= 4.5$
g	gravity	$= 9.812\ \mathrm{m\,s}^{-2}$
M_{air}	molecular weight air	$= 28.96\ \mathrm{g/mol}$
M_{CO_2}	molecular weight carbon dioxyde	$= 44.00\ \mathrm{g/mol}$
μ_{CO_2}	dynamic viscosity of CO_2 at 20°C	$= 14.85 \cdot 10^{-6} \mathrm{Pa\,s}$
μ_{air}	dynamic viscosity of air at 20°C	$= 18.24 \cdot 10^{-6} \mathrm{Pa\,s}$
ν_{CO_2}	kinematic viscosity of CO_2 at 20°C	$= 8.1 \cdot 10^{-6} \mathrm{m}^2\,\mathrm{s}^{-1}$
ν_{air}	kinematic viscosity of air at 20°C	$= 1.519 \cdot 10^{-5} \mathrm{m}^2\,\mathrm{s}^{-1}$

List of Main Symbols

a_i	deterministic acceleration	$\mathrm{m\,s^{-1}}$
b_{ij}	stochastic diffusive term	$\mathrm{m\,s^{-3/2}}$
c	concentration	ppm or $\mathrm{kg\,m^{-3}}$
C	particle concentration Lagrangian model	$\mathrm{kg\,m^{-3}}$
c'	concentration fluctuations	$\mathrm{kg\,m^{-3}}$
c_s	concentration at the source	$\mathrm{kg\,m^{-3}}$
D	Diffusivity	$\mathrm{m^2\,s^{-1}}$
D_t	turbulent dispersion coefficient	$\mathrm{m^2\,s^{-1}}$
d_s	source diameter	m
E	flux of air entrained into the plume	$\mathrm{kg\,s^{-1}\,m^{-1}}$
g'	reduced gravity	$\mathrm{m\,s^{-2}}$
H	height Irwin spires	m
h_s	source height	m
i_c	intensity fluctuations	-
k	parameter Gamma distribution	-
K	turbulent kinetic energy	$\mathrm{m^2\,s^{-2}}$
m	mass at the source	kg
m_p	mass of the tracer	kg
m_{nc}	n-order moment concentration	$\mathrm{kg\,m^{-3}}$
$\overline{M}$	molecular wight of the plume	g/mol
N_ϕ^+	upcrossing mean frequency	s
p	fluctuating kinematic pressure	Pa
P_K	internal production term turbulent kinetic energy equation	$\mathrm{m^2\,s^{-3}}$
P_{K_s}	buoyancy production term turbulent kinetic energy equation	$\mathrm{m^2\,s^{-3}}$
Q	flowrate	$\mathrm{m^3\,s^{-1}}$
Q'	fluctuations flowrate	$\mathrm{m^3\,s^{-1}}$
Q_s	source flowrate	$\mathrm{m^3\,s^{-1}}$
r	ratio between carbon dioxide and ethane	-
R	top-hat radius	m
t	time	s
T	temperature	°C
T_{Lv}	Lagrangian time scale transversal velocity	s
T_{Lw}	Lagrangian time scale vertical velocity	s
T_ϕ^+	upcrossing time	s
T_{tot}	signal duration	s

$u*$	friction velocity	$\mathrm{m\,s^{-1}}$
U_∞	free stream velocity boundary layer	$\mathrm{m\,s^{-1}}$
u	longitudinal velocity	$\mathrm{m\,s^{-1}}$
$\overline{u}$	mean longitudinal velocity	$\mathrm{m\,s^{-1}}$
$\overline{u}_{MC}$	mean longitudinal velocity at centre of mass height	$\mathrm{m\,s^{-1}}$
$\mathbf{u}_p$	velocity of the plume centroid	$\mathrm{m\,s^{-1}}$
u_e	entrainment velocityvelocity	$\mathrm{m\,s^{-1}}$
u'	longitudinal velocity fluctuations	$\mathrm{m\,s^{-1}}$
$\overline{u'c'}$	longitudinal turbulent mass fluxes	$\mathrm{kg\,s^{-1}\,m^{-2}}$
U	velocity from flowmeter	$\mathrm{m\,s^{-1}}$
U_i'	Lagrangian velocity fluctuation	$\mathrm{m\,s^{-1}}$
v	transversal velocity	$\mathrm{m\,s^{-1}}$
v'	transversal velocity fluctuations	$\mathrm{m\,s^{-1}}$
$\overline{v}$	mean transversal velocity	$\mathrm{m\,s^{-1}}$
$\overline{v'c'}$	transversal turbulent mass fluxes	$\mathrm{kg\,s^{-1}\,m^{-2}}$
V_p	volume particle Lagrangian model	$\mathrm{m^3}$
w	vertical velocity	$\mathrm{m\,s^{-1}}$
$\overline{w}$	mean vertical velocity	$\mathrm{m\,s^{-1}}$
w'	vertical velocity fluctuations	$\mathrm{m\,s^{-1}}$
$\overline{w'c'}$	vertical turbulent mass fluxes	$\mathrm{kg\,s^{-1}\,m^{-2}}$
w_s	source emission velocity	$\mathrm{m\,s^{-1}}$
x	horizontal coordinate	m
$\mathbf{x}_p$	location of the plume centre of mass	m
X_i	particle position Lagrangian model	m
y	transverse coordinate	m
z	vertical coordinate	m
z_0	roughness	m
Z_{MC}	centre of mass height	m
Γ	Gamma function	-
δ	Boundary Layer height	m
$\Delta\rho$	density difference mixture-air	$\mathrm{kg\,m^{-3}}$
ε	dissipation rate turbulent kinetic energy	$\mathrm{m^2\,s^{-3}}$
$\varepsilon_{\sigma_c^2}$	dissipation rate concentration variance	$\mathrm{kg^2m^{-6}s^{-1}}$
ϑ	integral time scale	s
ν	kinematic viscosity	$\mathrm{m^2\,s^{-1}}$
ρ	density	$\mathrm{kg\,m^{-3}}$
ρ'	density fluctuation	$\mathrm{kg\,m^{-3}}$
ρ_a	density air	$\mathrm{kg\,m^{-3}}$
ρ_c	critical density	$\mathrm{kg\,m^{-3}}$
ρ_m	density gas mixture	$\mathrm{kg\,m^{-3}}$
ρ_s	density at the source	$\mathrm{kg\,m^{-3}}$
ρ_p	plume density	$\mathrm{kg\,m^{-3}}$

σ_y	transversal plume spread	m
σ_z	vertical plume spread	m
σ_c	concentration standard deviation	$\mathrm{kg\,m^{-3}}$
σ_c^2	concentration variance	$\mathrm{kg\,m^{-3}}$
σ_u	longitudinal velocity standard deviation	m
σ_v	transversal velocity standard deviation	$\mathrm{m\,s^{-1}}$
σ_w	vertical velocity standard deviation	$\mathrm{m\,s^{-1}}$
τ	turbulent time scale	s
τ_m	micromixing time scale	s
τ_{m_c}	micromixing time scale with IEM model	s
$\tau_{m_{c\|u}}$	micromixing time scale with IECM model	s
χ	concentration normalised over mean concentration	-
Fr	Froude number	-
Nu	Nusselt number	-
Re	Reynolds number	-
Ri	Richardson number	-
Ri_b	bulk Richardson number	-
Ri_f	flux Richardson number	-
Sc	Schmidt number	-

Alla mia mamma...

Chapter 1

Introduction

Nowadays the management of risk associated to accidental release of heavy gas has a relevant role in the design of industrial plants and facilities. The release of gases such as gasoline vapours, carbon dioxide (CO_2), cryogenic fluids (liquid nitrogen N_2, oxygen O_2, hydrogen LH_2 and liquefied natural gas LNG), or heated/vaporised products liquid at ambient conditions (e.g. liquefied propane gas LPG) may produce favourable conditions to asphyxia, explosions and fires. The consequences of these releases are today further enhanced by the proximity of urban area to industrial sites (Fig. 1.1).

The density difference between the heavy release and the surrounding air induces buoyancy and stratification effects that have a major impact on the dispersion of these gases. Once released, the heavy gas ends up spreading to the ground, producing a stable stratified flow configuration, that inhibits the dilution of the heavy gas with the ambient air. Consequently, the hazard threshold concentration limits (related to asphyxia, toxicity, explosiveness, flammability) can be locally exceeded by peaks of concentration, increasing the risk for workers, people and structures. Furthermore, the presence of gas heavier than air may produce significant density gradients that can locally alter the dynamical properties of the atmospheric turbulence, inducing effects that are difficult to predict. In order to correctly estimate the risk associated to these phenomena by means of operational dispersion models, all these physical phenomena have to be suitably parameterised. The reliability of these parameterisations have in turn to be tested by using accurate data obtained by laboratory experiments and/or well controlled field trials.

The aim of this study is to experimentally investigate the dynamics of a heavy gas release, enlightening its main differences compared to that of a passive scalar (i.e., same density as ambient air), and to use the acquired data to evaluate the reliability of an Integral and a Lagrangian dispersion model.

1.1 Social and economic context

In the last decades, the management of industrial and environmental risks played a central role in the social, economic and political decision-making process. The growing urbanisation led to the reconciliation between industrial sites and residential

Figure 1.1: Pollutant gas emission of an industrial site near a residential area (Benxi Steel Industries, China - credit: Andreas Habic).

areas or sites of social interest (schools, sport areas, shopping centres, underground car park). This proximity represents a major concern, not only for surrounding population, but also for the industrial groups, whose business and activities may be heavily affected by strict regulations. Furthermore, increasing interest and sensitivity of citizens to environmental risk exposure is fed by concerns due to recurring major technological accidents, e.g. Seveso, Italy 1976 (Homberger et al., 1979), Bhopal, India 1984 (Broughton, 2005), Chernobyl, Russia 1986 (McCall, 2016), Fukushima, Japan 2011 (Aliyu et al., 2015), Lubrizol, France 2019 (Negre, 2021). These provide evidence of the consequences related to accidental releases, and induce also a suspicion in the public about the ability of public authorities and industrial groups to manage and reduce these technological risks. Another major concern is the increasing exposure of industrial sites to terrorist actions.

In this frame of work, the role of Research & Development centres (R&D), universities and research establishments is to lead industry towards a sustainable and responsible business growth assuring a reliable risk management. The main goal has to be the life safety of the workers and of the people living in the surrounding areas, the reduction of the economics consequences of an accident and the reassurance of investors, banks and authorities.

Increasingly stringent regulation puts the burden of producing exhaustive risk prevention plans on industrial groups and private companies. In particular, the so called “risk law”, established in France in 2003 (Loi n° 2003-699 du 30 juillet 2003), defines the technological risk prevention plan (PPRT, Décret n° 2005-1130 du 7 septembre 2005) as a new tool for managing land-use planning in the vicinity of industrial establishments. The PPRT applies to all establishments classified as SEVESO, according to the current European directive. These Directive applies to more than 12 000 industrial establishments in the European Union (European-Commission,

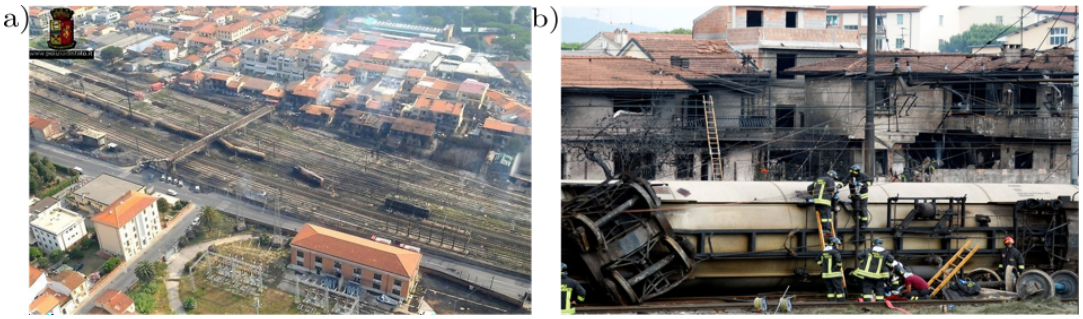

Figure 1.2: The destructive consequences of the Viareggio accident (2009) on the surrounding residential area (credit: a) the archive of the Italian Polizia di Stato, b) Stefano Rellandini, Reuters/Contrasto).

2017) that employ and store hazardous material, such as chemical and petrochemical substances.

Several scenarios were related to the accidental release of harmful gases whose density is higher than that of air, such as liquid N_2 and O_2, LNG, LPG, LH_2 gasoline vapours and CO_2. The high gas density can significantly inhibit its atmospheric dispersion and therefore its dilution with ambient air, raising the risk of possible environmental consequences, such as explosions and fires. This was the case, for instance, of the explosions that took place on the site of the La Mede refinery in 1992 (causing 6 fatalities, ARIA-Developpement-durable, 2008) and that in the oil depot of Saint-Herblain in 1991 (2 people died and 2 others were severely injured, ARIA-Developpement-durable, 2006). This was also the case of other two accidents involving trains: the flash-fire close to the Viareggio railway station, in 2009, (Landucci et al., 2011), that claimed 31 lives and whose consequences on the surrounding residential area are reported in Figure 1.2; the Ufa disaster in Russia (Chernov and Sornette, 2016) where a low velocity leak of LNG from the pipeline accumulated in the valley, creating a flammable cloud and wheel sparks ignite the explosion, leading to hundreds of victims (more than 500) and injured (almost 800).

The management of the risks associated to these accidental releases and its minimisation, for instance by protective barriers or alarm systems, represent nowadays an important technical challenge. In order to face these new regulations and operational constrains, private companies and public authorities require simulation tools to predict the impact of a potential industrial accident on the environment and the population.

1.2 Phenomenology of the dense buoyant flows

The atmospheric dispersion of a plume of gases heavier than air is driven by the atmospheric turbulence and by buoyancy effects induced by the density difference, between the air and the gas (Fannelöp, 1994). In a negative buoyant plume, the buoyancy affects the momentum and energy balance, and results in two main effects:

- altering the trajectory of the centre of mass of the plumes in case of elevated release;

Figure 1.3: a) Downburst over Pheonix, AZ (credit Bruce Haffner/Andrew Park/Jerry Ferguson). b) Haboob, a dust or sandstorm (credit Scott Griessel).

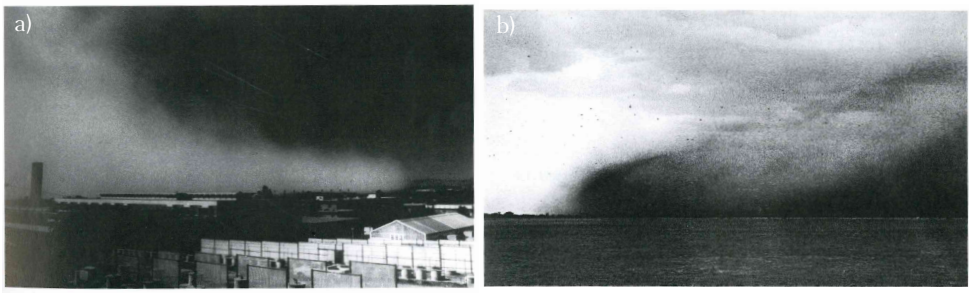

Figure 1.4: a) The front of a sea breeze polluted by photochemical smog in Riverside, CA, 1972 (credit G.R. Stephens). b) The form of a cold outflow outlined by flying locusts, Hergeisa, Somali Republic, 1960 (credit A.J.Wood).

- suppressing turbulent fluctuations and mixing.

From a phenomenological and physical point of view, the dispersion of dense gases is similar to a large variety of very well known phenomena in the field of the environmental fluid dynamics. Among these, we can cite the dynamics of downbursts (Fig. 1.3.a), cold fronts intrusions, haboob or dust/sand storms (Fig. 1.3.b), turbidity currents, avalanches, salty water intrusions and sea breeze fronts. The latter has been studied in connection to the transport of photochemical smog (Fig. 1.4.a) and to the influence on the behaviours of birds and insects, as the flying locust swarms that outlined a cold outflow in Figure 1.4.b (Simpson, 1999). In all these cases, the flow configuration is referred to as a gravity current, since the motion is driven by gravitational effects induced by density differences.

When dealing with industrial releases, classical configurations are a ground source or an elevated source of pollutant. In the latter case (Fig 1.5), the interaction of the gas release with the wind flow results in a plume bend over in the streamwise direction, as a results of the inertial effect of the flow on the plume and the exchange of momentum with the ambient air. When the density of the released gas is equal or higher than that of air, the plume reaches the maximum height (usually referred as the penetration depth) before bending over (Fannelöp, 1994). Downwind the source, the behaviour of the heavy gas plume is driven by the interaction of the inertial and buoyancy forces. As the plume is bent over, the momentum and the buoyancy are equally important, influencing the trajectory. When the plume touches the ground,

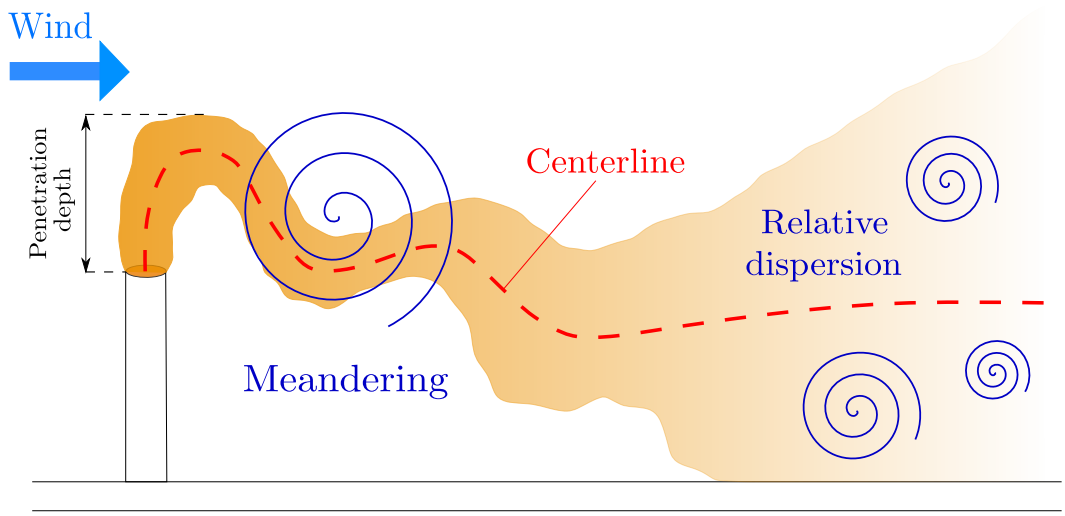

Figure 1.5: Dispersion of a heavy gas from an elevated source, characterised by meandering motion in the near field and relative dispersion in the far field.

the motion of the dense gas clouds becomes then similar to that of a gravity current. This behaviour persist until the density differences are negligible and the heavy gas plume spreads as a passive scalar.

Usually, this process of turbulent dispersion of the plume is considered from a phenomenological point of view as driven by two bulk mechanisms (Gifford, 1959): the meandering, which is the transport of the plume centre of mass by the large-scale turbulence, and the relative dispersion of the plume around the plume centreline (Fig 1.5). Close to the source, the meandering is the dominant mechanisms, since the plume size is sufficiently small to be transported as a whole by large-scale turbulence. In the far field, as the plume spreads and exceeds the size of layer eddies, the meandering becomes negligible compared to the relative dispersion and the plume is blended following concentration gradients. In the middle field, both process occur, influencing the plume dynamics.

The simulation of these phenomena in laboratory experiments requires a dynamical similarity, which means a geometric similarity between the model and the large-scale flow and the equality of the most relevant dimensionless numbers (Simpson, 1999), notably the Reynolds Re, the Froude number Fr. The Reynolds number is defined as the ratio between inertial and viscosity forces $Re = UL/\nu$, with U the flow velocity, L the characteristic characteristic length and ν the kinematic viscosity. Typically, when Re is sufficiently large and the flow is fully turbulent, it is possible to neglect the viscosity effect and assume the laboratory results to be representative to those in real scenarios (Turner, 1973). The Froude number is defined as the ratio between inertial and buoyancy forces $Fr = U/\sqrt{g'L}$, with $g' = g\Delta\rho/\rho_a$ the reduced gravity and $\Delta\rho$ is the difference between the density of the gas and that of the ambient, referred to as ρ_a. The lower Fr, the higher the buoyancy effects. The Froude number similarity (same Fr in the experiments and the real case) is then necessary to maintain the correct balance between buoyancy forces and the inertial effects induced by the atmospheric

flows. Alternatively, these effects are often taken into account by another dimensional parameter, the bulk Richardson number Ri, which is however strictly related to the Froude number, i.e. $Ri = 1/Fr^2$.

1.3 State of the art

Historically, mixing mechanisms in a stable stratified fluids have been studied for geophysical applications (e.g. atmospheric downburst, sea breezes, mesofronts in the atmosphere and cold fronts in the ocean). These provided the basic knowledge to investigate the physical phenomena relevant to the dispersion of dense gases, the main mechanism for mixing with ambient fluid (air or water) and of the development of operational models. An exhaustive review on the dynamics of stratified flows can be found in classical text books, such as Turner (1973) and Simpson (1999). The interest in heavy gas dispersion grew around the '80s when urban development led to the overlap of cities and industrial areas. The role of dense gases in the assessment of industrial hazards became important and both open field and wind tunnel experimental campaigns were conducted (Britter and Griffiths, 1982). At the same time, as far as the computer power increased, these phenomena were tackled numerically, with models of varying complexity. In what follows, we briefly review the state of the art concerning the experimental (both in open field and in wind tunnels) and numerical studies on this topic. In 1985, the milestone experiments of Thorney Island (McQuaid, 1985) was performed, consisting in a release of a volume of dense gases over flat terrain in calm wind conditions. This field experiment were subsequently used as benchmark in the study of heavy gas dispersion (Hall and Waters, 1985; Carpenter et al., 1987; Fannelöp, 1994; Anfossi et al., 2010). In the early '80s, small scale simulations in wind tunnel experiments of heavy gas emission were also performed (Meroney, 1982; Heidorn et al., 1992; Ayrault, Balint, and Morel, 1991; Britter, 1989), mainly focusing on dispersion in 'open' terrain. Later studies focused then on the effects of obstacles and stable/neutral atmospheric conditions (Heidorn et al., 1992; Snyder, 2001; Robins et al., 2001b; Robins et al., 2001a; Briggs et al., 2001; Zhu, Arya, and Snyder, 1998), comparing results with field measurement such as the Kit Fox field experiment (Hanna and Chang, 2001) and Jack Rabbit field experiment (Hanna et al., 2012).

Major finding of this body of work led to the parameterisation of the rate of dilution of the dense gases with the ambient air, as quantified by an entrainment velocity u_e, and on its dependence on the 'local' Richardson number, defined as:

$$Ri = \frac{g'L}{u_*^2} = \frac{g\Delta\rho/\rho_a L}{u_*^2} \tag{1.1}$$

where u_* the friction velocity of the atmospheric flow and L is the gas cloud depth. This functional dependence, used in dispersion models for operational purposes (e.g. DEGADIS, SLAB), evaluates the dilution of the pollutant concentration as a function of the distance from the source depending on local atmospheric conditions. These models

are essentially focused on the quantification of time or ensemble averaged pollutant concentrations, but do not provide information on the statistics of concentration fluctuations around the mean. As far as we are aware, only few studies have so far provided information about the higher order moments of gas concentration. Among these we cite Britter and Snyder (1988), who used a Flame Ionisation Detector (FID) to measure the mean and the standard deviation of the concentration field for steady releases, and Ayrault, Simoëns, and Méjean (1998), who quantified the first four moments of the concentration ensemble statistics concerning the spread of an unsteady ground release. Furthermore, in the existing literature concerning the atmospheric heavy gas dispersion, there is a lack of experimental data on the evaluation of the turbulent mass fluxes, i.e. the correlations between velocity and concentration fluctuations.

1.3.1 Modelling of atmospheric dispersion of dense gases

The main approaches for the modelling of the dispersion of an accidental or deliberate release of pollutant in the atmosphere are:

- Integral and Gaussian models;
- Lagrangian stochastic models;
- Computational Fluid Dynamics (CFD) models.

Integral and Gaussian models (softwares like Safesite, Phast, Effects, SLAB, Degadis, Venjet etc.) are based on simplified formulation of balance equations. These latter (conservation of mass, momentum and energy) are averaged in each plume section and solved along the plume axis, as a function of the distance from the source. These models provide extremely rapid results but do not allow for the simulation of the dispersion phenomena in complex areas (presence of buildings, walls, industrial environments and complex topographies).

Lagrangian stochastic models are widely used to compute the gas dispersion in industrial sites. For a long time, such models were applied to simulate the pollutant mean concentration in the evaluation of the chronic risk (Tinarelli et al., 2000; Carvalho et al., 1999; Trini Castelli, Anfossi, and Finardi, 2010). The prediction of accidental releases of flammable or toxic gases required to develop new strategies, in order to estimate the concentration fluctuations by means of 'micro-mixing' models (Sawford, 2004; Cassiani, Franzese, and Giostra, 2005a; Cassiani, Franzese, and Giostra, 2005b; Cassiani, 2013). In case of dense releases these models have to include specific parameterisation, to take into account the effects of buoyancy. Lagrangian model can be coupled with simplified models of the velocity field, likewise operational integral models, or with velocity fields driven by the output of the CFD simulations. The validation of operational plume rise models integrated in a Lagrangian approach was performed against wind tunnel experiments (Marro et al., 2013) and open terrain

data (Webster and Thomson, 2002). Conversely, few works concerned the simulation of dense gases dispersion. Among these, we cited the model of Anfossi et al. (2010), who simulated the negative buoyancy and the gravity spreading induced from the emissions of dense gases and tested the accuracy of the model against open terrain measurements.

CFD codes solve the Navier-Stokes equations with different turbulence closure models, i.e RANS - Reynolds Averaged Navier Stokes, LES - Large Eddy Simulation, DNS - Direct Numerical Simulation. These approaches allow for a detailed description of the three dimensional structure of the velocity field within complex geometries and therefore for the simulation of the dispersion patterns within them. Since these models are conceived for a wide range of dynamical conditions of the atmosphere and geometrical characteristics of the domain, their application requires a rigorous methodology to implement appropriate boundary conditions, for the topography and the thermodynamics state of the atmosphere (Blocken et al., 2008; Gavelli, Bullister, and Kytomaa, 2008; Pontiggia et al., 2011; Gousseau et al., 2011). It is worth mentioning that the computational resources needed to run these models are much larger than those required by operational models. This feature limits therefore their use for operational purposes, that requires to model an accidental scenario in a limited amount of time.

1.4 Scientific, technical hurdles and impacts

The first and main challenge of this thesis is to achieve a gain of understanding of fundamental physical phenomena governing the dynamics of dense gas releases. In particular, it is of primary interest to identify the influence of the local stratification, as characterised by the local Richardson number Ri (Eq. 1.1) and the relative density difference $\Delta\rho/\rho_a$, on the mixing between the gas cloud and the ambient fluid. Nowadays, this lack of understanding is mainly due to scarce experimental data concerning a detailed description of the turbulence structure within the dense gas clouds and at its edges, where the mixing with ambient air takes place. On its turn, the lack of experimental results is motivated by inherent experimental difficulties in the investigation of these flows, since the high density gradients within the plume are critical conditions for several experimental techniques. Therefore, the metrological aspects of this work represent themselves a significant difficulty that will have to be overcome.

Most of the published studies (Meroney, 1982; Britter and Griffiths, 1982; Heidorn et al., 1992; Snyder, 2001; Hanna and Chang, 2001; Robins et al., 2001a; Briggs et al., 2001; Zhu, Arya, and Snyder, 1998) quantified the spatial distribution of time (or ensemble) averaged concentration. However, it is worth mentioning that the hazards related to the atmospheric transport of these substances are mainly linked to peak values of concentration, that may exceed flammability or toxicity limits. In that sense, modelling these phenomena require the estimation of the intensity of

the concentration fluctuations. The focus has then to be set on the concentration probability density function (PDF), and on its dependence on source and atmospheric conditions. However, knowing the PDF of the concentration does not imply having access to the information on the structure of the signal. Understanding the time series of the concentration signal is therefore also crucial in the risk assessment, especially to identify the hazardous threshold crossing, its time and frequency.

Based on the elements presented so far, it is clear that we need to perform measurements at high frequencies, in order to characterise heavy releases, by reconstructing the PDF of velocity and concentration and their joint PDF. Such measurement can further provide information on the spectra, the turbulent kinetic energy budget, the large and small mixing, as well as the temporal structure of the signal.

1.5 Aim and structure of this thesis

The aim of this thesis is to investigate experimentally the dynamics of an elevated dense gas release and to test the ability of operational dispersion models to simulate it. The studied scenario was defined according to the interest of the industrial partner Air Liquide, mainly focused on the emission from an Air Separation Unit (ASU). These plants separate air through cryogenic process into oxygen, nitrogen and argon products, emitting low temperature plumes that are heavier then air. So far, Air Liquide based the validation of the prediction models of heavy gas dispersion on the operational dataset provided by Schatzmann, Snyder, and Lawson (1993) and Donat and Schatzmann (1999). They tested different release scenarios from an elevated source with a wide range of emission conditions and densities mixture, obtaining information on the mean concentration field, the plume rise and the plume touchdown. The same configuration, corresponding to a real case scenario of O_2 release from an ASU at a temperature of -40°C in the atmospheric boundary layer, was then identified as the configuration of interest in this studies. From the same elevated source, we also simulated a release of a passive scalar, obtaining measurements useful for the comparison with the heavy gas release.

In this work we address three main issues: the metrological aspect related to the simultaneous measurements of velocity and concentration of a dense gas, the analysis of the results of the experimental campaign simulating a dense and a passive gas release, and the simulation of these releases by means of operational models. The structure of this thesis is by article, which means that each chapter treats each subject independently and some repetition may occur, especially when dealing with the metrology and the description of the experimental set up and measurement techniques.

In Chapter 2, we discuss the metrological hurdles and describe the calibration procedure of the coupled system used to simultaneously measure the concentration and the velocity fields. We present the methodology and introduce the set-up for the elevated source emission experiments.

In Chapter 3, we present the main results of the coupled measurements of the velocity and the concentration, comparing the passive scalar and the heavy gas plumes. The velocity and concentration field and their statistics are reported, in particular the mean, the standard deviation and the higher order moments. We analyse the concentration PDF and the turbulent mass fluxes. Furthermore, we quantify the production, transport and dissipation terms in the balance equation of the turbulent kinetic energy and of the concentration variance. The estimate of typical mixing time scales is also discussed and compared with the estimates of theoretical model.

Finally, the data collected during the experiments was used in order to test and validate operational dispersion models (Chapter 4). To that purpose we considered an integral model (Ventjet, Miller et al., 2021), developed by Air Product and Air Liquide, and a Lagrangian model (SLAM, Vendel et al., 2011), developed by the team AIR of the École Centrale de Lyon. We completed the study by investigating the structure of the concentration time series, estimating the level crossing time and rate.

Chapter 2

Wind tunnel experiment on atmospheric heavy gas dispersion: metrological aspects

2.1 Abstract

We propose a new experimental protocol to investigate the atmospheric dispersion of a dense gas in wind tunnel experiments. Simultaneous measurements of concentration and velocity are performed by coupling Flame Ionization Detection (FID) and hot-wire Anemometry (HWA), whose probes were located sufficiently close to each other so that respective measurements could refer to a same sampling volume. The heavy gas emission consists in a mixture of air, carbon dioxide and ethane. Carbon dioxide is used as a buoyant agent, and ethane is used as tracer, its concentration being detect by the FID. In this context, the main metrological issue of the setup concerns the response of the FID and the HWA to different proportions of the gases in the mixture. Notably, the presence of carbon dioxide affects the linear response of the FID by a saturation process, and modifies the calibration of the HWA by density effects. This can be compensated by performing a non-linear calibration of the FID, and by using the instantaneous density value given by the FID to apply a time-dependant correction of the HWA response. We demonstate the capability of our coupled HWA-FID measurement system in the case of a negatively buoyant emission in a turbulent boundary layer. The estimation of mass fluxes through different sections downwind the source enlightens the reliability of the experimental results.

2.2 Introduction

Experimental studies in atmospheric wind tunnels still play a major role for our understanding of pollutant dispersion physics. These studies provide reference datasets, that can be subsequently used to validate and improve numerical models. If many datasets exist in the case of neutrally buoyant plumes, it is still necessary to improve the characterisation of turbulent fluctuations and mass fluxes, by means of combined statistics of concentration and velocity, in the presence of density gradients. These

experiments can be performed in both wind tunnel and water flumes. However, the latter are not suited for the simulation of releases characterised by large density differences with the ambient air. We will therefore focus here only on wind tunnel experiments, in which gases with molecular weight higher than that of air are employed for the simulation of heavy releases.

Combined statistics of concentration and velocity can be actually acquired adopting suitable measurement techniques. Different systems have been developed and employed in wind tunnel experiments, involving techniques for the measurements of velocity as the Hot-Wire Anemometry (HWA) and the Laser Doppler Anemometry (LDA). Measurements of concentration include instead either the Photo Ionization Detector (PID), the cold film/wire, and the Flame Ionization Detector (**FID**)Fackrell80.

The HWA (Comte-Bellot, 1976) is a well established technique, widely employed to measure fluctuating fluid velocities. The calibration procedure is well defined in isodensity flows, but is more complicated for gases with different densities (Simpson and Wyatt, 1973; Wasan and Baid, 1971; Pitts and McCaffrey, 1986; Banerjee and Andrews, 2007; Way and Libby, 1970).

In order to measure the velocity in the bi-gases turbulent mixing in isothermal conditions, Corrsin (1947) combined the calibrations of HWA obtained for each gas. However, this method led to systematic error in the estimate of the coefficients of the calibration King's equation. Pitts and McCaffrey (1986) calibrated the hot-wire and film anemometers in different gases and defined an empirical correction of the calibration parameters as a function of the Reynolds (Re) and Nusset (Nu) numbers. Wasan and Baid (1971) focused on the HWA response in carbon dioxide-air mixture by performing a calibration in pure gas and then used a linear interpolation to estimate velocities. All this methods are characterised by a considerable uncertainty, especially if the two components have molecular weights significantly different one to the other (Banerjee and Andrews, 2007). McQuaid and Wright (1973) examined the response of HWA in gas mixtures defining an empirical law relating the molal concentration of the second component gas mixture to the voltage response. The main result of this study was the empirical correction on the response of HWA in presence of gases other than air. A different approach was proposed by Talbot et al. (2009). They performed neon doping in a variable-viscosity flows of propane-air mixture, obtaining hot-wire response to be insensitive to the concentration field. Zhu, Arya, and Snyder (1998) analysed velocity and turbulence within the dense gas plumes by using hot film anemometry with an optimum overheat ratio that allowed them to perform measurements in a range of carbon dioxide (CO_2) concentration (less then 25%) that did not affect the probe sensitivity. Over the range of 0.3 - 1.1 m/s, the errors in the mean wind speeds were generally less than 5%. Finally, Banerjee and Andrews (2007) performed a detailed procedure to investigate helium-air mixture with HWA, employing a multiposition-multioverheat hot-wire technique to estimate both velocity and density fluctuations and defining a calibration surface in function of density and velocity.

Coupled measurements of velocity and concentration were most commonly performed with a HWA-FID or HWA-PID system, with the exceptions of Raupach and Legg (1983) and Stapountzis et al. (1986), who employed the HWA and a cold wire to measure the velocity and concentration field respectively, simulating the scalar source with a heated wire. Fackrell and Robins (1982) measured with HWA-FID the first two moments of the concentration field of a passive scalar plume and estimated the turbulent fluxes from the mean concentration and velocity field. Koeltzsch (2000) used the same technique to estimate the turbulent mass fluxes in a turbulent boundary layer, focusing on the dependence of the turbulent Schmidt number on the distance from the wall. Metzger and Klewicki (2003) developed a sensor combining respectively HWA and a PID, Talluru et al. (2017) used the same system to investigate passive scalar dispersion in a turbulent boundary layer.

Others studies used a coupled system of LDA-FID to directly estimate turbulent fluxes of passive scalar (Contini, Hayden, and Robins, 2006; Carpentieri and Robins, 2010; Carpentieri, Hayden, and Robins, 2012). Employing the LDA (Abbiss, Chubb, and Pike, 1974) for the velocity measurements, prevents any calibration uncertainty related to a varying density difference, but may imply other complications. Notably, the aerosols used to seed the flow may affect the concentration statistics measured by the FID. To analyse these and other metrological aspects of these coupled measurements techniques, Marro et al. (2020) compared the HWA-FID and the LDA-FID systems, notably concerning the optimal distance between the probes, the effect of the seeding on concentration statistics, the evaluation of the signal resampling and the synchronisation of the measured signals of concentration and velocity. Beside defining the optimal setting of the probes, they highlighted the reliability of both systems for simultaneous measuring of high-frequency signals of velocity and concentration in a turbulent boundary layer.

It is worth noting that these coupled techniques have not been used so far to investigate the dispersion of heavy gas releases. To that purpose, the release of a heavy gas can be conveniently produced by a mixture of air and carbon dioxide (Meroney, 1982; Schatzmann, Snyder, and Lawson, 1993; Snyder, 2001; Briggs et al., 2001; Hanna and Chang, 2001; Britter and Snyder, 1988). The local density within the turbulent flow can then be estimated by a direct estimate of the heavy gas concentration (Briggs et al., 1998; Meroney, 1982) or, alternatively, by adding a tiny quantity of a gas tracer, whose presence can be detected with a FID. Common tracers are propane (Robins et al., 2001a) and ethane (Schatzmann, Snyder, and Lawson, 1993; Zhu, Arya, and Snyder, 1998; Britter and Snyder, 1988). Schatzmann, Snyder, and Lawson (1993) and Donat and Schatzmann (1999) used a gas-probe sampling system connected to a FID to analyse time-mean concentrations and velocities of heavy gas plumes. Robins et al. (2001a) collected simultaneously 16 air samples using a vacuum system and analysed it with a FID, to obtain information on the mean concentration in neutral turbulent boundary layer. They used two additional channels for the calibration, one to determine the background hydrocarbon concentration in the wind tunnel

and the other to obtain the sensor response of the calibration gas of known and certified composition, used also at the source. This provided the most direct way of determining the required concentration, normalised by source conditions. Britter and Snyder (1988) measured with a FID the time averaged concentration field induced by a steady emission of a passive scalar and a heavy gas. They calibrated the FID using an ethane/air mixture and investigated separately the response of the FID to ethane/carbon dioxide/air mixture, and corrected the measurement accordingly. Zhu, Arya, and Snyder (1998) investigated a ground level emission of heavy gas, using ethane (C_2H_6) as tracer and CO_2 as heavy gas, imposing a ratio between carbon dioxide and ethane $r = C_{CO_2}/C_{C_2H_6} = 33.3$. Moreover, they tested the response of the FID to ethane/air and CO_2/ethane/air mixtures in a series of measures where the source mixtures were diluted with air at constant rates in a dilution chamber. They found a deviation from the theoretical exponential curve for high ethane concentration and for lower concentration of ethane in presence of CO_2. The same method was employed by Snyder (2001).

This work is part of a project that aims at studying heavy gas dispersion from an elevated point source in a turbulent atmospheric boundary layer. Following the recent works of Iacobello et al. (2019) and Marro et al. (2020) in the context of passive emissions, we use a coupled system of FID-HWA to investigate the release of a dense mixture of air, CO_2 and ethane. The aim of the present study is to define a calibration procedure for both the FID and the HWA that takes into account the influence of the mixture density. In this new approach, the instantaneous measurements of concentration are used to provide a time-dependant correction of the HWA response.

We first present the experimental set-up used for the calibration and the wind tunnel experiments (Section 2.3.1). We continue by describing the characteristics of the instruments (Section 2.3.2 and 2.3.3) and the coupled measurement system (Section 2.3.4). The calibration procedures are detailed for the FID (Section 2.4) and the HWA (Section 2.5). Finally, we present results on the concentration mean field, the turbulent mass fluxes and the total mass fluxes estimated in the cross-wind section, verifying the conservation of the mass within the plume and thus the reliability of the coupled measurements technique (Section 2.6).

2.3 Experimental methods

2.3.1 Experimental set-up

The experiments are conducted in the atmospheric wind tunnel of the Laboratoire de Mécanique des Fluides et d'Acoustique at the École Centrale de Lyon in France. The recirculating wind tunnel is 14 m long and 3.7 m wide, with an adjustable ceiling to control pressure gradients. The temperature in the vein is regulated, to limit the temperature variation during a one-day experiment in the range ±0.5°C. The wind tunnel temperature is chosen to minimise the temperature difference between the emitted gases (coming from pressurised bottles) and the wind tunnel flow.

In order to calibrate the instruments, a mixture of air, ethane and carbon dioxide is used to generate density controlled gas mixtures. Ethane is employed as a tracer as the FID (Fackrell, 1980) is sensitive to its concentration. Ethane has almost the same density of air (ρ_a), while the density of CO_2 is $1.5\rho_a$. Different percentage of carbon dioxide are used to modify the density of the gas mixture during the calibration and the experiments. The mixture device is composed of three different lines, one for each gas. Every line is equipped with a mass flow controller that provides for each gas the volumetric flow rate Q. The mass flow controller works in a range between 1 and 200 Nl/min for CO_2 and air, and between 0.50 Nml/min and 200 Nml/min for ethane. The error on the mass flow rate is estimated by comparison with measurements provided by a volumetric counter. The maximal difference between the measurements of the two instruments does not exceed $\pm 3\%$ (Nironi et al., 2015). Between the CO_2 tank and the flowmeter is placed a heater, to avoid the presence of condensed CO_2 droplets that could change the dynamics of the dispersion and the instruments response. All the lines are connected to a valve in which gases are blended together before being directed to the source, as shown in Figure 2.1. The concentrations of ethane and CO_2 at the source are computed in volumetric ppm, with $c_s = Q/Q_s$, where Q is the flowrate of the considered gas and Q_s the total flowrate at the source.

The steady release of a heavy gas and a passive scalar is investigated in a neutral turbulent boundary layer characterised by free-stream velocity $U_\infty = 1.45\, m/s$ and height $\delta = 0.8\, m$. The turbulent boundary layer is generated by combining the effects of spires and wall roughness as described in Nironi et al. (2015). The plume is released from a metallic source of internal diameter $d_s = 0.012\, m$ and placed at $h_s = 0.076\, m$ from ground level and at 7.5δ from the beginning of the working section, where the boundary layer can be considered fully developed (Fig. 2.1). The passive scalar release is obtained by a mixture of air and ethane and the heavy gas release with a mixture of air, ethane and CO_2. The sampling duration is 300 s, allowing the stochastic uncertainty of the concentration statistics due to the finite size of the sampling to be of order 0.1 % (Nironi et al., 2015). The flowrate at the source is $Q_s = 16\, l/min$ for both heavy and passive releases, corresponding to a vertical velocity of $w_s = 2.37\, m/s$. For the heavy gas emission the volume flow of CO_2 is $14,8\, l/min$, which corresponds to a density at the source $\rho_s = 1.78\, kg/m^3$ and to a relative density difference $\Delta\rho/\rho_a = (\rho_s - \rho_a)/\rho_a \approx 50\%$, depending on the air temperature in the wind tunnel.

2.3.2 Concentration measurements

Concentration is measured with the FID (Fackrell, 1980) that is sensible to the presence of hydrocarbons. The air sample is sucked and burned in the combustion chamber where a cathode collects ions. The instrument returns the electric potential difference induced by the ionization current, proportional to the number of atoms of carbon in the sampling. The complex combustion process produces a series of chemical reactions that occur in the combustion chamber. The presence in the air sample of gases other

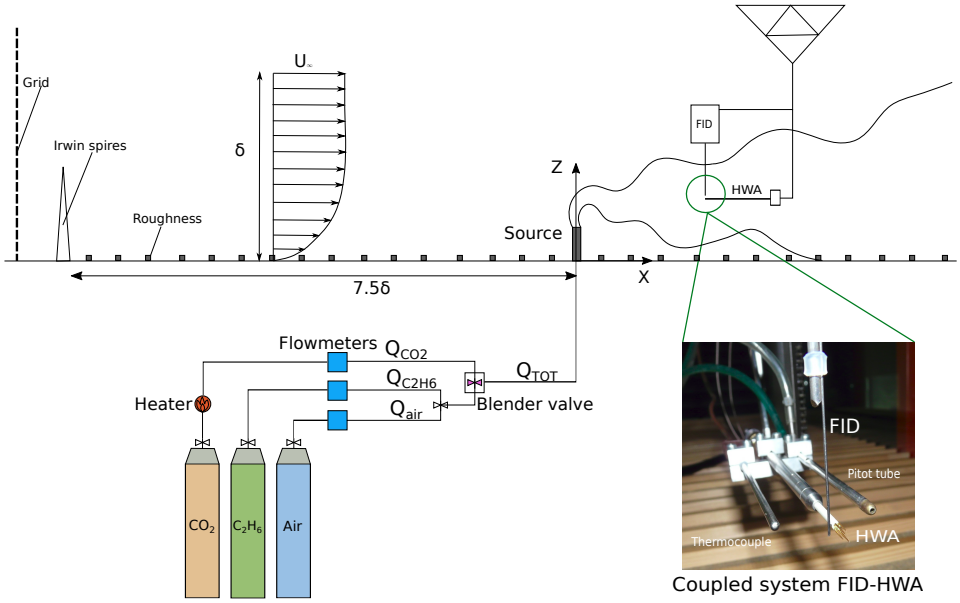

Figure 2.1: Experimental setup of gas lines and coupled measurements system

than the tracer, such as CO_2, influences these reactions, changing the instrument response. We fixed the ratio $r = C_{CO_2}/C_{C_2H_6}$ between carbon dioxide and ethane concentration at the source and we assume that r is constant all along the dispersion process. This is justified by the fact that molecular diffusion coefficient in air for CO_2 and ethane are comparable $D_{CO_2} = 1.61 \cdot 10^{-4}\ m^2/s$ and $D_{C_2H_6} = 1.48 \cdot 10^{-4}\ m^2/s$ at 20 °C (Pritchard and Currie, 1982) and that the gases are well blended at the emission. The FID frequency response is approximately at 400 Hz with a sampling tube 0.3 m long and with a diameter of 0.125 mm (Marro et al., 2020).

Since the experiments on gas dispersion are performed in a recirculating wind tunnel, the increase of background concentration over time has to be taken into account. We therefore measure the background concentration before and after every acquisition. We interpolate linearly over time the initial and final value and we subtract the obtained background concentration from the signal.

2.3.3 Velocity measurements

Velocity measurements are performed with a two probes HWA at constant temperature (Perry and Morrison, 1971; Bruun, 1996). The platinum probe has a volume sample of $5\mu m \times 5\mu m \times 1mm$ and a velocity-vector acceptance angle of 45°. In our set-up, the HWA has frequency response of about 5kHz. The yaw calibration is not performed. After the calibration procedure, described in Section 2.5, we apply a yaw correction with constant coefficients $k_1^2 = k_2^2 = 0.0225$ to decompose velocities from the X-probe into longitudinal and transverse velocity components (Jørgensen, 2002). Since the HWA response is influenced by the CO_2 concentration, it is necessary to know the instantaneous value of this concentration in the sampling volume to correct the HWA

response. This is made possible trough the coupled measurement system that combines FID and HWA.

2.3.4 Coupled measurement system

A coupled system of FID and HWA requires the setting of an optimal distance between the two probes in order to: I) avoid any perturbation on the response of one instrument on the other and II) be close enough to consider measurements as performed in the same sampling volume (Marro et al., 2020). According to the analysis performed by Marro et al. (2020) this distance is set equal to $5\,mm$. Further information is provided by a Pitot tube and a thermocouple, monitoring during the experiment the flow velocity and the temperature. Sampling frequency for coupled measurements is set at 1000 Hz. Signals of concentration are shifted in time by $15ms$ with respect to velocity, which is the time required for the gas sample to reach the FID combustion chamber (Marro et al., 2020). Once shifted the signals, these are resampled to obtain cross statistics. According to the measurements of Nironi et al. (2015) the experimental error of repetitive measurements for the mean and the standard deviation of velocity and concentration are 2% and 3%, respectively. With a similar experimental set-up, Marro et al. (2020), assessed likewise values for the LDA-FID system. Both studies were however performed with passive scalar releases.

2.4 FID Calibration in the presence of CO_2

We perform the calibration by connecting the output of our three lines mixture device to a pipe of diameter 0.005m. The FID is placed at the exit of this pipe and we investigate the response of the probe for different mixtures of CO_2 and ethane. In Figure 2.2a we show the response of FID, in volt $E(V)$, as a function of the ethane concentration, for different ratio $r = C_{CO_2}/C_{C_2H_6}$ in the gas mixture. We note that $E(V)$ decreases as the ratio r increases. That means that, for constant $C_{C_2H_6}$, the presence of C_{CO_2} lowers the voltage response. Secondly, for pure ethane or low value of r, it is possible to define the ethane concentration as a one-to-one function of the FID volts ($r = 36$ in Fig. 2.2a). As C_{CO_2} increases ($r \geq 75$), a saturation of the signal occurs and the relation between $E(V)$ and $C_{C_2H_6}$ is no longer one-to-one. The calibration curves collapse on a single curve when the products between $E(V)$ and the ratio r is plotted versus the density of the mixture ρ (Fig. 2.2b). This analysis allows us to identify a unique critical density ρ_c for all r value considered (red line in Fig. 2.2b), corresponding to $\rho_c = 1.56\,kg/m^3$ and 58% of CO_2. Measurements performed in a mixture with density $\rho < \rho_c$, are calibrated with a bijective function. In planning the wind tunnel experiments, we accurately defined the amount of CO_2 at the release to have concentration values significantly lower than the critical value at the measurement locations, thus avoiding the saturation. As a general rule, FID calibration is performed twice a day during the whole measurement campaign.

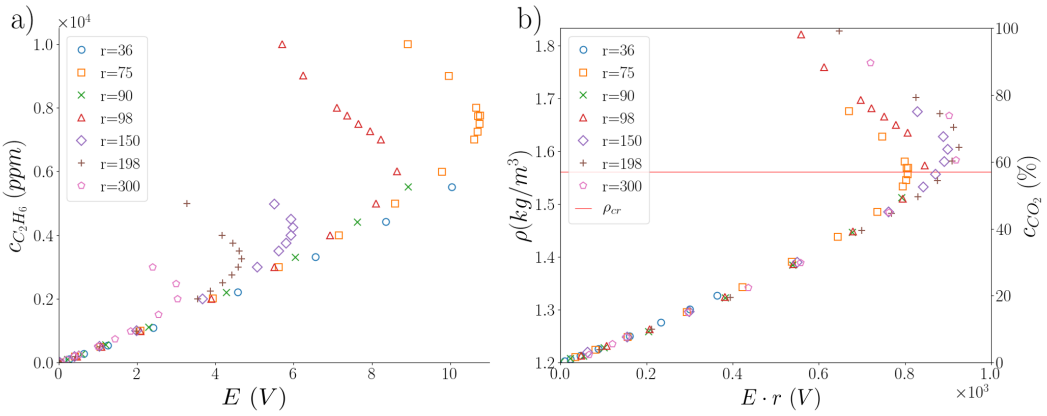

Figure 2.2: FID calibration curves for varying $r = C_{CO_2}/C_{C_2H_6}$. a) Ethane concentration as a function of volt response E. b) Normalized gas mixture density as a function of rE.

2.5 HWA Calibration in CO_2-air gas mixtures

When performing the HWA calibration, the standard procedure determines the sensitivity coefficients of the two wires with respect to different flow variables (Comte-Bellot, 1976). This relation depends on velocity, ambient temperature and gas mixture density. Here we are particularly concerned of the density effect on the HWA response. In this study, we use a similar approach to Banerjee and Andrews (2007) for the HWA calibration in the context of a heavy gas atmospheric dispersion. The main conceptual difference between our work and the one of Banerjee and Andrews (2007) is that we use this calibration to perform simultaneous and distinct measurements of concentration and velocity. As explained, the temperature in the vein of the wind tunnel is kept constant during one experiment, but the HWA calibration needs to be repeated every time the temperature varies more than ±0.5°C. The calibration of the hot-wire anemometer is performed at the exhaust of a pipe of 25 mm in diameter and 700 mm long. We use a gas mixture of CO_2 and air with five different ratios of the mixture, between 0 and 100%. The procedure includes a velocity correction using Pitot tube measurements, to take into account the difference between the velocity at the centre of Poiseuille profile and the average velocity over the tube section, as estimated by the flowmeters. From the measurements with the Pitot tube, we identify a 3rd degree polynomial linking the flow rate and the velocity in the range 0 to 3 m/s, that is the velocity range in which we are going to work during the experiments. The velocity is reported in Figure 2.3 as a function of the volt response; each set corresponds to a different percentage of carbon dioxide. These data can be fitted by a bi-dimensional function that takes into account the dependence of the velocity on both $E(V)$ and ρ (Fig. 2.3). The surface interpolation is a polynomial of 5th and 4th degree, with a the maximum estimated error of 2.7% for $U = 0.58\,m/s$, probably due to the uncertainties of the flowmeter. In order to use the calibration surface for instantaneous velocity measurements, the coupled system is essential. Through the

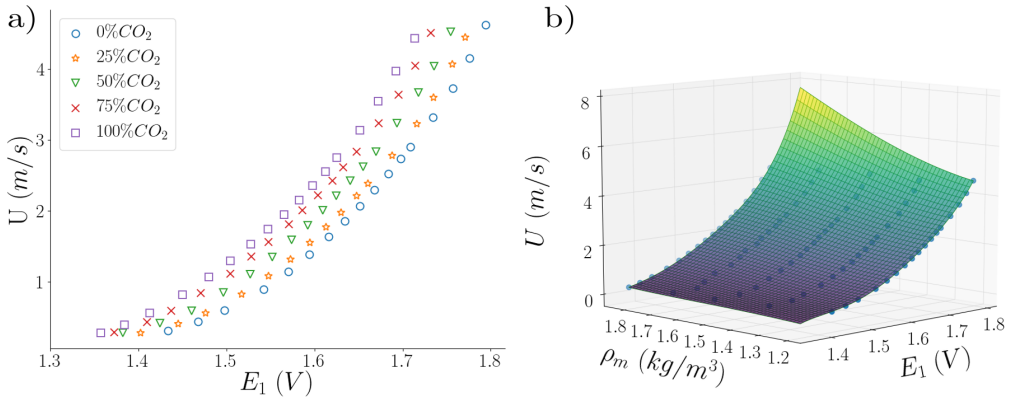

Figure 2.3: a) HWA calibration curves for gas mixture with increasing quantities of CO_2: velocities in function of volt response. b) HWA calibration surface velocities in function of volt response and gas mixture density.

FID acquisition of concentration we are able to evaluate the instantaneous density of the fluid and thus convert accordingly the HWA volt response.

2.6 Measurements

We investigate the steady release of a heavy gas and a passive scalar in a neutral turbulent BL (Section 2.3.1), performing simultaneous measurements of concentration and velocities profiles downwind the source with the coupled system FID-HWA. The first measurement section is located 200 mm downwind the source, where the dilution is sufficiently effective so that the density is below the critical value identified during FID calibration. We adjust the flowrates of ethane and air to reach Q_s as a function of the distance from the source, regulating the amount of C_2H_6 to avoid the FID saturation during one-point measurement, without changing ρ_s.

To compare the results we employ dimensionless concentration and velocities. The latter are defined as u^*, w^*, v^* and are rescaled by the free-stream velocity U_∞, while c^* is normalised in function of the mass flow rate at the source $Q_s\rho_s$, U_∞ and δ (assumed as the reference length scale), as:

$$c^* = c\frac{U_\infty \delta^2}{Q_s \rho_s}. \tag{2.1}$$

In Figure 2.4 is reported the normalised time averaged concentration $\overline{c^*}$ for a heavy gas plume and a passive scalar. Each profile corresponds to a section at increasing distances from the source. We observe that $\overline{c^*}$ decrease downstream the source. The mean concentration profiles show that the plume develops close to the ground, due to buoyancy effects.

Employing our coupled measurement systems, adjusted with the surface calibration of the HWA and the FID calibration, we can also obtain simultaneous measurements of concentration and velocity, that allow us to measure vertical profiles of streamwise

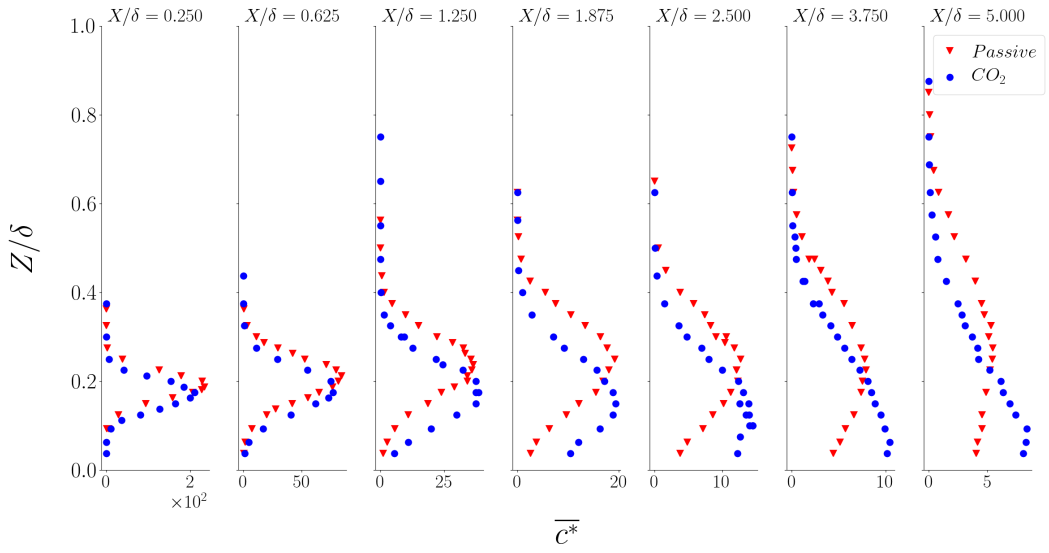

Figure 2.4: Vertical profiles of the normalized mean concentration at increasing distance from the source for passive (red) and heavy (blue) gas plumes.

turbulent mass fluxes ($\overline{u'c'}^*$), reported in Figure 3.16 in dimensionless values. The intensity of $\overline{u'c'}^*$ decreases with increasing distance from the source as the plume spreads. The vertical displacement of the plume also has a role on the evolution in space of $\overline{u'c'}^*$ in case of heavy gas emission. Close to the source, the dispersion dynamics is significantly influenced by the emission condition, with sharper profiles of turbulent mass fluxes. Furthermore, in this region, the source momentum and the buoyancy alter the velocity field, thus $\overline{u'c'}^*$ are lower in the plume centre in case of heavy gas emission. Further away from the source, the horizontal turbulent mass fluxes are not affected by the buoyancy effect and minimum and maximum values of $\overline{u'c'}^*$ are almost the same for both the heavy gas and the passive scalar plumes. Further discussion on these results, presented here to validate the coupled measurement technique, are beyond the scope of the present study.

In order to verify the reliability of our measurements, we have estimated mass conservation within the plume, by comparing the integrated mass flux at different cross-flow sections $Q(x)$ with the mass flow rate at the source and Q_s, i.e.:

$$\frac{Q}{Q_s} = \int\int \overline{uc}^* \, dy^* dz^*, \tag{2.2}$$

where $y^* = y/\delta$ and $z^* = z/\delta$.

Following the Reynolds decomposition, the mass fluxes can be expressed as the sum of the mean and the fluctuating component:

$$\overline{uc}^* = \overline{u^*}(z) \cdot \overline{c^*}(x,y,z) + \overline{u'c'}^*(x,y,z). \tag{2.3}$$

The available information on $\overline{c^*}(x,y,z)$ and $\overline{u'c'}^*(x,y,z)$ are limited on the vertical and transverse profiles, crossing at the plume centre. To evaluate the mass fluxes on the

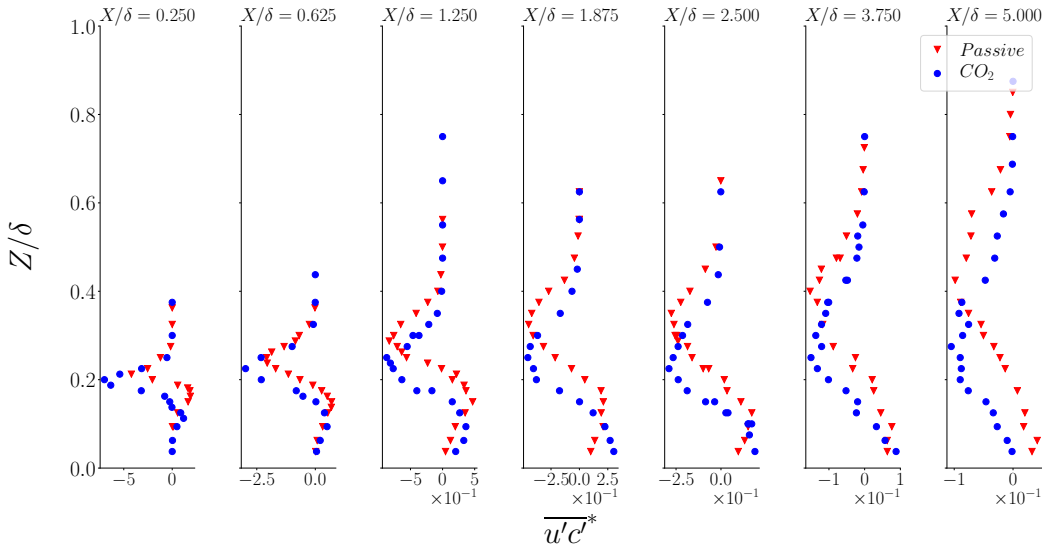

Figure 2.5: Vertical profiles of normalised horizontal turbulent mass fluxes for sections at increasing distance from the source for passive and heavy gas plume.

entire cross-section, some interpolation and hypothesis has to be made. Concentration profiles are interpolated with a Gaussian distribution for the transverse profiles and a symmetric Gaussian profile in the vertical direction (to take into account the reflection of the plume to the ground). We assume a velocity profile homogeneous in the horizontal direction, while the dependence on the distance from the wall follows the power law as has been characterised by Nironi et al. (2015) for the same velocity field. For the turbulent mass fluxes $\overline{u'c'}^*$, we interpolate linearly the measured vertical profiles and we assume a Gaussian distribution for the transverse profiles, since the information collected from the measurements were not sufficient to estimate a more specific interpolation.

In Figure 2.6 are compared the non dimensional mass fluxes in the cross-flow section for heavy gas (Fig. 2.6.a, c, e and g) and passive scalar (Fig. 2.6.b, d, f and h) releases at increasing distance from the source, with contour values that span every decade, from 10^{-3} to 10^{2}. Mass fluxes visualisation confirm what has been discussed in the previous paragraphs. It is visible the vertical displacement of the heavy gas plume, that develops near the ground, as it has been observed for the mean concentration field. Moreover, the shape of the plume, that depends on the dispersion mechanisms, is similar between heavy and passive scalar plume.

We plot Q/Q_s as a function of the longitudinal distance from the source (Fig. 2.7). The fluxes of both passive and heavy gas release are slightly underestimated, with an acceptance range of 20%. The estimated fluxes are here reported with error bars of 10%. Similar comparisons where performed by Raupach and Legg (1983) and, more recently, by Marro et al. (2020) in the case of passive emissions. Raupach and Legg (1983) evaluated the streamwise heat flux induced by a elevated linear source, obtaining values that are similar to ours, with a range of variation up to 20%. The reliability of

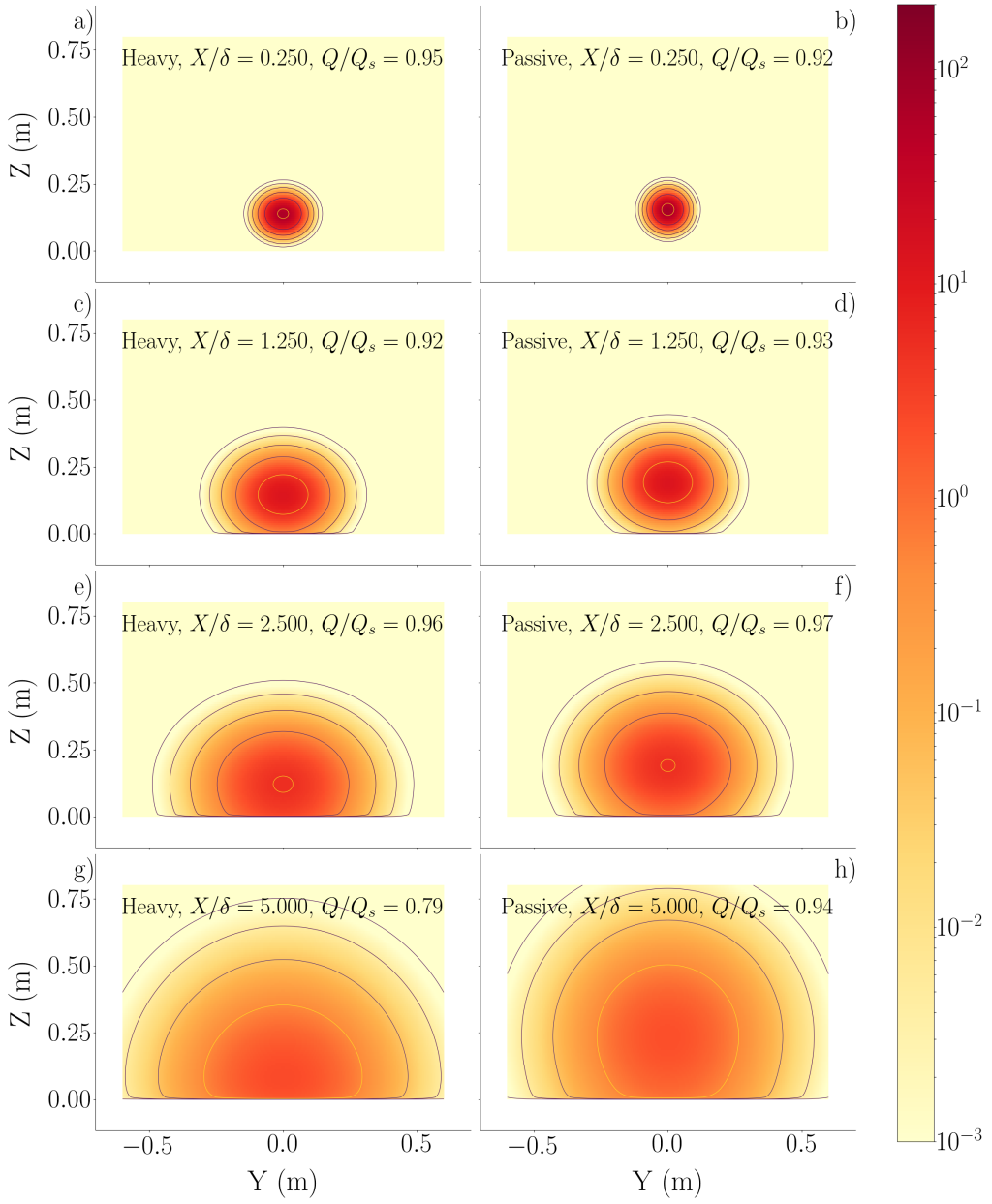

Figure 2.6: Mass fluxes in the cross-flow section for increasing section from the source for a), c), e), g), heavy gas and b), d), f), h), passive plume.

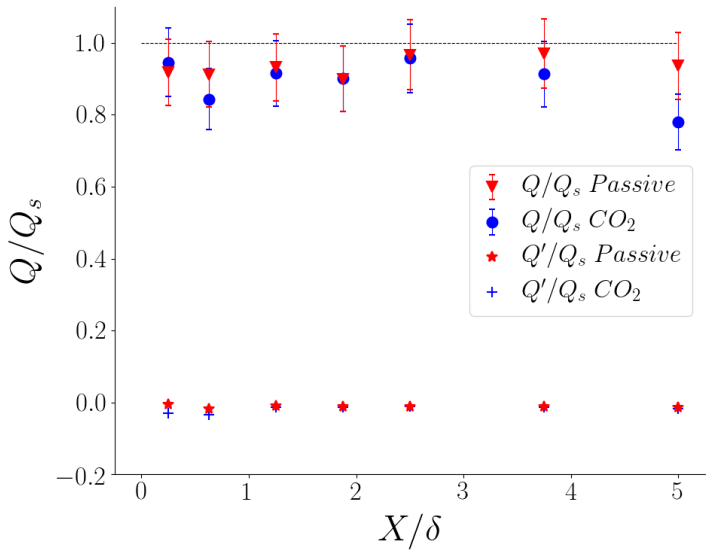

Figure 2.7: Integrated flux over transverse sections normalized by the flow rate at the source Q_s, for increasing distance from the source.

the coupled measurement system has been verified by Marro et al. (2020) for passive scalar emission from a ground line source. They computed a simple mass balance over the domain, observing a good agreement with the measurements provided by the mass flow rates, with a global uncertainty of 8%. In the case of Marro et al. (2020), the homogeneity in the horizontal direction simplified the horizontal interpolation of the vertical profiles, since the data were acquired in a grid. We apply the same approach to the case of a 3D plume disposing of information only on a vertical and a transverse profiles for each cross-wind section. The computed mass fluxes prove that the measurements in the heavy gas plume are as reliable as the one performed in a passive scalar plume.

In Figure 2.7 are also reported the normalized fluctuation fluxes (Q'/Q_s), that have small negative values. For this reason their contribution to the total fluxes is almost negligible. Note that their value is tiny, and that that they contribute for less than 2% to the total mass flux, a value which is systematically lower than that estimated by Marro et al. (2020) for a line-grounded source.

2.7 Conclusions

We have defined a procedure to calibrate a coupled system of FID-HWA in order to measure velocity and concentration statistics within heavy gas plumes. This system simultaneously measures concentration and velocity in the same sampling volume. The heavy gas mixture was composed by CO_2, air and C_2H_6, the latter used as a tracer, since its concentration was detected by the FID. The presence of CO_2 in the mixture alters the volt response of both instruments. For this reason, we have analysed the FID response as a function of the density of the mixture and

$r = C_{CO_2}/C_{C_2H_6}$, identifying a critical density that corresponds to $\Delta\rho = 30\%\rho_a$. For a density of the mixture below this value, we could define a one-to-one function to calibrate the FID. The HWA response depends on both the flow control velocity and the density of the gas mixture. We have therefore defined a calibration procedure aiming at estimating a calibration surface to take into account the dependence on both quantities. As a demonstration, we employed the coupled system HWA-FID in wind tunnel experiments, simulating a passive scalar and a heavy gas release from an elevated chimney. We measured the pollutant dispersion downwind the source and analysed the dimensionless mean concentration $\overline{c^*}$. We observed from the mean concentration profiles that the plume develops close to the ground. Simultaneous measurements of concentration and velocity allowed us to obtain vertical profile of streamwise turbulent mass fluxes $\overline{u'c'}^*$. Near the source, the dispersion dynamics is shown to be significantly influenced by the plume emission velocities, with sharper profiles of turbulent mass fluxes. To verify the reliability of our measurements, we estimated the total mass fluxes in the cross-flow section of the plume at increasing distance from the source. While the vertical displacement of the plume is affected by the buoyancy of the heavy gas, the shape of the plume is similar in both plumes. Furthermore, we normalised the total fluxes for each section by the total flow at the source Q_s, and verified mass conservation for both passive and heavy gas cases.

Chapter 3

Wind tunnel experiments on heavy gas and passive scalar emission in a turbulent boundary layer

3.1 Abstract

Understanding the physics of the atmospheric dispersion of heavy gases is essential to the evaluation and management of risks associated to accidental releases. Heavy gas dispersion is characterised by a reduced dilution with ambient air (compared to a passive gas) and a stagnation close to the ground level, with serious consequences on health and environment. The aim of this study is to investigate experimentally the dynamics of a heavy gas release and to enlighten its main differences compared to that of a passive gas. To that purpose we analyse the emission of a heavy and a passive gas from an elevated source placed within a turbulent boundary layer. In the wind tunnel experiments, we perform simultaneous velocity and concentration measurement for vertical and transverse profiles at several distances downwind the source. We analyse the mean and the fluctuating field of both concentration and velocity and deduce turbulent mass fluxes. With the information provided by the dataset, we characterise the plume, evaluating its vertical and transverse spread, the height of its centre of mass and the turbulent dispersion coefficients. We further evaluate the intensity of the concentration fluctuations and the concentration probability density function, which is shown to be well modelled by a Gamma distribution. Moreover, we analyse the production and dissipation terms of the mean turbulent kinetic energy equation, estimating the flux and bulk Richardson numbers within the plume. Similarly, we analyse the terms of the balance equation of the concentration variance focusing in particular on the production and dissipation. Finally, we estimate the typical time scale for the turbulent mixing, according to two different micro-mixing models parameterising the effects of molecular diffusion.

3.2 Introduction

The management of risks associated to accidental releases of heavy gases requires modelling tools that are able to predict the exceess of given concentration thresholds. Developing these models is nowadays a challenge and requires a deep understanding of the physics of the dispersion and mixing of dense gas releases. The spreading of a plume of gases heavier than air determines a stable stratified flow condition that influences the dispersion process. In case of either inflammable or toxic gases, the reduced dilution with ambient air and the stagnation close to ground level may imply exceeding the threshold concentrations for flammability and toxicity. For this reason the dense releases are generally associated to higher environmental risks. Modelling these phenomena requires to resolve the fluctuations of pollutant concentration and velocities.

Experimental campaigns in wind tunnels and water channels are the basis to understand the physics of pollutants dispersion. Water channels were successfully used to study passive scalar dispersion in boundary layers (Crimaldi, Wiley, and Koseff, 2002; Hilderman and Wilson, 2007) and urban flows (Yee et al., 2006; Di Bernardino et al., 2019; Hsieh, Lien, and Yee, 2007), obtaining information on plume meandering, concentration fluctuations and mass fluxes. However, in water channel, the density difference between the plume and the water is limited to a few percent. Furthermore, wind tunnels are more convenient in terms of available measuring equipment and more adequate to simulate the neutral and stratified atmospheric boundary layer (Meroney, 1987). These aspects make them preferable to investigate heavy gas dispersion over water facilities.

Most of the experimental studies on atmospheric pollutant dispersion have been so far performed in wind tunnels. Warhaft (2000) reviewed the studies concerning the passive scalar dispersion, enlightening how the intermittency of the scalar field influences the local isotropy of both the inertial and dissipation scales. Few works focused on the estimation of both the turbulent fluxes and the concentration fluctuation field of a passive scalar release, that are fundamental to characterize the plume structure and its development. Fackrell and Robins (1982) explored the plume emitted from a point source at different heights and size, observing the behaviour of the concentration fluctuation in terms of variance, intermittency, PDFs and spectra. They estimated the vertical and lateral turbulent fluxes and the terms of the balance equation of the concentration variance. Nironi et al. (2015) extended this work studying the spatial distribution of the first four moments of concentration and velocity. Coupled measurement system for concentration and velocity were used to measure the turbulent fluxes within a passive scalar plume from a point source (Koeltzsch, 2000; Talluru, Philip, and Chauhan, 2018) and a line source (Raupach and Legg, 1983; Marro et al., 2020). Contini, Hayden, and Robins (2006) used a coupled LDA-FID system to estimate the fluxes in a passive and positive buoyant plume (using helium) and investigated the mixing of the two plumes. More recent

studies have instead investigated the turbulent fluxes in presence of obstacles and urban canopies (Carpentieri and Robins, 2010; Carpentieri, Hayden, and Robins, 2012; Yee and Biltoft, 2004).

In the last decades, wind tunnel experiments on heavy gas dispersion in the atmospheric boundary layer have been undertaken. To simulate the buoyancy effect of a heavy gas emission in the wind tunnel, a mixture of air and a gas with higher molecular weight has to be used. Commonly employed are mixtures of air and carbon dioxide, CO_2 (Meroney, 1982; Schatzmann, Snyder, and Lawson, 1993; Snyder, 2001; Briggs et al., 2001; Hanna and Chang, 2001; Britter and Snyder, 1988). Larger density difference could be obtained with mixture of air and SF_6 (Schatzmann, Snyder, and Lawson, 1993; König-Langlo and Schatzmann, 1991) or Freon (F. T. Bodurtha, 1961; Hoot, Meroney, and Peterka, 1973; Ayrault, Balint, and Morel, 1991), but their use has nowadays been restricted due to safety and pollution limitations.

Previous studies focused on the experimental characterisation of the mean concentration field of a heavy gas release emitted from elevated and grounded sources (Meroney and Lohmeyer, 1984; Heidorn et al., 1992; Britter, 1989; Schatzmann, Snyder, and Lawson, 1993; Donat and Schatzmann, 1999). Later studies focused on the effects of obstacles (König-Langlo and Schatzmann, 1991; Roberts and Hall, 1994; Snyder, 2001; Hanna and Steinberg, 2001; Briggs et al., 2001; Zhu, Arya, and Snyder, 1998) and stable/neutral atmospheric conditions (Robins et al., 2001a; Robins et al., 2001b). To our knowledge only few study delivered some insight on higher order moments of gas concentration statistics. Britter and Snyder (1988) used CO_2 to reproduce a steady dense gas emission over a ramp and measured with a Flame Ionisation Detector (FID) the concentration field quantifying mean concentration and its standard deviation within the plume. Meroney and Lohmeyer (1984) examined the behaviour of suddenly released volumes of dense gas in a turbulent boundary layer. They obtained statistics on the mean concentration field and departure/arrival time by reproducing multiple times each cloud volume, while the analysis of the PDFs and standard deviations of each plume permited to gain knowledge on the concentration fluctuations. Ayrault, Simoëns, and Méjean (1998), investigated the dispersion of an unsteady ground release and provided the ensemble statistics of the first four moments of the concentration.

The review of the literature in this field clearly shows a lack of experimental data concerning the higher-order statistics of the concentration, as well as the turbulent mass fluxes. Our work aims at filling this gap, by analysing the velocity and concentration statistics of a heavy and a passive scalar release, emitted from an elevated source. To produce the heavy release, we employ a mixture of CO_2, air and ethane (C_2H_6), the latter used as a tracer for concentration measurements. We perform simultaneous measurements of concentration and velocity using a X-Probe Hot Wire Anemometry (HWA) and a Flame Ionization Detector (FID), respectively. This measurements techniques allow us to analyse higher-order statistics of plume concentration and velocity and to provide experimental evaluation of the turbulent mass fluxes.

In what follows, we introduce the experimental set-up and methods, the governing parameters of the dispersion process for a heavy gas emission, including the similarity condition between our experiment, the real case scenario and the Schatzmann, Snyder, and Lawson (1993) configuration (Section 3.3). In Section 3.4 we present the velocity field and its statistics and in Section 3.5 the mean concentration field and its higher-order moments analysis. The turbulent mass fluxes and the estimation of the turbulent dispersion coefficient are reported in Section 3.6. The analysis of the flux, production and dissipation terms of the mean turbulent kinetic energy and the transport equation of the concentration variance are reported in Section 3.7 and Section 3.8, respectively. Finally, in Section 3.9, we present the estimation of the mixing time scale with different methods, comparing the results with a theoretical model.

3.3 Experimental methods

3.3.1 Governing parameters and similarity conditions.

We study the atmospheric dispersion of a heavy gas and a passive scalar emission from an elevated source. The source has diameter d_s, height h_s and velocity emission w_s. The mass flow rate at the source is expressed as the product of the volumetric flow rate and the density at the source $Q_s\rho_s$. The turbulent boundary layer (BL), in which the emission take place, is characterised by a wind profile schematically reported in Figure 3.1 that has a free stream velocity U_∞, a friction velocity u_* and height δ.

The concentration field can be then generally expressed as a function of the governing parameters as:

$$c = f(w_s, \rho_a, \rho_s, h_s, d_s, \delta, U_\infty, u_*, \nu_a, \nu_s, D, g), \tag{3.1}$$

where D is the diffusivity of the gas mixture in air and ν_a and ν_s are the kinematic viscosity of air and the gas mixture, respectively.

Rewriting Eq. 3.1 in dimensionless form, we obtain:

$$\frac{c}{c_{scale}} = f\left(V_r, \frac{\rho_s}{\rho_a}, \frac{h_s}{\delta}, \frac{d_s}{\delta}, \frac{u_*}{U_\infty}, Re, Fr, Sc, Sc_s\right), \tag{3.2}$$

with $c_{scale} = Q_s\rho_s/(U_\infty\delta^2)$ the scale of the concentration variation, $V_r = w_s/U_\infty$ the ratio between the source and the boundary layer velocities, $Sc = \nu_a/D$ and $Sc_s = \nu_s/D$ the Schmidt numbers of the flow and at the source, respectively, Fr and Re the Froude number the Reynolds number, respectively. The Froude number is the ratio between inertial and buoyancy forces, while the Reynolds number is the ratio between inertial and viscosity forces. The definition of these numbers can be based on different scales, related to the boundary layer parameters or the source ones. In Table 3.1 are reported the possible formulations for the Fr and Re numbers, usually adopted in the literature.

Name	Symbol	Definition
Source Froude Number	Fr_s	$w_s / \sqrt{g d_s \frac{\rho_s - \rho_a}{\rho_s}}$
BL Froude Number	Fr_∞	$U_\infty / \sqrt{g d_s \frac{\rho_s - \rho_a}{\rho_s}}$
Source Reynolds Number	Re_s	$w_s d_s / \nu_s$
BL Reynolds Number	Re_∞	$U_\infty \delta / \nu_a$

Table 3.1: Formulation of the Froude and the Reynolds numbers at the source and in the turbulent boundary layer.

The dynamical similarity between the small scale experiments and the real scenario requires all non-dimensional parameter in Eq 3.2 to be constant. However, strictly speaking, these conditions cannot hold in wind tunnel experiments, notably for what concerns the source Reynolds number and the geometrical ratios (d_s/δ and h_s/δ).

Concerning the former, it is generally assumed that the dynamical similarity can be guaranteed even lowering Re_s by one or two orders of magnitude, provided that the flow in which the dispersion takes place is fully turbulent. For a buoyant release in a co-flow a criterion is provided by Arya and Lape (1990) who states that the Reynolds critical value above which the value of Re_s does not influence the plume dynamics is equal to 2000 for momentum dominated plumes and around 600 for buoyancy dominated plume.

Concerning the geometrical parameters, the condition that is generally imposed is that of a clear gap between the typical scale of the source diameter and the boundary layer height (Nironi et al, 2015; Marro et al, 2013). In this way the initial size of the plume will be smaller than the scale of the larger eddies of the boundary layer flow, therefore simulating the typical meandering motion characterising the early stages of the dispersion of a pollutant plume in the lower atmosphere.

In the settings of the parameters particular care has to be taken in the definition of the Fr_s, because its similarity is necessary to maintain the correct balance between buoyancy forces and the inertial effects induced by the atmospheric flows.

3.3.2 Experimental set-up

The atmospheric wind tunnel of the Laboratoire de Mécanique des Fluides et d'Acoustique (LMFA) of the École Centrale de Lyon (France) is a recirculating wind tunnel with a working section of $14m$ long, $3.7m$ wide and has an adjustable ceiling ($2 - 2.5m$) to control longitudinal pressure gradients (Fig. 3.1). The facility is regulated in temperature, to contain the temperature variation during a one-day experiment in the range $\pm\, 0.5$°C.

We generated a neutral turbulent boundary layer by means of floor roughness combined with a grid and a row of spires placed at the entrance of the test section. (Fig. 3.1). The roughness elements on the floor are equally spaced cubes of height $h_r = 0.02m$, that simulate a rural environment roughness. The grid at the entrance is

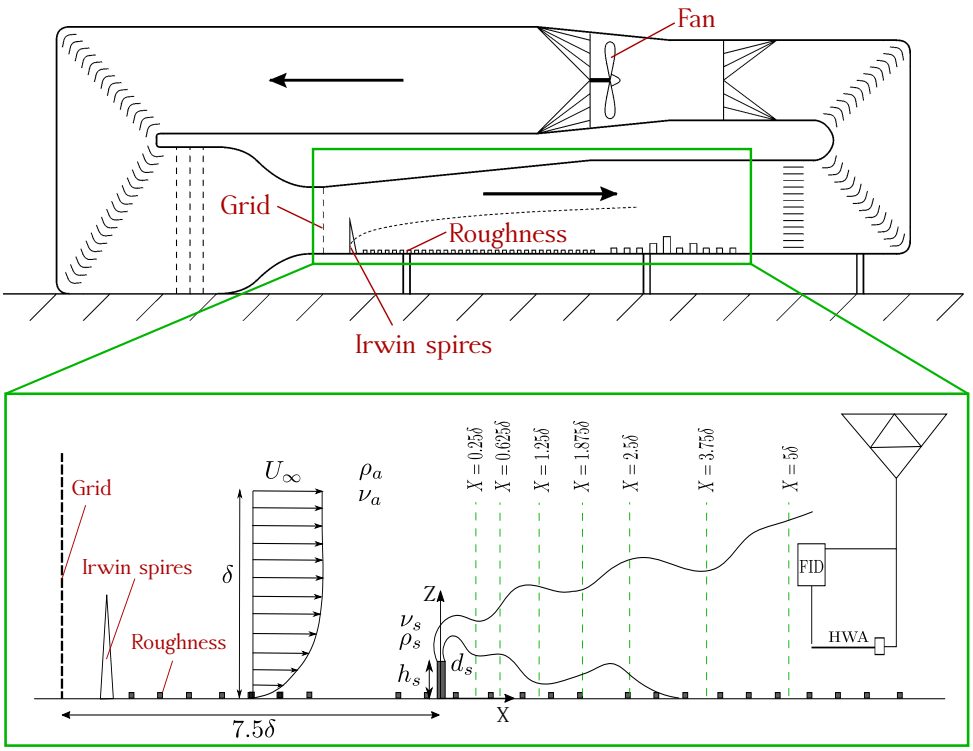

Figure 3.1: The LMFA atmospheric wind tunnel with a scheme (not in scale) of the experimental setup of the source, the coupled measurements system, the test sections and the governing parameters.

used to stabilise the flow and to reduce inhomogeneities in the transverse direction. The Irwin spires (Irwin, 1981) are $H = 0.5$ m high and spaced by $H/2$. A fully turbulent flow is created imposing a free stream velocity $U_\infty = 1.45$ m/s, the resultant boundary layer height is $\delta = 0.8m$ and the corresponding Reynolds number $Re_\infty = U_\infty \delta / \nu_a \approx 7.63 \cdot 10^4$ (Tab. 3.1). As observed in Nironi et al. (2015), the wind tunnel flow drifts in the transverse direction of less than 2%. In order to focus on the turbulent dispersion dynamics we decide to centre the profiles in the transverse direction that will be presented in the sections 3.5.1, 3.5.2 and 3.6.

The experiment set-up of the source and the emission conditions are fixed to reproduce a real case scenario of heavy gas release from a chimney into the atmospheric boundary layer. A similar configuration has been studied by Schatzmann, Snyder, and Lawson (1993) and we focus on the configuration named "3T" for the setting of the experimental parameters. The source size and the emission velocity are set to minimise Fr_s and maximise the buoyancy at the source, amplifying the effects of density diferences. For this reason, we decided to double the diameter of the source and to reduce by almost a half the emission velocity of the source compared to the Schatzmann, Snyder, and Lawson (1993) case. The parameters of the experimental set-up and the corresponding ones of Schatzmann, Snyder, and Lawson (1993) are reported in Table 3.2.

The considered configuration is a scale model for the real case scenario of the emission of oxygen O_2 at $T = -40$°C, corresponding to a density difference of

Name	Symbol	Experiments		Schatzmann	
		Value	Units	Value	Units
Boundary Layer Height	δ	0.8	m	1	m
Boundary Layer Velocity	U_∞	1.45	m/s	1.32	m/s
Source velocity	w_s	2.37	m/s	4.58	m/s
Source height	h_s	76	mm	76.2	mm
Source diameter	d_s	12	mm	6.35	mm
Velocity Ratio	Vr	1.63	[-]	3.47	[-]
Density ratio	ρ_s/ρ_a	1.5	[-]	1.56	[-]
Source Froude number	Fr_s	16.15	[-]	30.6	[-]
BL Froude number	Fr_∞	12	[-]	7.06	[-]
Source Reynolds number	Re_s	$3.4 \cdot 10^3$	[-]	$3.6 \cdot 10^3$	[-]
BL Reynolds number	Re_∞	$7.63 \cdot 10^4$	[-]	$8.69 \cdot 10^4$	[-]
BL velocity ratio	u_*/U_∞	0.04	[-]	n.a.	[-]
Source Schmidt number	Sc_s	0.50	[-]	n.a.	[-]
Flow Schmidt number	Sc	0.95	[-]	n.a.	[-]

Table 3.2: Governing parameters: experiments set-up vs. Schatzmann, Snyder, and Lawson (1993).

$\rho_s/\rho_a = 1.5$. The geometric scaling between the wind tunnel condition and the real case scenario is set on a ratio of $1:100$, imposing the similarity on the Fr_s, the resulting velocity scales are on a ratio $1:10$. In order to obtain the density difference corresponding to a real case of O_2 emission, we chose carbon dioxide as a buoyant agent in a mixture with air and ethane (as a tracer for concentration measurements). The density difference of the mixture is $\Delta\rho/\rho_a = (\rho_s - \rho_a)/\rho_a \approx 48.8\%$ (the gas density are reported in Table 3.3). We fix the ratio $r = C_{CO_2}/C_{C_2H_6}$ between carbon dioxide and ethane at the source and we assume that it is constant within the plume.

Name	Symbol	Value	Units
Density (at 20°C)	ρ_a	1.2007	kg/m^3
	ρ_{CO_2}	1.8332	kg/m^3
	$\rho_{C_2H_6}$	1.2560	kg/m^3

Table 3.3: Gas density at 20°C.

The source is made of a metallic pipe of internal diameter $d_s = 0.012$ m and height $h_s = 0.075$ m from ground level and the gas mixture is emitted with a vertical velocity of $w_s = 2.37$ m/s, corresponding to $V_r = w_s/U_\infty = 1.63$. The Froude Number at the source is then $Fr_s \approx 16$ while the Reynolds number at the source is $Re_s = 3.4 \cdot 10^3$, and the Froude number referred to the BL is $Fr_\infty \approx 12$ (Tab. 3.1). The source is placed at 7.5δ from the beginning of the working section, where the boundary layer can be considered fully developed (Fig. 3.1), i.e the velocity statistics are dependent on z only (except within the roughness sub-layer). The origin of the coordinate system is the source, with x, y and z as longitudinal, transverse and vertical axes,

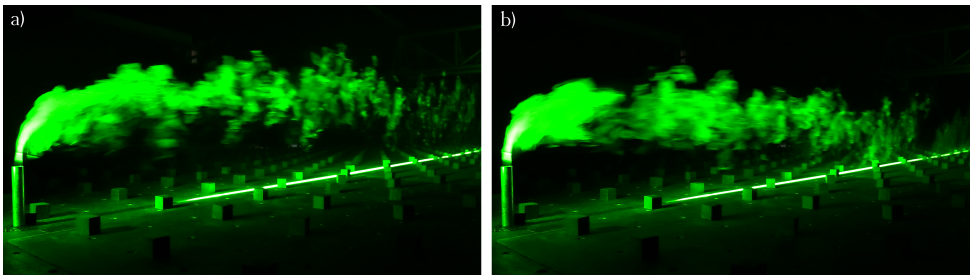

Figure 3.2: Laser tomographic visualisation of a) the passive scalar and b) the heavy gas plume, under the same experimental emission and flow conditions.

respectively. We define the measurement section for both vertical and transverse profile at increasing distance from the source, as schematically reported in Figure 3.1.

The passive scalar emission take place in the same BL under the same dynamic conditions (same Vr, Re and u_*/U_∞) with no density difference at the source, realising a mixture of air and ethane.

3.3.3 Measurement techniques

Laser tomographic visualisations have been performed at the beginning of the experimental campaign to verify the trajectories of the heavy gas and passive scalar plumes. As can be observed in Figure 3.2, the trajectories had different elevations and in case of the heavy gas emission the plume touched the ground closer to the source.

Concentration measurements are performed with a Flame Ionization Detector (FID), with a sampling tube 0.3 m long, permitting a frequency response of 400 Hz. In case of heavy gas experiments, the instruments response is influenced by the presence of CO_2 and a specific calibration procedure is established and repeated twice a day. Velocity measurements are performed with a X-Probe hot wire anemometry with constant temperature that provides simultaneous measurements of two velocity components. In our set-up, the HWA has a frequency response of about 5 kHz. The response of the HWA is corrected taking into account the local CO_2 concentration in the calibration procedure. Since the experiments on gas dispersion are performed in a recirculating wind tunnel, the increase of background concentration over time is also taken into account. Details on the procedure of the signal noise treatment is reported in Appendix A. We combined FID and HWA in a coupled measurement system (Fig. 3.3) and we perform simultaneous measurements of concentration and velocity. The combined HWA-FID system is therefore able to provide a signal for the joint statistics of concentration and velocity of 400 Hz, the one imposed by the frequency response of the FID. The main hurdle using this system is that the instruments responses vary with the ratio r between carbon dioxide and ethane and it has to be taken into account in the calibration procedure. During the experiments the sampling frequency is set at 1000 Hz and the sampling time at 300 s.

The detailed description of calibration procedure, the instrument and the coupled system configurations, along with the gas lines scheme is reported in Chapter 2.

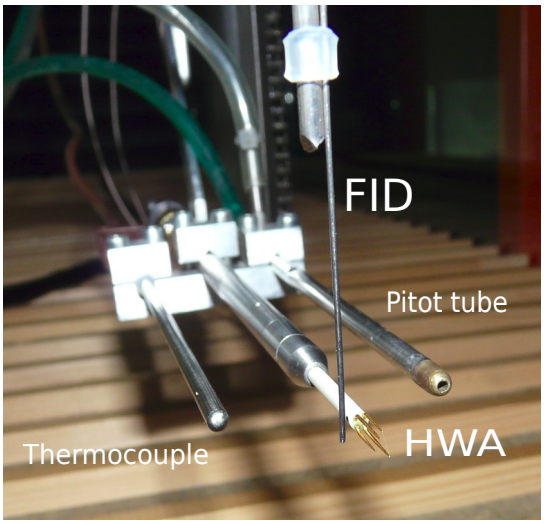

Figure 3.3: FID-HWA coupled measurement system, with the Pitot tube and the thermocouple monitoring during the experiment the flow velocity and the temperature.

3.4 Velocity field

In this section we present the vertical profiles of one point velocity statistics. The results are compared with those by Nironi et al. (2015), obtained with the same experimental set-up, but with higher stream velocity (5 m/s instead of 1,44 m/s). The BL develops over a rough surface with a light adverse longitudinal pressure gradient $\approx -0.095 Pa/m$, estimated by Nironi et al. (2015) by measuring the free stream velocity U_∞ for varying distance from the entrance of the test section. According to the principles of the similarity theory, we expect the profiles of the velocity statistics to collapse when rescaled with appropriate velocity and length scales. It is possible to select sensible scaling parameters to analyse non-dimensional data describing the boundary layer. The boundary layer is defined by an outer and a inner region, the latter including the inertial region and the underlying roughness sublayer (Raupach, Thom, and Edwards, 1980), extending for a few roughness heights away from the wall. A good fit of the mean velocity profile $\overline{u}(z)$ in the whole turbulent boundary layer is provided by the power law:

$$\frac{\overline{u}(z)}{U_\infty} = \left(\frac{z}{\delta}\right)^n, \tag{3.3}$$

with $n = 0.23$. Figure 3.4.a shows a good agreement with the results of the mean horizontal velocity profiles with Nironi et al. (2015) and the power law of Eq. 3.3. The set-up of U_∞ to a lower value compared to Nironi et al. (2015), induces a higher variability on the velocities profiles, especially for higher order moments and close to the wall. We can assume that this variability depends on the uncertainty of the measurement at low velocity. For this reason, in order to compare our set of data with the one of Nironi et al. (2015), we spatially average our results by means of binning technique for the velocity statistics with 13 equally spaced bins along the vertical direction. The binned data are represented in Figure 3.4.a-b-c, the error bars

corresponding to the standard deviation of the considered quantity in the bin. We observe in Figure 3.4.a a slight divergence near the wall where the turbulent intensity $\sigma_u/\overline{u}$ exceed 0.3 and an error is induced by the assumption of Taylor's hypothesis. We observe a good agreement for the standard deviation profiles in Figure 3.4.b, with higher variability for σ_v. The vertical profile of the Reynolds stress overlaps well to Nironi's data, as shown in Figure 3.4.c. We can notice a slight divergence in the higher part of the boundary layer and higher dispersion near the ground.

Since our set of data shows a good agreement with the Nironi's one, as highlighted by the overlapping of the vertical profiles of first and second order statistics, we can conclude that the dynamics of the BL is essentially the same. This implies, therefore, also the equivalence of the ratio $u_*/U_\infty = 0.04$ (where the friction velocity $u_* = 0.058m/s$ is estimated from the Reynolds stress profile) and of the typical boundary layer parameters, as estimated by fitting the mean longitudinal profiles with a logarithmic law:

$$\frac{\overline{u}(z)}{u_*} = \frac{1}{k} ln\left(\frac{z-d}{z_0}\right), \tag{3.4}$$

where $k = 0.4$ is the Von Karman constant, $z_0 = 1.13 \cdot 10^{-4}$ m is the surface roughness and $d = 0.013$ m is the displacement height (Nironi et al., 2015).

As already stated by Nironi et al. (2015) this velocity field is characterized by an equilibrium between the production and dissipation of the turbulent kinetic energy (TKE). The former term, defined as $P_K = \overline{\rho u_i' u_j'} \frac{\partial \overline{u_i}}{\partial x_j}$, can be conveniently approximated as $P_K \approx \overline{\rho u' w'} \frac{\partial \overline{u}}{\partial z}$. To estimate the dissipation rate we assume the Taylor's hypothesis of frozen turbulent and the local isotropy of the velocity field. We convert spatial gradients to temporal derivatives and we compute TKE dissipation rate according to Hinze (1975):

$$\varepsilon_{iso} = \frac{15\nu}{\overline{u}^2} \overline{\left(\frac{\partial u'}{\partial t}\right)^2}. \tag{3.5}$$

The obtained values of P_K and ε are reported in Figure 3.4.d. We observe a general good agreement between the production (pink rounds) and dissipation profiles (light blue squares), thus we can assume a local equilibrium between TKE production and dissipation.

3.5 Concentration fields

In analysing profiles of the concentration statistics, we will systematically compare the case of the heavy release with that of the passive scalar one. In presenting the data, the concentration will be normalised as:

$$c^* = \frac{c}{c_{scale}} = c\frac{U_\infty \delta^2}{Q_s \rho_s}. \tag{3.6}$$

All other quantities, denoted with the symbol "*", are normalised using U_∞ and δ as velocity and the length scale, respectively. We first analyse the mean concentration

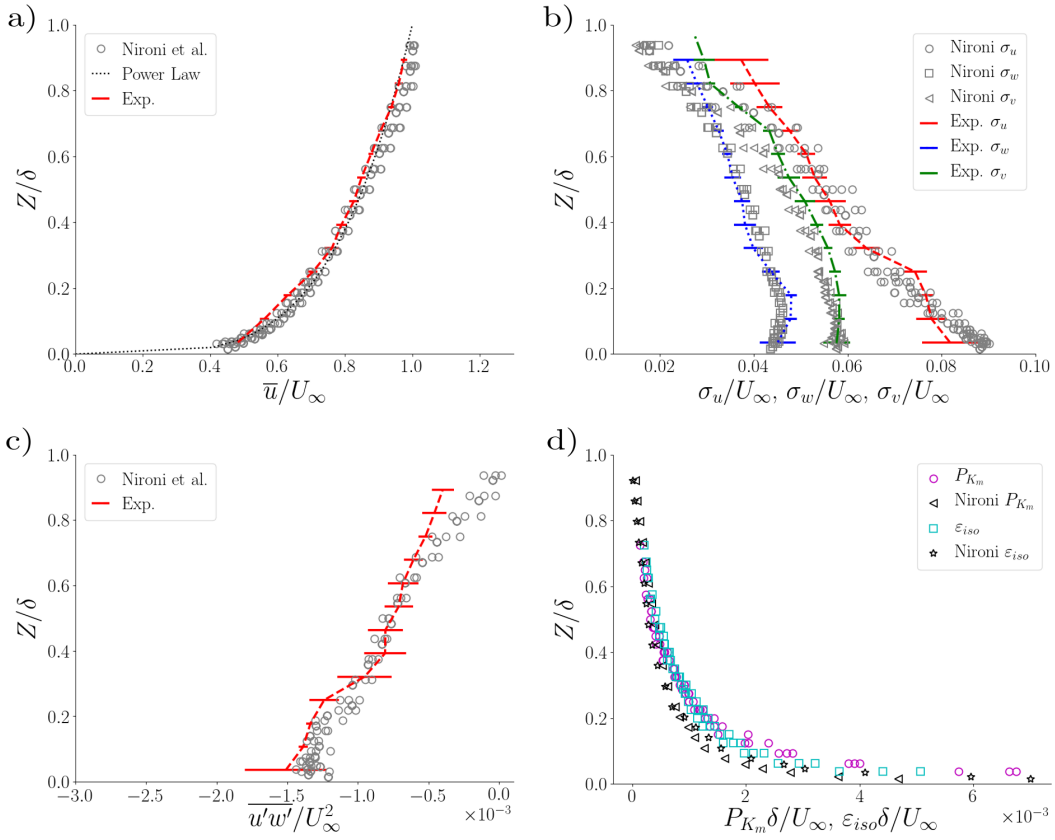

Figure 3.4: Vertical profiles (dimensionless) of a) mean velocity vertical profiles, b) standard deviation of horizontal, vertical and transverse velocity, c) Reynolds stress, d) TKE production P_k and dissipation ε, compared to benchmark Nironi.

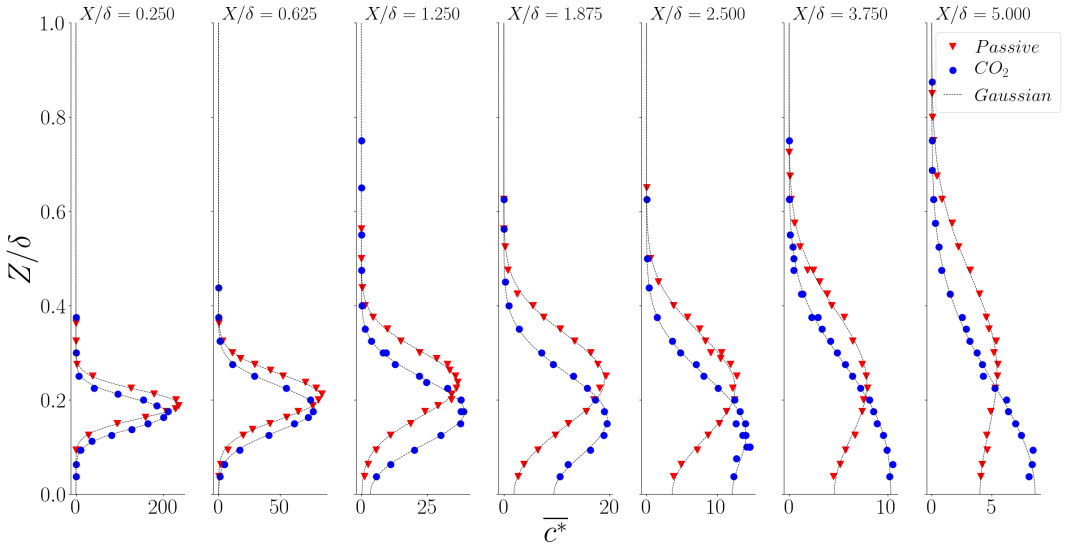

Figure 3.5: Vertical profiles of the normalised mean concentration for sections at increasing distance from the source for passive and heavy gas plume.

profiles $\overline{c^*}$ for both the vertical and transverse section, and we present the parameters that characterise the "mean" plume, such as the height of the centre of mass (Z^*_{MC}) and the vertical and transverse standard deviation (σ^*_z and σ^*_y).

The analysis of the concentration standard deviation σ^*_c provide an estimate the intensity of fluctuation i_c, the latter defined as the ratio between σ^*_c and $\overline{c^*}$. The information on the i_c and the study of the PDF concentration allow us to identify a good fit with the Gamma distribution. The higher order moments of concentration are computed as:

$$m^*_{nc} = \left[\frac{1}{N} \sum_{i=1}^{N} (c^*_i - \overline{c^*})^n \right]^{1/n}, \tag{3.7}$$

with $n = 2, 3, 4$ and N is the total number of sample in the measurement.

3.5.1 Mean concentration field

Figure 3.5 shows the dimensionless concentration profiles for sections at increasing distances from the source. Each point corresponds to the time average concentration $\overline{c^*} = \frac{1}{N} \sum_{i=1}^{N} c^*_i$. We observe that the mean concentration decreases downstream from the source. Furthermore, the heavy gas plume is deflected toward the ground, due to its negative buoyancy. At the furthest profile close to the ground, $\overline{c^*}$ is consistently higher for the heavy gas emission.

Figure 3.6 shows the transverse mean concentration profiles. These have been obtained at the height at which the vertical profiles showed a maximum value of concentration. For this reason, passive and heavy transverse sections are measured at different heights. The concentration of both heavy and passive plume decrease within the distance from the source. As for the vertical profiles, the maxima of concentration in the first two sections are higher for the passive scalar release.

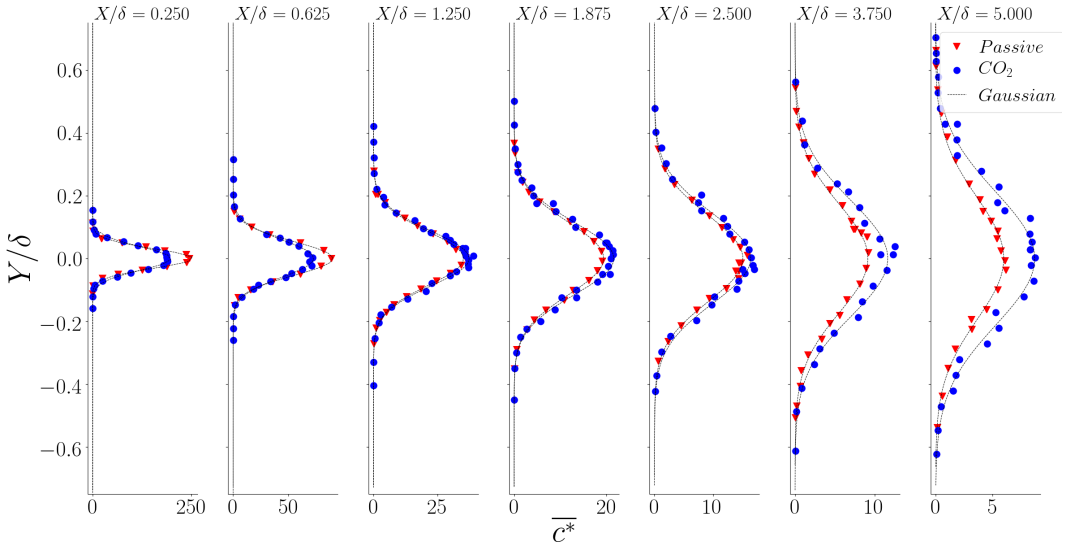

Figure 3.6: Transverse profiles of the normalised mean concentration for sections at increasing distance from the source for passive and heavy gas plume.

As customary, the vertical and transverse mean concentration profiles can be suitably remodelled by mean of a Gaussian model, taking into account an extra term to reproduce the effect of the reflection of the ground (Hay and Pasquill, 1959):

$$\overline{c}(x,z) = \frac{Q_s \rho_s}{2\pi\sigma_y\sigma_z\overline{u}_{MC}} exp\left(-\frac{y^2}{2\sigma_y^2}\right)\left[exp\left(-\frac{(z-h_{eff})^2}{2\sigma_z^2}\right) + exp\left(-\frac{(z+h_{eff})^2}{2\sigma_z^2}\right)\right], \tag{3.8}$$

where $\overline{u}_{MC}$ is the mean longitudinal velocity at the centre of mass of the plume and $h_{eff} = h_s + \Delta h$ is the effective height of the plume estimated at each section that take into account the plume rise Δh.

We fit the mean concentration profiles with the Eq. 3.8 imposing $y = 0$ for the vertical profiles and $z = h_0$ for the horizontal ones, using σ_z and σ_y as free parameters (Fig. 3.5 and 3.6). Figure 3.7.a-b show the values of σ_z and σ_y obtained from the fit adjustment. It can be noticed that there are no significant difference between the passive scalar and the heavy gas plumes in terms of vertical and transverse spread.

From the interpolation of the vertical profiles (Eq. 3.8) we estimate the height of the dimensionless centre of mass Z^*_{MC} as reported in Eq. 3.9.

$$Z^*_{MC} = \frac{1}{\delta}\left(\frac{\int_0^\infty (c(z)\cdot z)dz}{\int_0^\infty c(z)dz}\right). \tag{3.9}$$

The results show that the effect of buoyancy is to limit the height of the heavy gas plume (Fig. 3.7.c). It can be noticed that in the near field both plumes rise and reach a maximum and then start decrease. The maximum for the heavy gas is lower and it is reached closer to the source. In the far field, when the plume touches the ground, the height of the centre of mass tends to rise again, due to the vertical spread influenced by the reflection on the ground.

In Figure 3.7.a-b we also plot the values of σ_z and σ_y evaluated according the Taylor's formulation (Taylor, 1922):

$$\sigma_z^2 = \frac{d_s^2}{6} + 2\sigma_w^2 T_{Lw} \left\{ t - T_{Lw} \left[1 - exp\left(-\frac{t}{T_{Lw}} \right) \right] \right\}, \tag{3.10}$$

$$\sigma_y^2 = \frac{d_s^2}{6} + 2\sigma_v^2 T_{Lv} \left\{ t - T_{Lv} \left[1 - exp\left(-\frac{t}{T_{Lv}} \right) \right] \right\}, \tag{3.11}$$

where t is the flight time, T_{Lw} and T_{Lv} are the Lagrangian time scales in the lateral and vertical direction, respectively. The Lagrangian times are estimated as (Tennekes and Lumley, 1972):

$$T_{Lw} = \frac{2\sigma_w^2}{C_0 \varepsilon}, \tag{3.12}$$

$$T_{Lv} = \frac{2\sigma_v^2}{C_0 \varepsilon}, \tag{3.13}$$

where $C_0 = 4.5$ is the Kolmogorov constant (as estimated by Nironi et al., 2015), comparing the Lagrangian length scales and the dissipation profiles. To take into account the effect of the not homogeneity of the velocity field, the parameters σ_v, σ_w, T_{Lw} and T_{Lv} are evaluated at the height of the centre of mass of the plume (which varies as the plume travels downstream). The flight time t is expressed as a function of the mean longitudinal velocity at Z_{MC} as $t = x/\overline{u}_{MC}$. We derive along x Eq. 3.10 and Eq. 3.11 and we estimate the theoretical values of σ_z^2 and σ_y^2 with the following formulation:

$$\sigma_{i,n}^2 = \sigma_{i,n-1}^2 + 2\sigma_{j,n}^2 T_{Lj} \left(1 - exp\left(-\frac{t}{T_{Lj}} \right) \right) \frac{x_n - x_{n-1}}{\overline{u}_{MC}}, \tag{3.14}$$

where i refers to y or z, j refers to v and w,respectively, and n in the measurement section number.

In Figure 3.7.a we observe a general good agreement between σ_z, obtained from the interpolation of the experimental data with a Gaussian model and Eq. 3.10, even though the Taylor formulation tend to slightly overestimate the vertical spread. The results of Eq. 3.11 are considerably higher than the transverse spread computed from the Gaussian model, especially in the heavy gas case. In interpreting this differences, it is worth remembering that this model have been developed for the case of dispersion in homogeneous turbulence. In this case, the Eq. 3.10 and 3.11 are adapted to the case of not homogeneous turbulence, considering that the model parameters vary actually in the domain. Our results are in agreement with the results of Nironi et al. (2015), that observed a model overestimation of the transverse spread values compared to the one obtained with the interpolation of the Gaussian model.

The vertical profiles of the relative density difference of the plume to the air reported in Figure 3.7.d show the rapid decrease of $\Delta\rho/\rho_a$. With a density difference at the source around 48.8%, the maximum of $\Delta\rho/\rho_a$ in the first measurement section

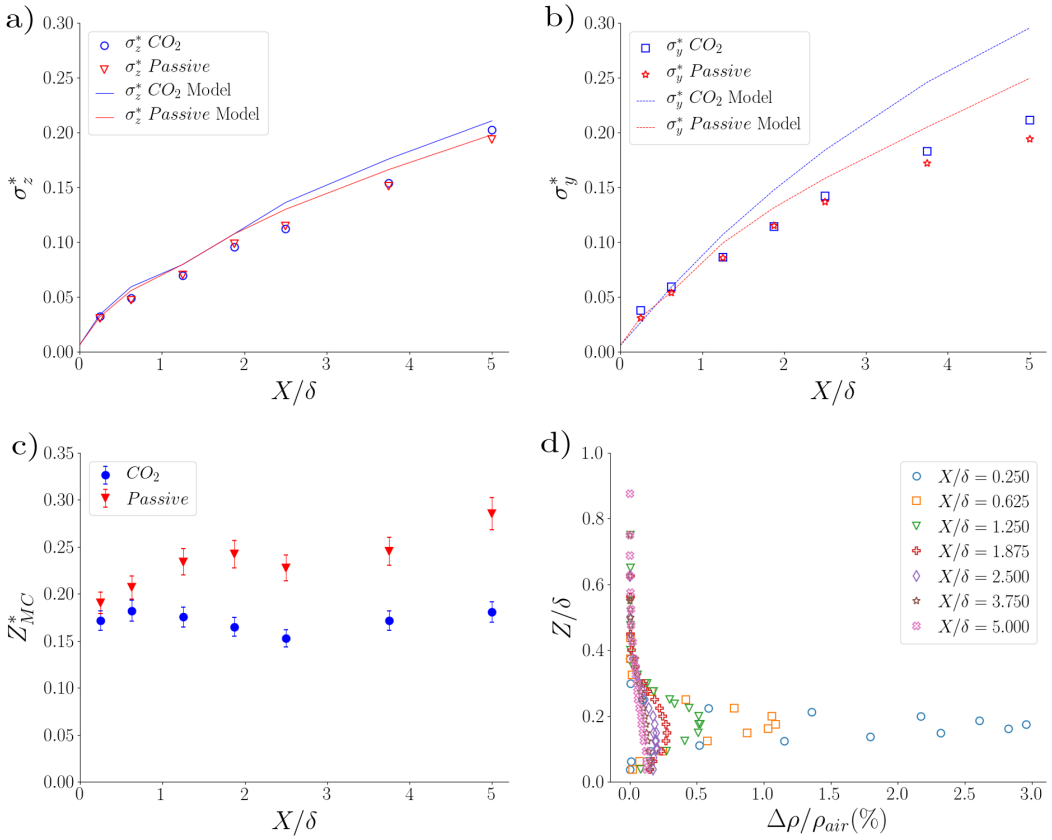

Figure 3.7: Longitudinal profiles of a) vertical and b) transverse standard deviation compared with theoretical laws, c) centre of mass height Z_{MC}^* for both heavy and passive scalar and d) relative density difference of the plume to the air.

is around 3%, and in the second decrease to almost 1%. In the far field, the buoyancy effect are clearly negligible.

From these results, we can assume that the momentum injected at the source leads to a jet effect that dominates the dispersion dynamics of the plume in the near field. In the region between the source and the first measurement section, the plume develops vertically and, in case of heavy gas emission, the negative buoyancy due to density difference limits the height at which the plume develops. This effect leads to differences that can be observed in the longitudinal distribution of the height of the centre of mass of the plume (Fig. 3.7.c) and the concentration field (Fig 3.5). The measurement profiles of the first two sections show higher values of $\overline{c^*}$ and σ_c^* for the passive scalar compared to the heavy gas. The effectiveness of the dispersion is confirmed by the same vertical and transverse spread of the passive scalar and heavy gas plumes and the rapid decrease of the density difference at increasing distance from the source. The saturation threshold of the FID at high CO_2 and C_2H_6 concentration (see Chapter 2) does not allow us to further investigate the region between the source and the first section.

The vertical spread, the centre of mass and the integral time scale are key parameters for the characterisation of the plume with integral models. Understanding the differences between the heavy gas and the passive release allows us to adapt and validate models that correctly simulate the plume dispersion in case of density differences, as will be discussed in Chapter 4.

3.5.2 Higher order moments

We analyse the standard deviation σ_c^* for vertical and transverse profiles, as shown respectively in Figure 3.8 and Figure 3.9. As for the mean concentration field, the vertical profiles (Fig. 3.8) of σ_c^* follow the trajectory of the plumes, with the heavy gas plume deflected through the ground. Furthermore, σ_c^* in the plume centre is lower for the heavy gas, especially in the near field, where the plume dispersion dynamics are more affected by the jet of the source and the buoyancy effect, due to the density difference, and where the concentration fluctuations are less intense. The transverse profiles (Fig. 3.9) show a similar distribution, with marked differences only in the first two sections, similarly to the vertical profiles, probably due to the effect of the source emission.

By comparing Figure 3.5 and Figure 3.8, it can be noticed that, at the border of the plume, $\sigma_c^* > \overline{c^*}$, whilst we have that $\sigma_c^* < \overline{c^*}$ in the core. The external part of the plume is characterised by entrainment of air into the plume and the signal is intermittent. At the centre, the fluxes are reduced and the value of σ_c^* has almost the same order of magnitude of $\overline{c^*}$. This behaviour is pronounced in the middle field. Conversely, in the far field the plume touches the ground and σ_c^* is consistently lower than the mean concentration.

Figure 3.10.a shows the longitudinal evolution of i_c at the maximum of the mean concentration field for both heavy and passive scalar emissions. In both cases i_c raises,

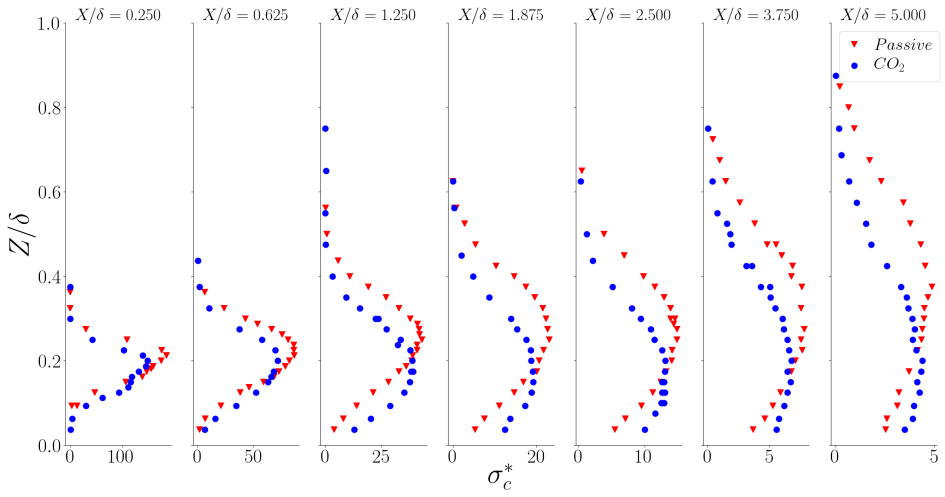

Figure 3.8: Vertical profiles of the normalised standard deviation for sections at increasing distance from the source for passive and heavy gas plume.

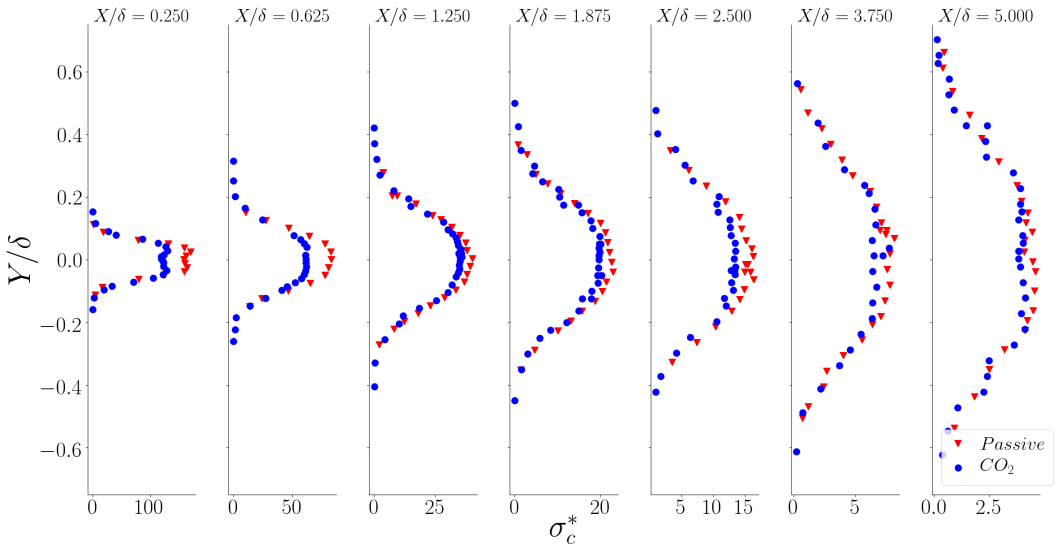

Figure 3.9: Transverse profiles of the normalised standard deviation for sections at increasing distance from the source for passive and heavy gas plume.

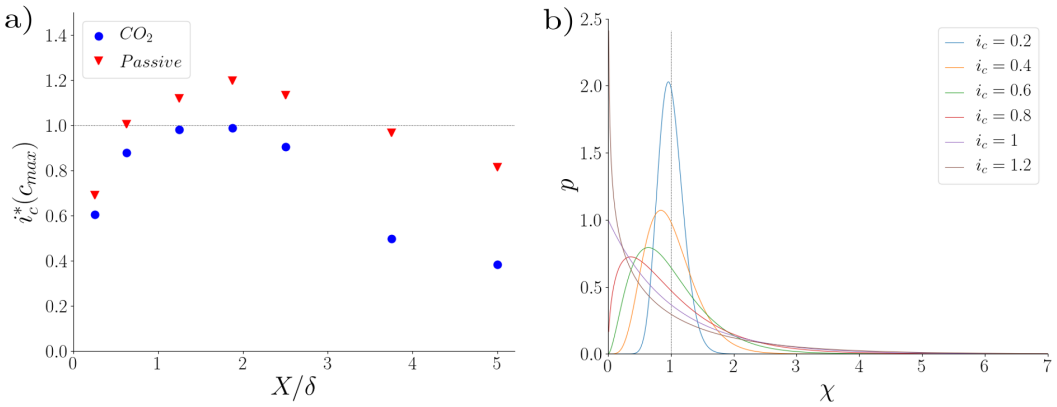

Figure 3.10: a) Longitudinal profiles of the concentration intensity fluctuation i_c for both heavy gas and passive scalar estimated at the maximum of the mean concentration. b) Example of the PDF Gamma distribution evolution for different values of i_c

reaches a peak and decreases, and the heavy gas plume is characterised by lower fluctuation intensity in the far field. The presence of CO_2 reduces the intensity of the fluctuations. Compared to the passive scalar, the density difference affects the concentration field increasing its mean values and reducing the standard deviation.

The interesting aspect of this parameter is related to the intermittency of the plume and the time distribution of concentrations. Previous studies (Villermaux and Duplat, 2003; Duplat and Villermaux, 2008; Yee and Skvortsov, 2011; Nironi et al., 2015) showed that the PDF of the concentration can be well modelled by a Gamma distribution of the form:

$$p(\chi) = \frac{k^k}{\Gamma(k)} \chi^{k-1} exp\left(-k\chi\right), \tag{3.15}$$

where $\Gamma(k)$ the Gamma function, $k = i_c^{-2}$ and $\chi \equiv c/\bar{c}$. The convenience of the Gamma distribution is its dependence on the parameter k, and therefore, on the first two statistical moments of concentration.

As discussed by Nironi et al. (2015) there is a clear link between the value of k (and therefore i_c) and the form of the PDF. Notably, as shown in Figure 3.10.b, the PDF has an exponential-like shape for values of the parameter i_c higher than 1, while for i_c less than 1 it shifts into a log-nomal-like distribution with short tail and tend then towards a Gaussian-like distribution as i_c decreases further.

Analysing the intensity of concentration fluctuations in the centre of mass of the plume allows us to relate i_c with the dynamics that drives the mixing between the plume and the surrounding air. Values of $i_c > 1$ correspond to a signal with high intermittency, due to the meandering motion of the plume. For $i_c < 1$ the intermittency is instead suppressed together with the meandering motion of the plume. Values of $i_c \approx 1$ corresponds to the transition between the two dynamics.

We analyse the correspondence between i_c and the PDF of the concentration signal, compared to the Gamma distribution. In Figure 3.11 are reported five PDF,

corresponding to the maximum of the vertical mean concentration profiles and to a value of i_c, as indicated in Figure 3.11.a. We also show a $10s$ sample of the concentration signal to visualise the differences of the instantaneous concentration field associated to the PDF. When the meandering motion is intense, the intermittency of the signal is high, therefore $i_c > 1$ (Fig. 3.11.b) and the PDF follows an exponential-like distribution. As the plume grows and evolves, the meandering motion is gradually suppressed, the intermittency is reduced, i_c reaches the unit and the PDF is in transition between the exponential shape and the log-normal (Fig. 3.11.c). In the far field the relative dispersion becomes the only mechanism controlling turbulent transfer, i_c is below one and the intermittence of the signal is reduced (Fig. 3.11.d). These results confirm that the Gamma distribution is a robust model for the concentration PDFs (Fig.3.11.b,c,d,). The exceptions are in the far field (Fig.3.11.e), where i_c reached a value around 0.4 and the PDF concentration approaches the normal distribution, and in proximity of the source (Fig.3.11.f), where the concentration PDF is not modelled with a Gamma distribution, due to the influence of the source emission. These results show that the Gamma distribution can be used to model, with good accuracy in the middle and far field, the changing in shape of PDF with increasing distance from the source for both heavy and passive plume.

From the Gamma distribution we can estimate higher order statistics of the concentration field, knowing the mean and the standard deviation of the concentration, i.e. i_c. Therefore, we compared the 3rd and 4th order moments estimated from the measurements (Eq. 3.7) to the corresponding moments of the Gamma distribution (Fig. 3.12, 3.13). We evaluate the 3rd and 4th order PDF moments as:

$$m^*_{3c\Gamma} = \left(\frac{2}{\sqrt{k}}\right)^{1/3} \sigma^*_c, \tag{3.16}$$

$$m^*_{4c\Gamma} = \left(\frac{6}{k} + 3\right)^{1/4} \sigma^*_c. \tag{3.17}$$

In Figure 3.12 and Figure 3.13 are reported the 3rd and 4th order moments vertical and transverse profile, respectively, for both passive scalar and heavy gas, for a section in the near ($X = 0.625\delta$) and in the far field ($Z = 5\delta$). For the experimental results we observe that the presence of a heavy gas in the plume affects the high order moments which show a significant reduction compared to passive scalar, especially in the near field (Fig. 3.12.a,b and Figure 3.13.a,b). In the far field (Fig. 3.13.c,d and Figure 3.12.a,b), the values of m^*_{3c} and m^*_{4c} decrease of almost two orders of magnitude, highlighting the dilution of pollutant within the plume. As can be expected from the PDF analysis, there are remarkable differences near the source between the Gamma distribution and the experimental results. These discrepancies are due to the effect of the jet emitted by the source. The momentum emitted at the chimney influences both the velocity field and the concentration fluctuations. In this conditions we observe that the Gamma distribution is not suited to describe the PDF concentration. In the far

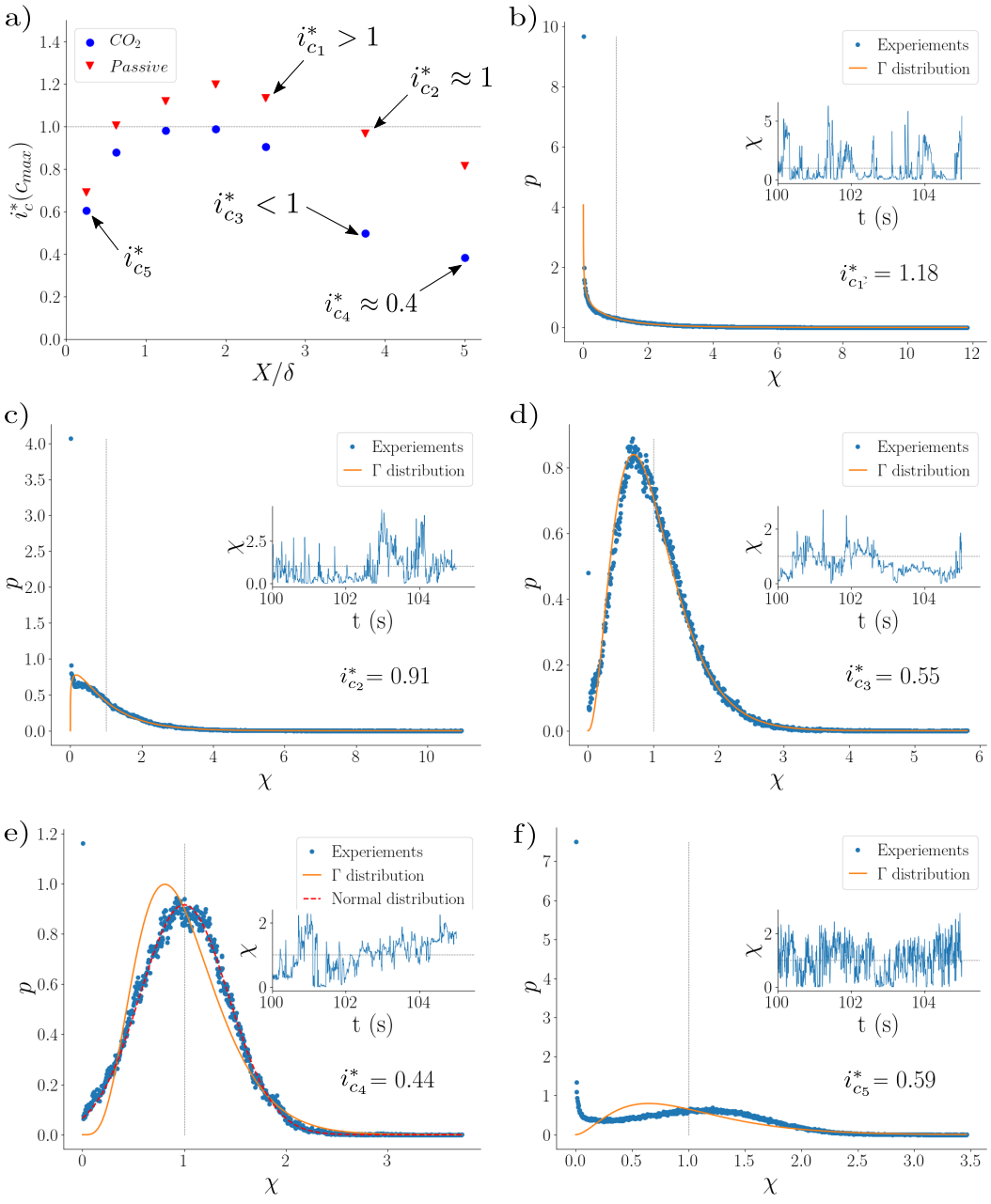

Figure 3.11: Analysis of the relation of concentration PDF and fluctuation intensity i_c. a) Longitudinal profile of the intensity of concentration fluctuation i_c for both heavy gas and passive scalar. Concentration PDF and signal sample for b) $i_{c_1} > 1$ in the middle field, c) $i_{c_1} \approx 1$, d) $i_{c_1} < 1$ and e) $i_{c_1} \approx 0.4$a in the far field, and f) $i_{c_1} < 1$ near the source.

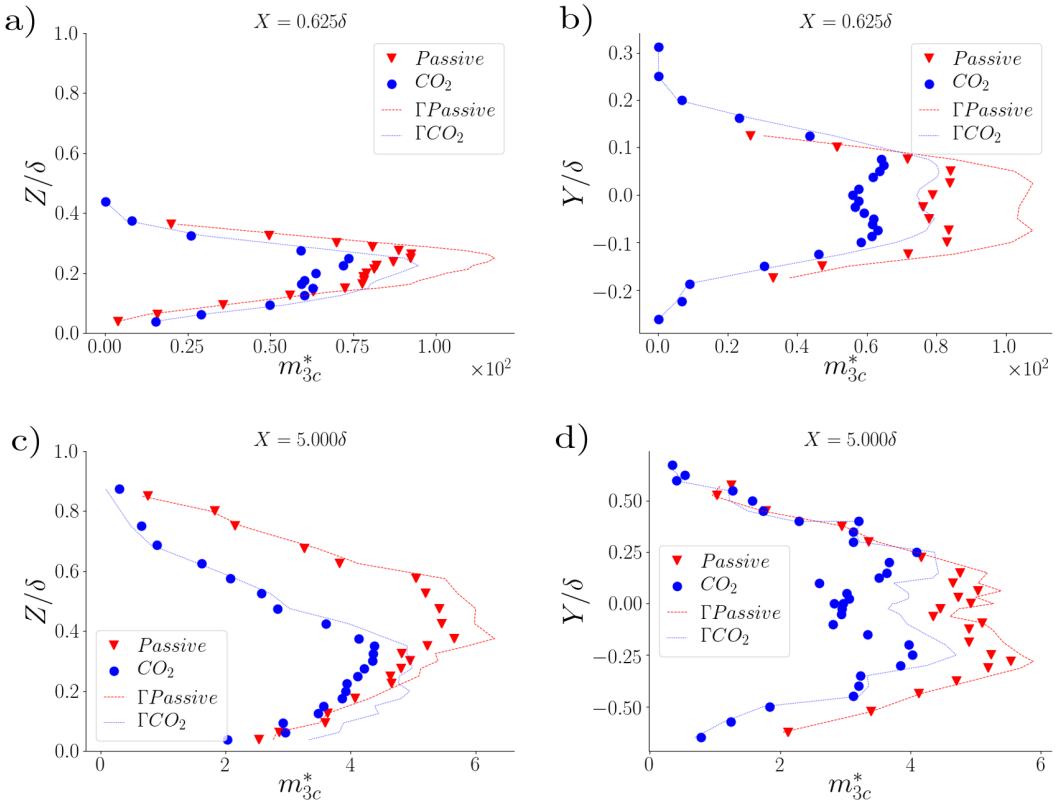

Figure 3.12: 3rd order moment a) vertical and b) transverse profiles near the source ($X = 0.625\delta$) and c) vertical and d) transverse profiles in the far field ($X = 5\delta$), for a passive scalar and a heavy gas, compared with the moments obtained from the Gamma distribution models.

field, concentration moments estimated by Eq. 3.16 and Eq. 3.17 slightly overestimate the concentration moments. Nevertheless, the spatial evolution of the values predicted by Eq. 3.16 and Eq. 3.17 show a good agreement with the experimental data. We can therefore conclude that, according to the present results, the Gamma distribution is a suitable model for the PDF also in case of a heavy release. This model is extremely useful, since it allows for the estimate of higher order statistic, based on the evaluation of the mean and the standard deviation, which can in turn be predicted by analytical (Bertagni et al., 2019) or Lagrangian (Marro et al., 2018) dispersion models.

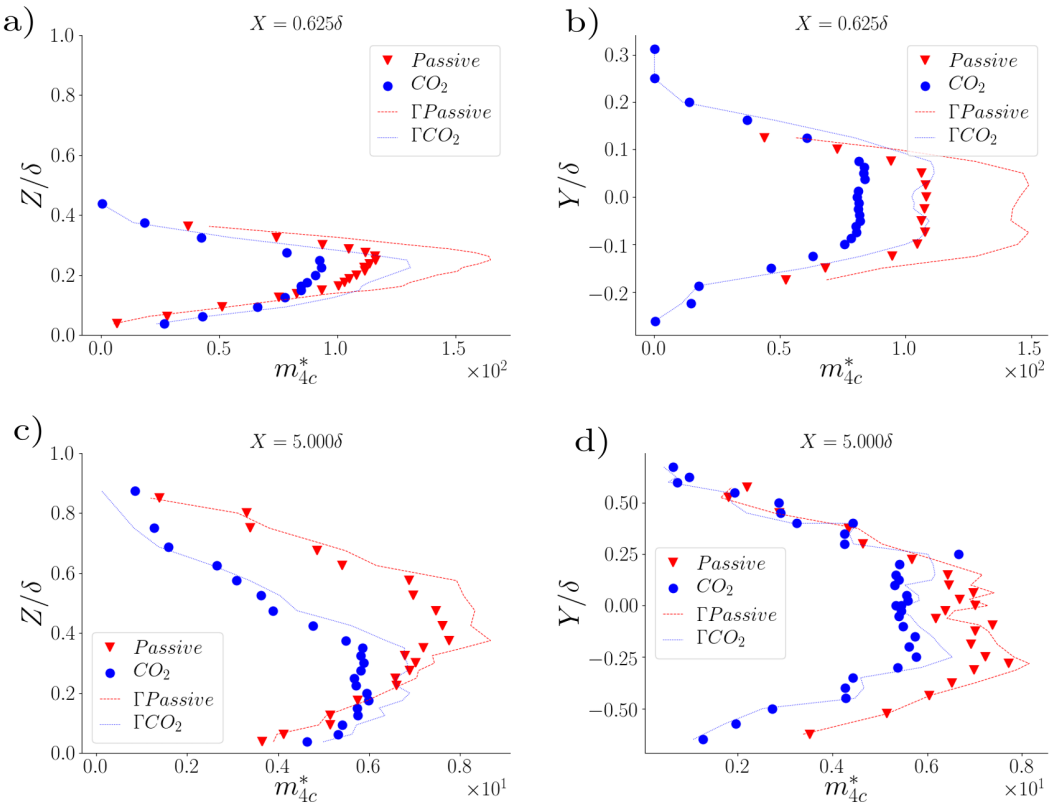

Figure 3.13: 4th order moment a) vertical and b) transverse profiles near the source ($X = 0.625\delta$) and c) vertical and d) transverse profiles in the far field ($X = 5\delta$), for a passive scalar and a heavy gas, compared with the moments obtained from the Gamma distribution models.

3.6 Mass fluxes

Simultaneous measurements of concentration and velocity allow us to compute profiles of turbulent mass fluxes at increasing distance from the source. In our analysis, we begin by focusing on the vertical fluxes $\overline{w'c'}^*$. These are presented in Figure 3.14, that shows the general decrease of $\overline{w'c'}^*$ as the plume travels downstream the source.

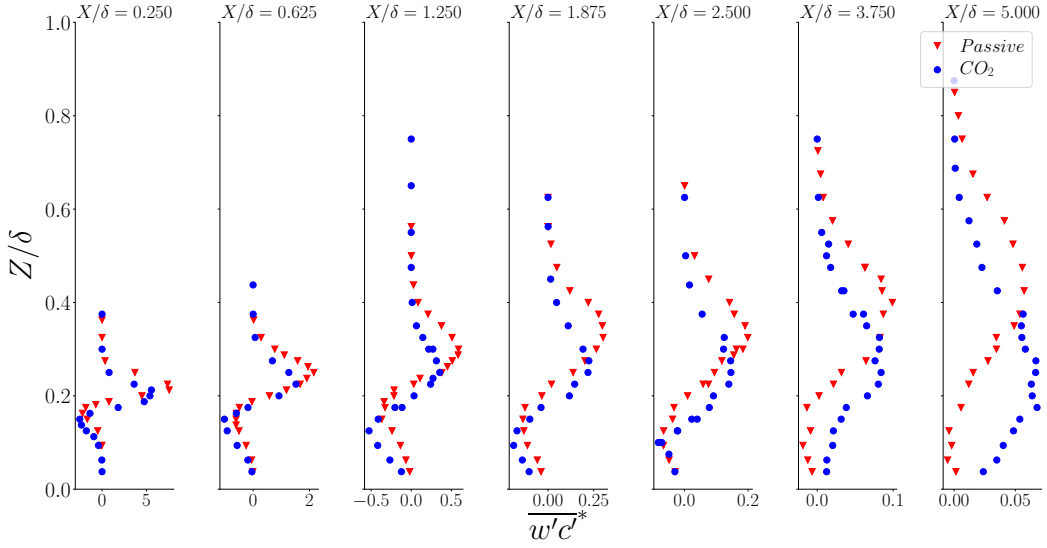

Figure 3.14: Vertical profiles of the normalised vertical turbulent mass flux for sections at increasing distance from the source for passive and heavy gas plume.

The heavy gas and passive scalar plumes vertical displacement is reflected in the distribution of $\overline{w'c'}^*$. In the near field, the dispersion dynamics is significantly influenced by the emission condition, which correspond to sharper profiles of the turbulent mass fluxes. Furthermore, vertical profiles of $\overline{w'c'}^*$ highlighted the role of buoyancy on the turbulent transfer, as the maximum near the source for the dense releases is slightly lower than that for the passive releases. However, this difference between the heavy gas and the passive scalar profiles is moderate, meaning that the negative buoyancy and the source conditions have more effect on the plume elevation and trajectory rather than on the turbulent fluxes.

Observing the mean concentration profiles in Figure 3.5, it can be noticed that $\overline{w'c'}^*$ has a counter gradient evolution. Combining this measurement with the evaluation of mean concentration vertical gradient and applying a standard gradient closure model:

$$\overline{w'c'*} = -D_t^* \frac{\partial c^*}{\partial z^*}, \tag{3.18}$$

we are then able to evaluate the dimensionless turbulent dispersion coefficient:

$$D_t^* = \frac{\int_0^\infty (\frac{\partial c^*}{\partial z^*} \overline{w'c'}^*) dz^*}{\int_0^\infty (\frac{\partial c^*}{\partial z^*})^2 dz^*}. \tag{3.19}$$

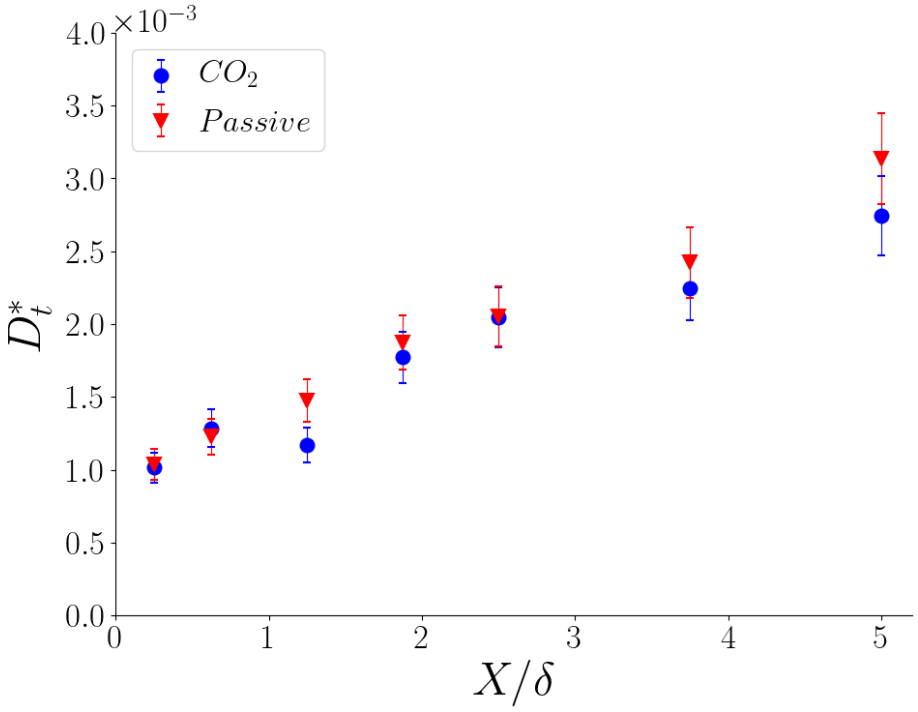

Figure 3.15: Longitudinal profiles of the normalised turbulent dispersion factor D_t^* for both heavy gas and passive scalar plumes.

The longitudinal profiles of D_t^* are reported in Figure 3.15, showing that D_t^* increases with the longitudinal distance. This trend follows the increasing of the size of the plume that interact with lager turbulent eddies, leading to a more effective turbulent dispersion. However, there is no significant difference between a passive and a heavy gas emission. As for σ_z, the profile of the turbulent dispersion coefficient suggests that vertical dispersion is not influenced by buoyancy effects, whereas the plume trajectory clearly is.

The vertical profiles of horizontal turbulent mass fluxes $\overline{u'c'}^*$ are reported in Figure 3.16. Likewise $\overline{w'c'}^*$, the intensity of $\overline{u'c'}^*$ decreases with increasing distance from the source, as the plume spreads, and significant differences between the passive scalar and the heavy gas profiles are observed in their vertical displacement. The streamwise turbulent mass fluxes are not affected by buoyancy and the minimum values of $\overline{u'c'}^*$ are the same for heavy gas and passive scalar plume, exception made for the first two sections. In this area the influence of the momentum ejected at the source on the velocity field is stronger and the fluxes $\overline{u'c'}^*$ are lower at the centre of the heavy gas plume. Comparing $\overline{u'c'}^*$ with the mean concentration field in Figure 3.5, it can be noticed that $\overline{u'c'}^*$ vertical profiles are not counter-gradient, thus, a more complex closure model has to be adopted (compared to the standard gradient closure model) to model the turbulent dispersion in the horizontal direction. This analysis is, however, beyond the scope of this thesis, since D_t^* does not show significant differences between the passive scalar and the heavy gas plume. For a discussion on higher-order model of

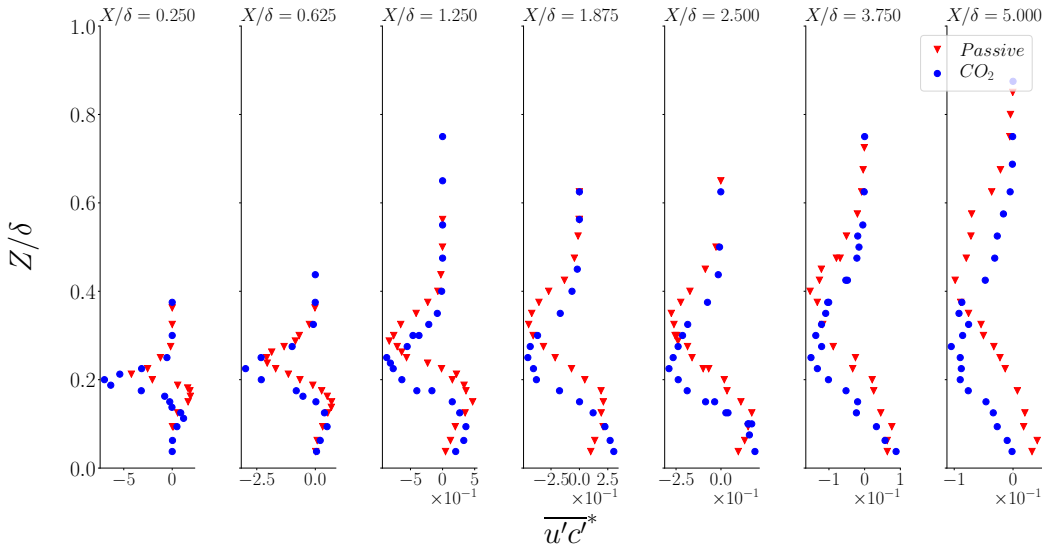

Figure 3.16: Vertical profiles of the normalised horizontal turbulent mass flux for sections at increasing distance from the source for passive and heavy gas plume.

the longitudinal turbulent fluxes, the reader is addressed to Gamel (2015). Our focus is here instead on the production and dissipation terms of the turbulent kinetic energy equation and the terms composing the balance equation of the concentration variance.

3.7 Turbulent kinetic energy equation

The balance equation of turbulent kinetic energy (TKE), taking into account the gravitational effects and the density variation and employing the Einstein notation, is (Tennekes and Lumley, 1972):

$$\begin{aligned}\frac{\partial}{\partial t}\left(\overline{\rho}K\right) = &-\frac{\partial}{\partial x_j}\left(\overline{\rho u_j}K + \frac{\overline{\rho}}{2}\overline{u_j' u_i' u_i'} + \overline{u_j' p'} - \overline{\mu u_i'\left(\frac{\partial u_i'}{\partial x_j} + \frac{\partial u_j'}{\partial x_i}\right)}\right) \\ &+ g_i\overline{u_i'\rho'} - \overline{\rho}\,\overline{u_i' u_j'}\frac{\partial \overline{u_i}}{\partial x_j} - \varepsilon,\end{aligned} \tag{3.20}$$

where $K = 0.5(\sigma_u^2 + \sigma_w^2 + \sigma_v^2)$ is the TKE, p' is the fluctuating kinematic pressure, ρ' the density fluctuation and ε the average energy dissipation rate, whose estimation is detailed in Section 3.4 and Appendix B.

In a boundary layer, we assume that the vertical and transverse velocity are negligible, and that the only non-null velocity component is the longitudinal one, i.e. $u_i = (\overline{u}, 0, 0)$. Furthermore, we assume that the flow statistics are homogeneous in the $x - y$ plane and the flow is statistically steady, so that Eq. 3.20 reduces to:

$$-\frac{\partial}{\partial z}\left(\frac{\overline{\rho}}{2}\overline{w' u_i' u_i'} + \overline{w'\delta p}\right) - g\overline{w'\rho'} - \overline{\rho}\,\overline{u' w'}\frac{\partial \overline{u}}{\partial z} - \varepsilon = 0, \tag{3.21}$$

where the gravitational field is $g_2 = -g$.

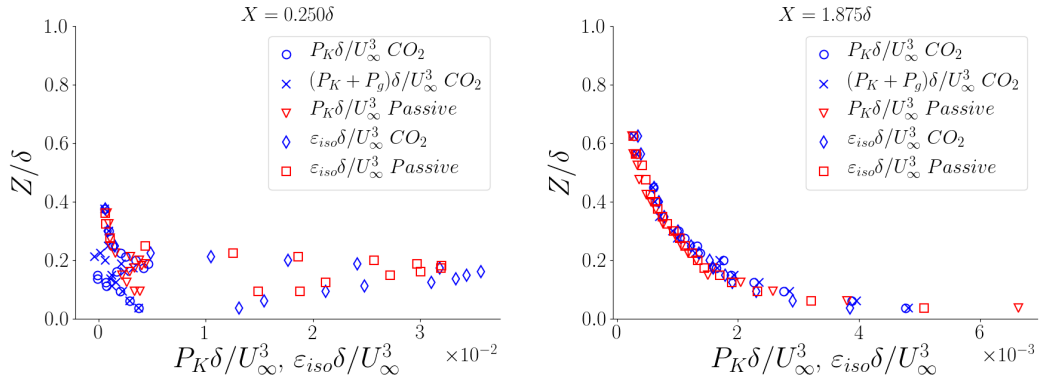

Figure 3.17: TKE production and dissipation profiles a) near the source ($X = 0.250\delta$), b) for a mean field section ($X = 1.875\delta$).

The inertial production term P_K, always positive, represent the rate of transfers (per unit of volume) of energy from the mean to the turbulent motion (Tennekes and Lumley, 1972):

$$P_K = -\overline{\rho}\overline{u_i' u_j'}\frac{\partial \overline{u_i}}{\partial x_j} \approx -\overline{\rho}\overline{u'w'}\frac{\partial \overline{u}}{\partial z}. \tag{3.22}$$

The gravitational term P_g is instead proportional to the flux driven by the density differences, and can change sign according to the turbulent density fluxes $\overline{u_i'\rho'}$:

$$P_g = -g_i\overline{u_i'\rho'} = -g\overline{w'\rho'}, \tag{3.23}$$

therefore acting as a source or a sink of turbulent kinetic energy.

Figure 3.17 shows the vertical profiles for the dissipation, estimated by means of Eq. 3.5 and referred to as ε_{iso}, and the TKE production terms, P_K (Eq. 3.22) for a passive scalar and P_K and $P_K + P_g$ (Eqs. 3.22, 3.23) for a heavy gas. It can be noticed that near the source (Fig. 3.17.a) there is a significant difference between production and dissipation for both plumes. In fact, due to the effect of the jet at the source on the velocities fields, the hypothesis of isotropic flow is in this region particularly inappropriate and therefore the model provided by Eq. 3.5 is highly inaccurate. In the intermediate field (3.17.b) the value of $P_K + P_g$ and ε_{iso} are similar, therefore at a certain distance from the source, the TKE local balance is verified. This is valid from section $X = 1.875\delta$ to the furthest section. Moreover, we observe that there is no significant difference between the heavy and the passive gas plume. Focusing on the heavy gas plume, the contribution of P_g is negligible compared to P_K in both sections, being $P_g \approx 0$.

Once compared the two terms P_K and P_g we can estimate, for the heavy gas plume, the flux Richardson number R_{if}, which expresses the ratio of the rate of removal (or production) of energy by buoyancy forces to its production by shear (inertial generated

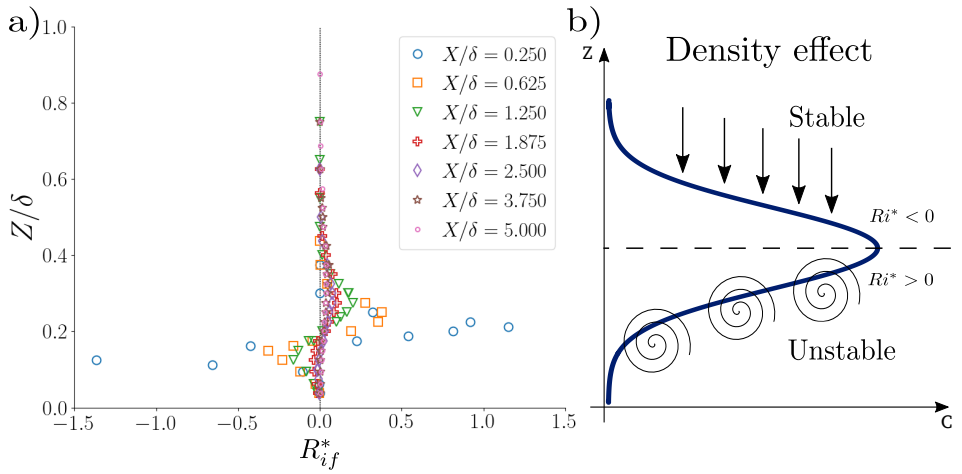

Figure 3.18: a) Vertical profiles of the flux Richardson number for heavy gas emission. b) Scheme of a plume concentration profile and the flux Richardson number.

turbulence) (Turner, 1973):

$$R_{if} = \frac{-P_g}{P_K} = -\frac{g\overline{w'\rho'}}{\overline{\rho}\overline{u'w'}\frac{\partial \overline{u}}{\partial z}}. \tag{3.24}$$

As said before, P_K is always positive while P_g changes sign depending on that of the turbulent density fluxes. Their ratio determines the characteristics of the turbulent field. The flux Richardson number is negative when the two terms are both positive. So, when $R_{if} < 0$ the plume is in an unstable condition, characterized by strong turbulent mixing. When $P_g < 0$ the fluctuating motion tends to be suppressed by the density differences, $R_{if} > 0$ and the plume is in stable conditions. In Figure 3.18.a are reported the vertical profiles of the flux Richardson number at increasing distance from the source. In the near field, R_{if} changes sign within the plume and we identify two different conditions, schematically represented in Figure 3.18.b. The bottom part of the plume is 'unstable' with $R_{if} < 0$, while the upper part is 'stable'. As the turbulent dispersion spreads the plume, this effect is reduced and we observe smaller differences on R_{if}.

In order to understand how the buoyancy affects the plume stability, we estimate another dimensionless parameter, the bulk Richardson number (R_{i_b}), defined in Eq. 3.25 as the ratio of gravitational to inertial forcing (Reeuwijk and Craske, 2015):

$$R_{ib} = \frac{\Delta\rho g \sigma_z}{\rho_a U_\infty^2}, \tag{3.25}$$

where $\Delta\rho = \rho_{max} - \rho_a$ is the difference between the maximum density of the gas mixture in the vertical section and the density of the air. Figure 3.19 shows the longitudinal profile of R_{i_b}, that decreases for increasing distance from the source and stabilises below 1 in the far field, as the density difference approaches zero. In literature (i.e. Turner, 1973; Miles, 1961), is commonly employed the gradient

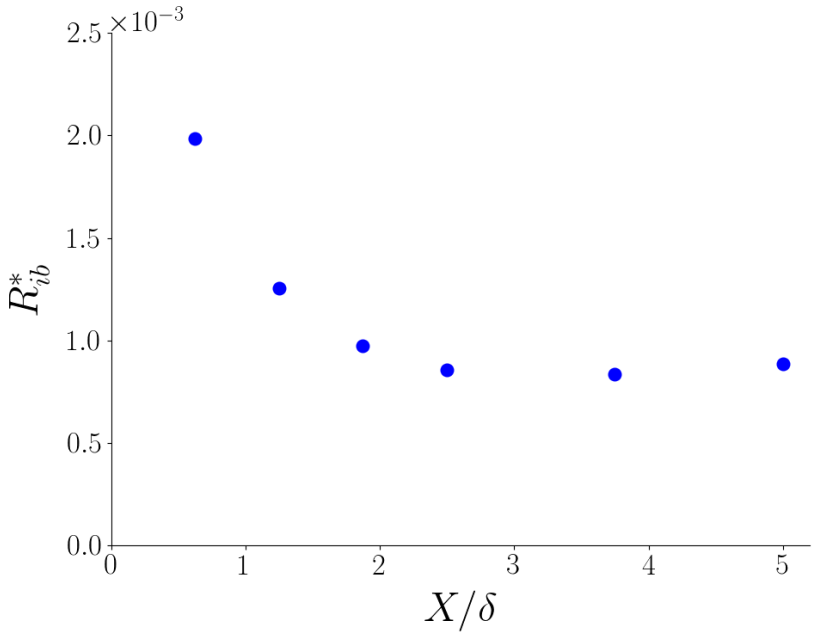

Figure 3.19: Longitudinal profile of the bulk Richardson number for a heavy gas plume, estimated in the maximum of density difference.

Richardson number:

$$R_{ig} = \frac{g\partial\overline{\rho}/\partial z}{\overline{\rho}\left(\partial\overline{u}/\partial z\right)^2}, \tag{3.26}$$

for which as been defined a critical value between 0.2 and 0.25, namely the linear stability threshold above which the laminarization of the flow occurs. A possible interpretation for our result is to relate the values of R_{ib} with this critical value of the R_{ig}. The observed R_{ig} are of the order of magnitude of $10^{-3} \ll 0.2$, therefore, we can assume that the negative buoyancy does not affect nor reduce the turbulence of the plume.

3.8 Concentration variance balance equation

The balance equation of the concentration variance σ_c^2 reads (Batchelor, 1959; Csanady, 1967):

$$\frac{\partial}{\partial t}\sigma_c^2 = -\underbrace{\frac{\partial}{\partial x_j}\overline{u_j}\sigma_c^2}_{Adv_{\sigma_c^2}} - \underbrace{\frac{\partial}{\partial x_j}\overline{u_j' c'^2}}_{T_{\sigma_c^2}} + \underbrace{\frac{\partial}{\partial x_j}D\frac{\partial}{\partial x_j}\sigma_c^2}_{Diff_{\sigma_c^2}} \underbrace{-2\overline{u_j' c'}\frac{\partial\overline{c}}{\partial x_j}}_{P_{\sigma_c^2}} - \underbrace{2D\overline{\frac{\partial c'}{\partial x_j}\frac{\partial c'}{\partial x_j}}}_{2\varepsilon_{\sigma_c^2}}, \tag{3.27}$$

where the terms under the divergence operator of the equation are fluxes of concentration variance due to advection ($Adv_{\sigma_c^2}$), diffusion by turbulent-velocity fluctuations ($T_{\sigma_c^2}$) and molecular diffusion ($Diff_{\sigma_c^2}$). The production term $P_{\sigma_c^2}$ is always positive and it express the generation of σ_c^2 by gradients of mean concentration field, while the dissipation rate $-2\varepsilon_{\sigma_c^2}$ is always negative.

We estimate the dissipation of concentration variance with two different methods. First, assuming the Taylor's hypothesis of frozen turbulent and the isotropic approximation, we compute it as:

$$\varepsilon_{\sigma_c^2 iso} = \frac{3D}{\overline{u}^2}\overline{\left(\frac{\partial c'}{\partial t}\right)^2}. \tag{3.28}$$

Secondly, we compute $\varepsilon_{\sigma_c^2}$ from the spectra of the concentration signal, as described in Appendix B. In this case, the relation between the spectra and the dissipation of the concentration variance for the inertial sub-range is on the form:

$$PSD_k = \alpha_c \cdot 2\varepsilon_{\sigma_c^2 sp} \cdot \varepsilon_{iso}^{\frac{1}{3}} \cdot k^{-\frac{5}{3}}, \tag{3.29}$$

where ε_{iso} is the rate of dissipation of turbulent kinetic energy (Eq. 3.5) and $\alpha_c = 0.5$ is a constant (Warhaft, 2000). These experimental estimates can be used to test models of $\varepsilon_{\sigma_c^2}$ that are widely used in literature. We consider here a simple model for parameterise $\varepsilon_{\sigma_c^2}$ (Eq. 3.30), derived from the ratio of the turbulence integral time scale to the scalar dissipation time scale (Hsieh, Lien, and Yee, 2007):

$$\varepsilon_{\sigma_c^2 mod} = \frac{1}{R_f}\frac{\varepsilon}{K}\sigma_c^2, \tag{3.30}$$

where R_f, a constant value in the range 0.5-0.8 (Marro et al., 2020; Warhaft, 2000), imposed here equal to $R_f = 0.7$.

Profiles of $\varepsilon^*_{\sigma_c^2}$ are reported in Figure 3.20 for both heavy gas and passive scalar at three different distances from the source. It can be noticed that $\varepsilon^*_{\sigma_c^2}$ decreases for increasing distance from the source by about three orders of magnitude. In the near field (Fig. 3.20.a,b), the vertical profiles of $\varepsilon^*_{\sigma_c^2}$, obtained with different methods, differ one to another. Due to the effect of the emission at the source the isotropic condition does not hold and $\varepsilon^*_{\sigma_c^2 iso}$ is underestimated, while $\varepsilon^*_{\sigma_c^2 mod}$ is overestimated. Further away from the source (Fig. 3.20.b,c), the three profiles are in very good agreement for the heavy gas plume, while for the passive scalar emission $\varepsilon^*_{\sigma_c^2 mod}$ is underestimated. In the far field, $\varepsilon^*_{\sigma_c^2 iso}$ and $\varepsilon^*_{\sigma_c^2 sp}$ and $\varepsilon_{\sigma_c^2 mod}$ show a good agreement one to the other in the upper part of the plume. Near the ground $\varepsilon^*_{\sigma_c^2 mod}$ is instead overestimated compared to the two others, especially in case of heavy gas emission. Probably, the interaction of the plume with the ground affects the ratio of the time scale and the model of $\varepsilon^*_{\sigma_c^2 mod}$ is no longer valid in this region. In conclusion, the model in Eq. 3.30 is less reliable compared to both the isotropic model and the spectra method (that will be used henceforth to estimate the dissipation rate of the concentration variance).

In steady condition, the time derivative in Eq. 3.27 is null and we are able to evaluate the production $P_{\sigma_c^2}$, transport $T_{\sigma_c^2}$, advection $Adv_{\sigma_c^2}$, and dissipation terms $\varepsilon_{\sigma_c^2}$. The diffusion components $Diff_{\sigma_c^2}$ are negligible compared to the others and thus they are not reported in this analysis. Furthermore, since we estimate the terms of Eq. 3.27 for the vertical profile in the centre of mass of the plume, it is reasonable to

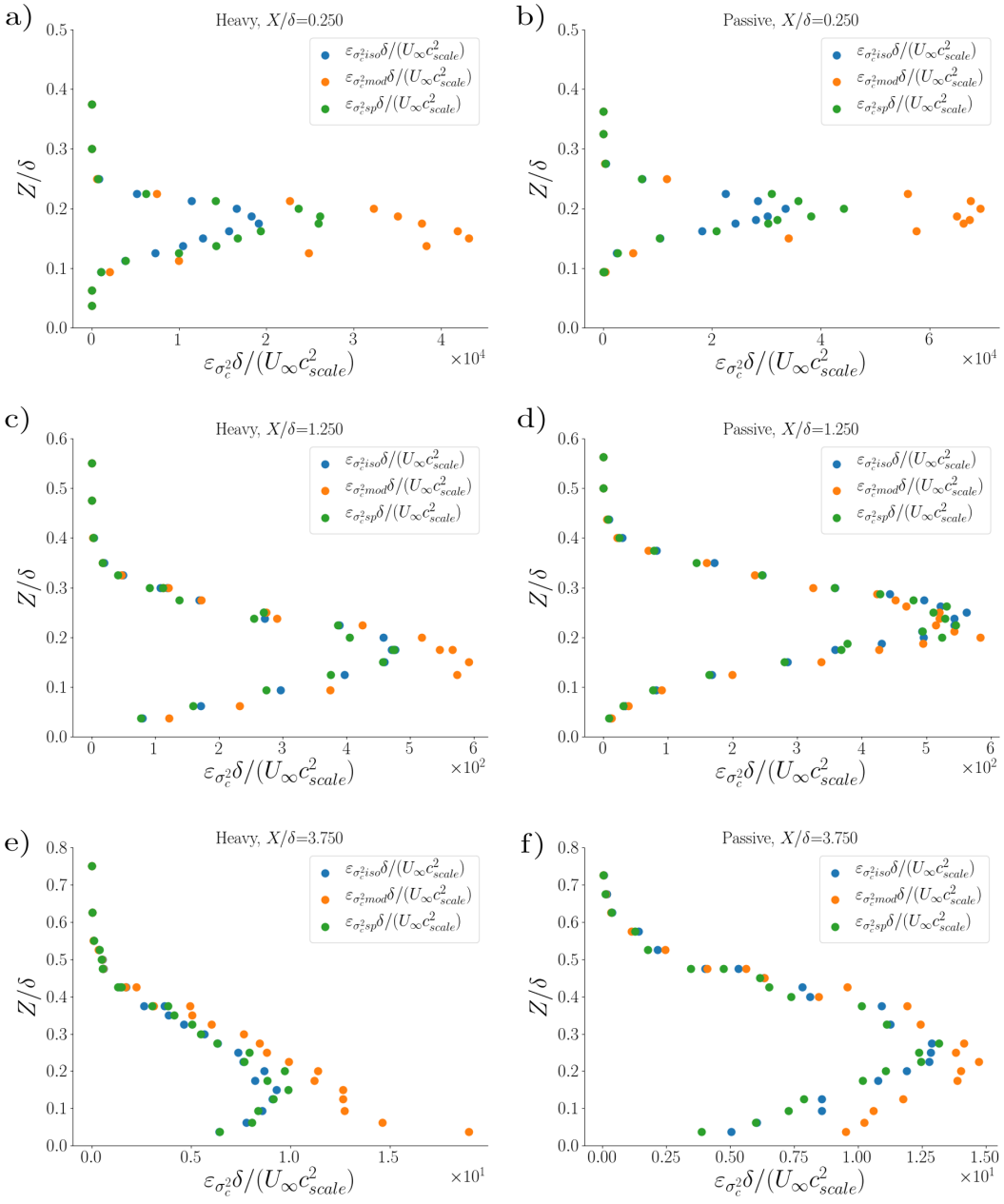

Figure 3.20: Vertical profiles of the dimensionless variance of concentration dissipation $\varepsilon_{\sigma_c^2}$, estimated with two different methods and a model for profile at increasing distance from the source for both a), c), e) heavy gas and b), d), f) passive scalar plume.

neglect all the components along the transverse direction y, as well as the advective terms along z, assuming $\overline{w} \approx 0$. A comparison between the different terms in Eq. 3.27, normalised by $\delta/(U_\infty c^2_{scale})$, is reported in Figure 3.21, including the estimation of the residuals of Eq. 3.27, referred to as $Res_{\sigma_c^2}$. The dissipation term is always negative, while $Adv^*_{x\sigma_c^2}$ and $P^*_{\sigma_c^2}$ are always positive and $T^*_{\sigma_c^2}$ changes sign according to the vertical profiles of the turbulent mass fluxes. It is worth noting that $Res_{\sigma_c^2} \neq 0$ within the plume, meaning that we are not able to verify the balance between the dissipation and the other terms. This imbalance of the terms of Eq. 3.27 is currently due to the role of turbulent transfer along the y-direction, that we could not estimate and that were here neglected. A more precise analysis can be performed by integrating each component in the cross section, this will be the subject of further studies and it will not be included in this work. In the near field, where the effect of the source injection of momentum and concentration lead to higher gradient of velocity and concentration, $P^*_{\sigma_c^2}$ and $Adv^*_{x\sigma_c^2}$ have the same order of magnitude. Further away from the source, the contribution of the horizontal advection is predominant compared to the other terms of the Eq. 3.27, as highlighted by the profiles of the residuals. In the far field, the heavy gas plume has higher density and higher concentration gradient near the ground, compared to the passive scalar case, for this reason the intake of $T^*_{\sigma_c^2}$ and $P^*_{\sigma_c^2}$ increases.

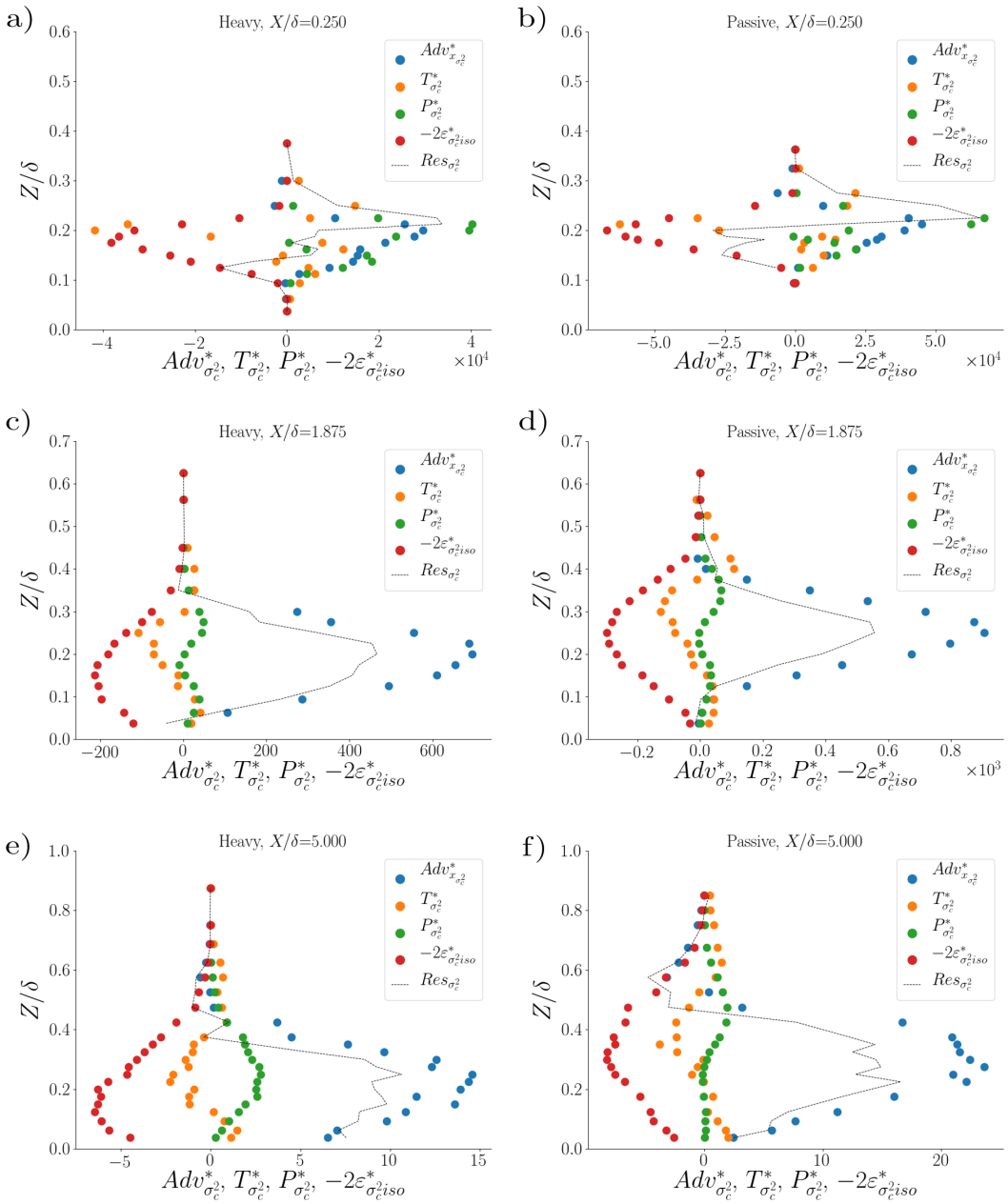

Figure 3.21: Vertical profiles of the dimensionless terms of the concentration variance equation, estimated for profile at increasing distance from the source for both a), c), e) heavy gas and b), d), f) passive scalar plume.

3.9 Mixing time scale

In evaluating the effect of the small scale turbulence on the dissipation of concentration variance, a key parameter is the so-called 'mixing time'. Notably, its parameterisation has to be included in analytical and stochastic models aiming at estimating the higher order moments of the concentration PDF (Marro et al., 2018; Bertagni et al., 2020).

In a general way, the mixing time scale, referred to as τ_m, represents the typical decay rate at which the dissipative action of small scale eddies tends to erase the inhomogeneities of the concentration field. Along the dispersion process, it is assumed that τ_m varies depending on the typology of the release (e.g. line or point source, elevated or ground level) and the flow dynamics (Cassiani et al., 2020).

In its simplest formulation, in the so-called 'interaction with the mean' (IEM) models, it is therefore linked to the concentration variance as:

$$\tau_m(IEM) = \tau_{m_c} = -\frac{\sigma_c^2}{\varepsilon_{\sigma_c}}. \tag{3.31}$$

A more complex parameterisation, referred to as 'interaction with the conditional mean' (IECM) can be instead achieved including also a term representing the meandering of the plume, through a mean concentration conditioned on the value of the local velocity $\langle c|u\rangle$. In this parameterisation the mixing time scale is expressed as:

$$\tau_m(IECM) = \tau_{m_{c|u}} = -\frac{1}{\varepsilon_{\sigma_c}}\left(\sigma_c^2 - \overline{c'\langle c|u\rangle}\right). \tag{3.32}$$

Note that when $\langle c|u\rangle$ tend to $\overline{c}$ and the mean concentration is no-longer linked to any particular class of the velocity vector (implying that the larger scale structure of the flow does not have an influence on the variance generation), the two models are identical one to the other.

In this section we provide experimental estimates of the micro-mixing time scale τ_m and we compare them to the turbulent time scale $\tau = K/\varepsilon$, defined as the ratio between the TKE and its dissipation.

Figure 3.22 shows the vertical profiles of τ_{m_c}, $\tau_{m_{c|u}}$ and τ for both heavy gas and passive scalar at increasing distance from the source. For sake of clarity we reported the micro-mixing time scale estimated in the core of the plume, i.e. only for $Z_{MC} - 2\sigma_z < z < Z_{MC} + 2\sigma_z$. We expect the vertical profile of τ to be equal at different downstream position, considering that all the velocity statistics depends only on z, as seen in Section 3.4. This condition actually holds in the whole flow field, except very close to the source, where the flow field is affected by the momentum and the buoyancy emitted at the source (see profiles of τ and τ_m (Fig. 3.22.a,b)). Amicarelli, Leuzzi, and Monti (2012) point out that the IEM model overestimates the dissipation of the concentration variance compared to the IECM model, i.e. $\tau_{m_c} < \tau_{m_{c|u}}$. In our case, however, the results show similar values of $\tau_{m_{c|u}}$ and τ_{m_c} in all the section, with the tendency of τ_{m_c} to be slightly higher then $\tau_{m_{c|u}}$. At $X = 1.250\delta$ (Fig. 3.22.c,d) and $X = 2.5\delta$ (Fig. 3.22.e,f), τ_{m_c} and $\tau_{m_{c|u}}$ have similar values to τ near the ground

and diverge in the higher part of the plume. In the far field, τ_m converge to τ with a general good agreement for both the heavy gas and the passive scalar plumes. This can also be observed in Figure 3.23, reporting the ratio between the micro-mixing time scale, estimated with the IEM model, and the turbulent time scale in the centre of mass of the plume. The longitudinal profiles show that τ_m/τ tends asymptotically to 1 far from the source, where the relative dispersion drives the mixing mechanisms.

In operational dispersion models, the value of τ_m has to be parameterised as a function of statistics of the velocity and concentration field. In what follows, we consider the micro-mixing time scale $\tau_{m_{mod}}$ presented by Cassiani, Franzese, and Giostra (2005a):

$$\tau_{m_{mod}} = \mu_t \frac{\sigma_r}{\sigma_{ur}}, \tag{3.33}$$

where $\mu_t = 0.44$ is an empirical constant (Marro et al., 2018), σ_r is the relative plume spread around the plume's centroid and $\sigma_{ur} = \sqrt{\overline{u_r^2}}$ is the r.m.s. of the relative velocity fluctuations. The term u_r represents the difference between a turbulent velocity component and the corresponding velocity component of the instantaneous centre of mass (meandering process). The relative plume spread σ_r is modelled as:

$$\sigma_{ur}^2 = \sigma_u^2 \left(\frac{\sigma_r}{L}\right)^{2/3} \tag{3.34}$$

where σ_u^2 is the variance of the turbulent velocity (this is assumed to be the average of the three components in case of an anisotropic flow), L is the Eulerian integral length scale parameterised as Sawford and Stapountzis (1986):

$$L = \frac{\left(3\sigma_u^2/2\right)^{3/2}}{\varepsilon}. \tag{3.35}$$

The meandering process becomes negligible with respect to the relative dispersion when $\sigma_r = L$ and all the energy contributes to the expansion of the plume. Consequently, we imposed $\sigma_{ur} = \sigma_u$ if $\sigma_r > L$ with σ_r^2 defined as:

$$\sigma_r^2 = \frac{d_r^2}{1 + (d_r^2 - d_s^2)/(d_s^2 + 2\sigma_u^2 T_L t)}, \tag{3.36}$$

where

$$d_r^2 = C_r \varepsilon (t_0 + t)^3, \tag{3.37}$$

is the inertial formulation for a dispersion from a finite source size d_s (with $C_r = 0.3$), and where $T_L = 2\sigma_u^2/C_0\varepsilon$ is the Lagrangian time scale (with $C_0 = 4.5$) (Marro et al., 2018)). The discretization in time of Eq. 3.37 is:

$$d_r^2(t + \Delta t) = d_r^2(t) + 3C_r\varepsilon(t_0 + t)^2\Delta t, \tag{3.38}$$

with the initial condition $d_r^2(t = 0) = d_s^2$.

Longitudinal profiles of τ, τ_{m_c}, $\tau_{m_{c|u}}$ and $\tau_{m_{mod}}$ at the centre of mass are reported in

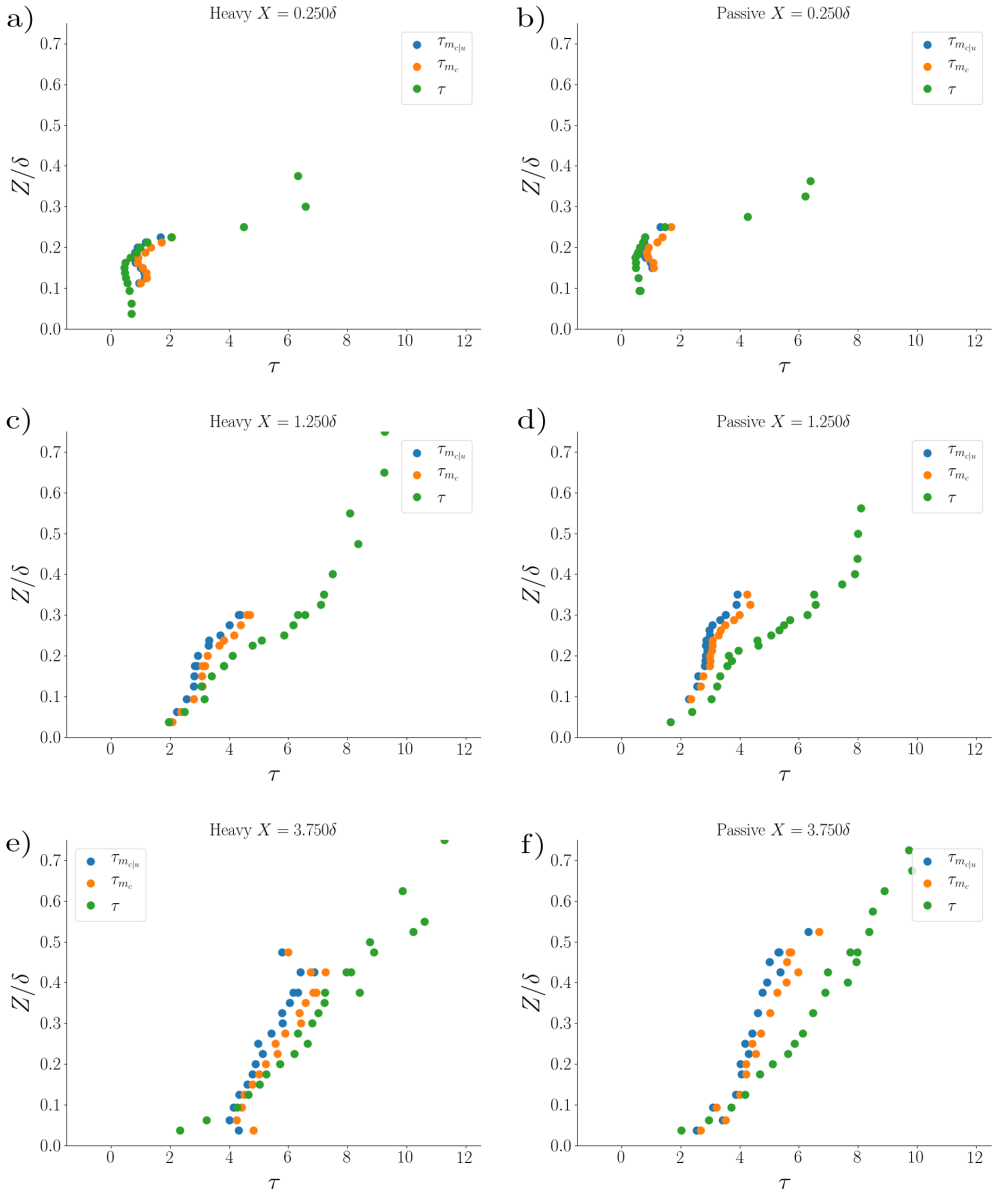

Figure 3.22: Vertical dimensionless profiles of the turbulent time scale τ and the mixing time τ_m, the latter estimated with two different models (IEM and IECM) for profile at increasing distance from the source for both a), c), e), g) heavy gas and b), d), f), h) passive scalar plumes.

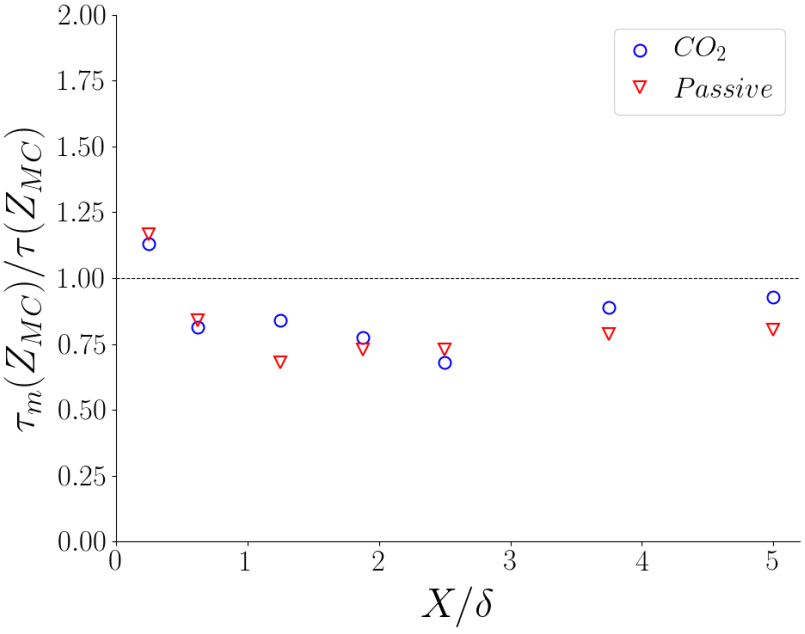

Figure 3.23: Longitudinal profiles of the turbulent mixing time τ_m, estimated with the IEM method, over the time scale τ in the centre of mass of the plume (Z_{MC}) for both heavy gas and passive scalar plumes.

Figure 3.24.a and 3.24.b for heavy gas and passive scalar respectively. We observe that, independently from the estimation method, the mixing time is always lower than τ and the difference between τ_m and turbulent time scale decreases for increasing distance from the source. It worth noting that the model of Cassiani, Franzese, and Giostra (2005a) underestimate the micro-mixing time scale, being $\tau_{m_{mod}} < \tau_{m_{c|u}} \approx \tau_{m_c}$.

3.10 Conclusions

In this study we highlighted the differences in the dynamics of the turbulent dispersion of a heavy gas and a passive scalar emission. In the atmospheric wind tunnel facilities of LMFA we characterised the pollutant plumes downwind the source by measuring simultaneously the concentration and velocity field, by means of a coupled system HWA-FID. Mean concentration vertical profiles showed how a plume of gas heavier than air develops closer to the ground. Comparing σ_c^* to $\overline{c^*}$, we identified the border of the plume as the region where entrainment of air into the plume is predominant for both passive scalar and heavy gas. From the interpolation of the plume concentration profiles we estimated the height of the centre of mass (Z_{MC}) and the vertical and transverse spread, σ_z and σ_y, respectively. We analysed the correspondence between the intensity of fluctuation i_c, defined as the ratio of σ_c^* and $\overline{c^*}$, to the concentration PDF, verifying the accuracy of the Gamma distribution model. In this way, knowing the mean and the standard deviation of the concentration field we were able to estimate the higher order moments. Furthermore, we compared all these parameters to understand if

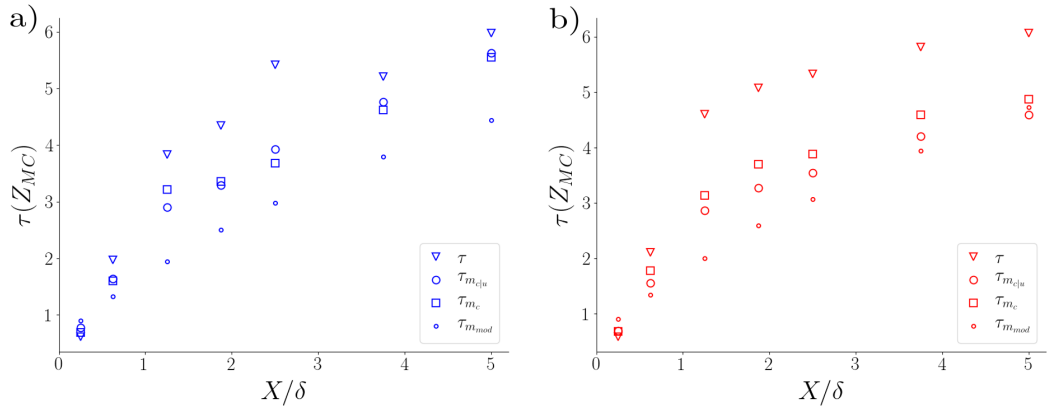

Figure 3.24: Longitudinal profiles of the turbulent time scale τ and the mixing time τ_m, the latter estimated with two different models (IEM, IECM) for a) the heavy gas and b) the passive scalar plume compared with τ_m estimated from the model of Cassiani, Franzese, and Giostra (2005a).

the dispersion dynamics of the plume centre is driven by the meandering motion or the relative dispersion. Simultaneous measurements of concentration and velocity allowed us to obtain vertical profiles of vertical and longitudinal turbulent mass fluxes, respectively $\overline{w'c'}^*$ and $\overline{u'c'}^*$. Near the source the dispersion dynamics was significantly influenced by the plume emission velocities, with sharper profile of the turbulent mass fluxes. Observing the mean concentration profiles, we noticed that only $\overline{w'c'}^*$ had counter gradient vertical evolution. By applying a standard closure hypothesis, we were then able to estimate the turbulent dispersion coefficient D_t^* for each profile, which was shown to increase for increasing distance from the source. Values of σ_z and D_t suggested that the vertical dispersion was not influenced by buoyancy effects, whereas the plume location Z_{MC} was clearly affected. The analysis of the mean TKE equation allowed us to verify the balance between production and dissipation in the middle and far field, with no significant difference for a plume of gas heavier than air. Moreover, for the case of heavy gas emission, we estimated the flux Richardson number, identifying a stable condition in the upper part of the plume and an unstable condition near the ground. We analysed the dissipation, transport and production terms of the concentration variance equation, in which, however, we were not able to properly estimate the transverse turbulent variance fluxes. Further analysis to integrate each component in the cross-flow section will be performed in future study. We focused in particular on the estimation of the concentration variance and its dissipation, which we could subsequently use to quantify typical mixing time scales τ_m of the flow.

Summarising, the experimental campaign allowed us to build a dataset characterising the concentration and velocity field of a heavy gas plume, through which we estimated the concentration PDFs, the micro-mixing time, the dissipation rate of the TKE and the concentration variance, which are essential to simulate the turbulent dispersion of heavy gas plume by means of analytical and stochastic models.

Chapter 4

Modelling atmospheric dispersion of elevated heavy gas releases

4.1 Abstract

The modelling of atmospheric gas dispersion has a key role in the management of risks related to accidental releases. In the industrial field, the main objective is to predict the pollutant concentration induced by these releases by means of operational models, i.e. with low computational costs. In case of inflammable, toxic or explosive substance even a local excess of the concentration hazard limit can lead to fatal consequences. Therefore, the risk assessment of pollutant dispersion requires the knowledge of the higher order concentration statistics as well as the insight on the temporal dynamics of the concentration. In this study we use the data of the wind tunnel experiments, on the heavy gas release from an elevated source in the atmospheric boundary layer, to validate an integral model, Ventjet (Air Product-Air Liquide) and a Lagrangian particle model, SLAM (AIR-LMFA-ECL). A first comparison between models and experimental data concerns the mean concentration and the plume centreline trajectory. Afterwards, we focus on the analysis of the higher order moments, obtained by the SLAM output (second order moment) and assuming a family of one parameter Gamma distribution to estimate the 3rd and 4th order moments. We complete the study by investigating the structure of the concentration time series, comparing the level crossing time and rate, estimated from the experimental signals with theoretical models based on the first two moments of the concentration and assuming as usual that the concentration PDF follows a Gamma distribution.

4.2 Introduction

The modelling of the plume dispersion in the atmosphere has a relevant role for both the risk assessment and design of the industrial gas facilities (i.e. dimension and position of vents, alarm system, barriers). A typical industrial scenario is provided by the Air Separation Units (ASUs), that separate air through cryogenic process into

oxygen, nitrogen and argon products. These plants emit continuously or intermittently oxygen/nitrogen/argon rich streams into the atmosphere. The dimension and position of the vents are defined during the plant design to respect safety distances, which are determined through gas dispersion models and correspond to poor (asphyxia) or too rich (fire) oxygen content. To simulate these phenomena, a variety of modelling approaches are available, characterised by mathematical formulations of very different complexity and, therefore, computational costs. Gaussian models are the most common air pollution models and describe the concentration field generated from a steady source of pollutant, and are mainly suitable for neutral gases (Zannetti, 1990). Integral models are one dimensional models and could take into account density difference, pressure at the source and two phase dispersion. Integral models are often coupled with a Gaussian model to estimate the plume spread. One of the most common integral model in the industrial gas plant design is PHAST (Witlox and Holt, 1999). Lagrangian particle dispersion models are valuable tools for the estimate of all moments of the concentration of non-reactive scalars in the boundary layer (Cassiani, Franzese, and Giostra, 2005a), often employed to achieve accurate concentration predictions over complex flow configurations (Marro et al., 2013). The evaluation of the concentration statistics may give insight on mixing time scale and on the concentration and velocity fluctuation, information that is extremely relevant in case of heavy gas plume of toxic, explosive or flammable gas. Another approach is provided by the Computational Fluid Dynamic (CFD), whose large computational costs can be, however an inconvenience in the industrial field, and therefore will not further discussed here.

In this chapter we use the experimental dataset of the heavy gas release, discussed in Chapter 3, to test the reliability of two models: Ventjet (Miller et al., 2021) and SLAM (Safety Lagrangian Atmospheric Model Vendel et al., 2011). These are both operational models that assume a simplified description of the wind profile over the domain and do not take into account the feedback of the buoyancy of the release on the velocity field. Ventjet is an integral model evaluating dispersion of a plume from a localised emission, developed by Air Product and Air Liquide as a joint program. Ventjet model was develop as a combination of previous models commonly employed in industrial risk analysis, such as the integral model of Ooms (1972), DEGAGIS (Havens and Spicer, 1988), HGSYSTEM (HGSYSTEM, 1990) and PHAST (Witlox and Holt, 1999) among others. The model performs a dispersion calculation on the top-hat model equation along the plume centreline and solves mass and momentum balances, adopting the entertainment assumption and considering a Gaussian solution for the mean concentration field. Ventjet has been validated against a wide range of test data (wind tunnel and full-scale field experiments), CFD results and actual incidents and near misses Miller et al. (2021). It showed good agreement with the Schatzmann, Snyder, and Lawson (1993) and Donat and Schatzmann (1999) experimental study on heavy gas dispersion. Ventjet is an effective model to estimate the mean concentration and the plume centreline position with very low computational costs. The main inconvenience is that the model does not take into account the reflection of the plume

at the ground and assumes the flow field shape, by means of similarity laws; thus it is not suited for complex environment.

The Lagrangian model SLAM is instead a stochastic model that was developed by the Atmosphere, Impact and Risk (AIR) team at the atmospheric wind tunnel of the Laboratoire de Mécanique des Fluides et d'Acoustique (LMFA) of the École Centrale de Lyon. SLAM is a software for the simulation of gas dispersion on industrial site and urban environment, that simulates the transport of pollutant in the atmosphere in function of the meteorological conditions. It is made of two modules, the first is dedicated to the evaluation of the meteorological data and the extraction of the wind field and the second to the evaluation of the pollutant dispersion. The velocity field can be uniform, evaluated from the atmospheric condition as wind profile, or characterised through 3D CFD simulation (in case of simulations in complex environments). Since the velocity field and the pollutant dispersion are evaluated separately, the running time for each simulation is of the order of magnitude of seconds. SLAM is based on a Lagrangian approach, evaluating the trajectory of a high number of pollutant particles in a mean velocity field, which is increased at each iteration by an aleatory component that represents the fluctuating turbulence (Marro et al., 2013; Vendel, 2011)

We complete the study by investigating the structure of the concentration time series, estimating the level crossing time and rate. This analysis is always possible with direct measurements of the mean concentration and its fluctuations. When these are not available, the information on the behaviour of time series is obtained by employing theoretical models based on the knowledge of the first two moments of the concentration and assuming that the concentration PDF follows a Gamma distribution (Bertagni et al., 2020).

4.3 One-point concentration statistics

In this section we introduce the equation of the integral and Lagrangian models and we discuss the respective results, relating them to the wind tunnel data. First we present the first order moment of the concentration field comparing Ventjet, SLAM and the experimental results. Then we focus on the higher order statistics, obtained from the SLAM simulation (second order moment) and assuming a family of one parameter Gamma distribution to describe the higher moments of the concentration PDF (3rd and 4th order moments).

4.3.1 Ventjet

Ventjet is based on PHAST equations and it performs a dispersion calculation on the top-hat model equation along the plume centreline. The top-hat model assumes no gradient of concentration, velocity and density within the plume, which is symmetric in the radial direction. A Gaussian concentration profile is then superimposed to predict the centreline concentration and the width of the plume to a specified concentration (Miller et al., 2021). The touchdown on the ground is taken into account, by changing

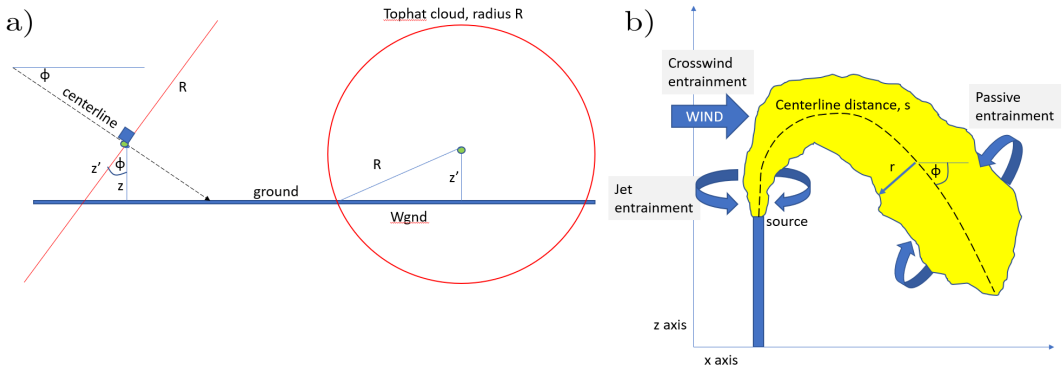

Figure 4.1: Schematic representation of the plume geometry a) interacting with the ground, b) spreading after being released from the source. Images credit Miller et al. (2021).

the perimeter available for the air entrainment, but the reflection of the plume on the ground is neglected. The coordinate system is centred at the source, with x the longitudinal direction downstream the source, z the vertical axis and s the plume centreline. For an extended and detailed explanation and validation of the model please refer to Miller et al. (2021).

Wind profile and balance equations

The mean wind velocity is assumed to be logarithmic:

$$\frac{\overline{u}(z)}{u_*} = \frac{1}{k} \ln\left(\frac{z}{z_0}\right). \tag{4.1}$$

For practical purposes it is usually determined by measuring the velocity at the reference height (usually $z_{ref} = 10m$) and estimated the roughness length z_0 through morphological criteria, being k = 0.4 the Von Karman constant.

The gas plume is emitted into the atmosphere by a round source of diameter d_s with given concentration, mass rate, velocity, temperature and orientation. The mass rate m at the source is defined as:

$$m = \pi R^2 u \rho, \tag{4.2}$$

where ρ and u are the top-hat density and velocity respectively and R is the top-hat radius:

$$R = R_s \left[0.2701 \left(\frac{z'}{R_s}\right) - 0.695 \left(\frac{z'}{R_s}\right)\right], \tag{4.3}$$

with $R_s = \sqrt{A/\pi}$ the radius of circular top-hat cloud not impacted by the ground (A is the top-hat cross section area) and it is equal to R when the plume is away from the ground (see Figure 4.1.a).

The mass balance along the plume centreline s is:

$$\frac{dm}{ds} = E, \tag{4.4}$$

where E is the flux of air entrained into the plume. As the plume disperses in the atmosphere, E dilutes the gas and modifies the plume momentum and direction. The entrainment is defined as the sum of three different mechanisms (Fig. 4.1.b):

$$E = E_{jet} + E_{cw} + E_p, \tag{4.5}$$

where E_{jet} is the jet entrainment, driven by the difference between the jet and the ambient air velocity, E_{cw} is the cross wind entrainment, induced by the wind velocity, and E_p is the passive entrainment, created by atmospheric turbulence. The parameterisation of E_{jet} is derived from Morton, Taylor, and Turner (1956) and Ooms (1972) as:

$$E_{jet} = \alpha_1 P \rho_a |u - u_a \cos\Phi|, \tag{4.6}$$

where u_a is the wind velocity at centreline elevation, $\alpha_1 = 0.08$ (Miller et al., 2021), Φ is plume trajectory angle determined from the horizontal and vertical velocities $\tan\Phi = u_z/u_x$, and P is the top-hat cloud wetted perimeter, defined in function of the ground contact radius W_{gnd} (Fig. 4.1.a) as:

$$P = R\left[2\pi - 2\arcsin\left(\frac{W_{gnd}}{R}\right)\right], \tag{4.7}$$

where

$$W_{gnd} = \sqrt{\left(R^2 - \left(\frac{z}{\cos\Phi}\right)^2\right)}. \tag{4.8}$$

The cross-wind entrainment E_{cw} (null when the cloud is vertical, i.e. $\Phi = 0$) is defined as:

$$E_{cw} = \alpha_2 P \rho_a u_a |\sin\Phi\cos\Phi|, \tag{4.9}$$

with $\alpha_2 = 0.5$ (Ooms, 1972).

Finally, E_p, for a D stability class of the atmosphere, is obtained as:

$$E_p = \alpha_3 P \pi \rho_a \beta^{1/3}, \tag{4.10}$$

where $\alpha_3 = 1$ (Witlox and Holt, 1999), $\beta = (u_*^3)/(k(z + z_0))$ is the passive turbulence parameter.

The momentum balance equation in the longitudinal and vertical directions are:

$$\frac{dM_x}{ds} = Eu_a + C_{drag}\frac{P}{2}\rho_a u_a^2 |\sin(\Phi)^3|, \tag{4.11}$$

$$\begin{aligned}\frac{dM_z}{ds} =& -g(\rho - \rho_a)A \\ &+ if(\Phi > 0, -1, 1)C_{drag}\frac{P}{2}\rho_a u_a^2 \sin(\Phi)^2\cos(\Phi) \\ &- if(z > z_{min}, 1, 0)W_{gnd}0.5\rho u_x^2,\end{aligned} \tag{4.12}$$

where $C_{drag} = 0.3$ is the drag of the atmospheric flow on the plume Ooms (1972). M_x changes when the air is entrained with a velocity equal to the wind velocity and M_z is affected by the buoyancy and the drag. The third term at the right side of the Eq. 4.12 has been added by Miller et al. (2021) to address the impact of the ground in pulling the cloud downwards by the Coanda effect and it is only active when the lower edge of the top-hat cloud has reached the ground.

Once the momentum balance is set, the centreline velocity can be estimated as $u^2 = u_x^2 + u_z^2$, with $u_x = M_x/m$ and $u_z = M_z/m$, and the centreline step size as $dx = u_x \sin\Phi$ and $dz = u_z \cos\Phi$. The centroid elevation has been estimated by Miller et al. (2021) as the mean between the upper bound and the lower bound of the top-hat model.

Concentration and Gaussian distribution

The cloud density is defined by linking it to the gas concentration:

$$\frac{1}{\rho} = \frac{c_m}{\rho_s} + \frac{1 - c_m}{\rho_a}, \tag{4.13}$$

with $c_m = m_0/m$ the top-hat mass fraction and m_0 the mass at the source.

As customary done in a integral plume model (Morton, Taylor, and Turner, 1956), the concentration can be determined as a top-hat variable (averaged over the plume section) and computed through a mass balance. This top-hat concentration can be then converted to a Gaussian distribution for the plume concentration to express the concentration as a function of the plume radius r:

$$\frac{c(r)}{c_{centreline}} = exp\left(\frac{-0.5r^2}{\sigma^2}\right), \tag{4.14}$$

where the centreline concentration $c_{centreline}$ is linked to the top-hat concentration trough the relation $c_{centreline}/c_{top-hat} = CR = 1.7$ (Witlox and Holt, 1999).

4.3.2 SLAM

SLAM couples a Lagrangian particle dispersion model to the velocity field, evaluated separately, without taking into account the density and momentum effects of the emission on the turbulence of the velocity field (i.e. the model assumes that there is no feedback on the atmospheric turbulence dynamics). In the SLAM code are implemented a plume rise model, a Lagrangian stochastic model and a micro-mixing model.

The plume trajectory is simulated by an integral model solving the mass, momentum and heat balance equations with an additional equation to parameterise the air entrainment within the plume. The variables that describe the plume dynamics are obtained by space and time averaging on the circular cross-section. A detailed description of the plume rise model, is reported in Appendix C (Robins et al., 2009).

A Lagrangian stochastic model is implemented to estimate the pollutant dispersion and dilution of the plume. This approach takes into account the influence of the plume buoyancy on the particles and it maintains the independence of the particle motions, as typically done in the Lagrangian models in anisotropic and inhomogeneous turbulence. For these reasons, following Marro et al. (2013) and Webster and Thomson (2002), we assume that the mean advection velocity of each particle is equal to the velocity of the plume centre of mass, that was previously computed by an integral plume rise model.

A micro-mixing model based on the volumetric particle approach (VPA) estimates the first two moments of the concentration without taking into account the background particles, simplifying the representation of the mixing and simulating explicitly only the plume particles.

The boundary conditions defined to ensure the well-mixed condition (Thomson, 1987) as follows:

- on the top and lateral boundaries, the particles go out the computational domain;
- on the ground, the particles are elastically reflected and they conserve their concentration.

The latter is a criterion by which, for a fixed temporal instant and a space position, if the particles distribution in the domain is homogeneous, the velocity statistics of each particle have to be equal to the statistics of the Eulerian velocity. As a consequence, the particles have the same dynamical properties of the fluid. The well-mixed condition is guaranteed by the elastic reflection of the particles if the turbulence is Gaussian and homogeneous. In case of asymmetry of the velocity PDF or local inhomogeneities the well-mixed condition is no longer valid (Wilson and Flesch, 1993; Wilson and Sawford, 1996). However, Wilson and Flesch (1993) demonstrated that the perfect reflection is acceptable in bounded Gaussian inhomogeneous turbulence, as the neutral BL.

In what follows, we present the main features of the model, describing the Lagrangian particle approach and the micro-mixing VPA model with references to the works of Marro et al. (2013) and Marro et al. (2018).

Lagrangian stochastic model

The fluid particles velocity and position evolve in time as described by the following stochastic differential equations:

$$dU_i' = a_i(\mathbf{X}, \mathbf{U}', t)dt + b_{ij}(\mathbf{X}, \mathbf{U}', t)d\xi_j, \tag{4.15}$$

$$dX_i = (\overline{u}_i + U_i')dt, \tag{4.16}$$

where $\overline{u}_i$ is the Eulerian mean velocity, U_i' is the related Lagrangian velocity fluctuation, $d\xi_j$ is an incremental Wiener process (Gardiner, 2004) with zero mean and variance, dt the time increment, X_i is the particle position, a_i is the deterministic acceleration and

b_{ij} is the stochastic diffusive term. The term a_i depends on the turbulent statistics and is computed by imposing the well-mixed condition (Thomson, 1987) as:

$$a_i = -\frac{U_i'}{T_{Li}} + \frac{1}{2}\frac{\partial \sigma_{ui}^2}{\partial x_i} + \frac{U_i'}{2\sigma_{ui}^2}\left(U_j \frac{\partial \sigma_{ui}^2}{\partial x_j}\right) \qquad \text{with} \qquad i = 1, 2, 3, \tag{4.17}$$

where σ_{ui} represents the standard deviation of the Eulerian velocity components ($\sigma_u = \sigma_{u1}$, $\sigma_v = \sigma_{u2}$, and $\sigma_w = \sigma_{u3}$) and $T_{Li} = 2\sigma_{ui}^2/C_0\varepsilon$ the Lagrangian integral time scales ($T_{Lu} = T_{L1}$, $T_{Lv} = T_{L2}$ and $T_{Lw} = T_{L3}$). The term b_{ij} is defined from the Kolmogorov's hypotheses of self-similarity and local isotropy in the inertial subrange (Pope, 2000):

$$b_{ij} = \delta_{ij}\sqrt{C_0\varepsilon}, \tag{4.18}$$

where δ_{ij} is the Kronecker delta. To take into account the effects of the momentum and buoyancy fluxes of the source on the plume in the near field, the Lagragian model is coupled with the plume rise module by replacing in Eq. 4.15 the Eulerian mean velocity $\overline{u}_i$ with the velocity of the plume centre of mass $\overline{u}_p$, estimated by means of the equation of Appendix C (Webster and Thomson, 2002; Marro et al., 2013; Robins et al., 2009). In this way we assume the plume as an ensemble of puffs that are constituted by a set of particles. At each time step we estimate the velocity of the puffs with the integral model, associating it to the corresponding particles.

In case of buoyant releases in a cross-flow, Webster and Thomson (2002) proposed to add a random displacement at each time step in Eq. 4.16 to take into account the growth of the plume size, as modelled by the plume rise module, and related to the generation of turbulence. Assuming an additional spread $r = (r_x, r_y, r_z)$ with zero mean and variance σ^2 depending on the variation of b_0 between two time steps:

$$\sigma^2 = \frac{b_0^2(t + \Delta t) - b_0^2(t)}{4}. \tag{4.19}$$

Eq. 4.16 can be rewritten as:

$$dX_i = (\overline{u}_p + U_i')dt + r_i. \tag{4.20}$$

It is worth noting that the random displacement r is a Wiener process and the trajectories of the particles (Eq. 4.16) are a second-order Markov process. Adding r in Eq. 4.20 is an empirical procedure which is in contrast with the theoretical bases of the Lagrangian models (Gardiner, 2004). This approach was applied to model the wind tunnel experiments of a buoyant plume by Marro et al. (2013).

Volumetric Particle Approach

The micro-mixing models aim at suitably approximating the concentration PDF accounting for the effects of the molecular diffusivity (Pope, 1998). One way to simulate the micro-mixing process, applyed in the PDF micro-mixing models, is considering it as mass exchanges between the fluid particles of the pollutant particles of

the ambient air (e.g. Sawford, 2004; Cassiani, Franzese, and Giostra, 2005a)), requiring high computational costs to deliver accurate solutions. The Volume Particle Approach (Cassiani, 2013) is a simpler model that does not take into account the background particles and allows us to estimates the first two moments of the concentration, saving computational resources.

Since Eqs. 4.15 and 4.16 give information about the first-order statistics only, the simulation of the higher-order moments of the concentration field requires the introduction of another Markovian state variable C representing the particle concentration, and of a drift coefficient ϕ responsible for the dissipation scalar variance (Sawford, 2004; Cassiani, Franzese, and Giostra, 2005a):

$$\frac{dC}{dt} = \phi(C, \mathbf{X}, \mathbf{U}', t), \tag{4.21}$$

To that purpose, the VPA uses the IEM model ($dC/dt = -(c - \overline{c})/\tau_m$) and defines a "fictitious" volume V_p, associated to the plume particles, whose variation stimulates the micro-mixing proces and in which the dissipation of the scalar fluctuations is related to a sort of dilution of the marked particles. The volume $V_p = m_p/C$ is a function of the mass of tracer m_p carried by a particle and, for non-reactive scalar, is conserved ($dm_p/dt = 0$). The evolution of V_p over time is:

$$V_p(t + dt) = V_p(t)\frac{C(t)}{C(t + dt)}, \tag{4.22}$$

where the concentration C can be modelled through Eq. 4.21. We define a computational domain discretised with Cartesian grid of fixed dimension. The mean concentration $\overline{c}$ over this domain depends on the global mass M_c in each space element:

$$\overline{c} = \frac{M_c}{V_c} = \frac{1}{V_c}\sum_{i=1}^{N_c} m_{p_i} = \sum_{i=1}^{N_c} C_i \frac{V_{p_i}}{V_c}, \tag{4.23}$$

where N_c is the particle number held in the generic cell of volume V_c. The term V_{p_i}/V_c can be seen as the probability that the particle i takes the concentration C_i. With this assumption the second-order moment $\overline{c^2}$, in analogy to Eq. 4.23, is computed as:

$$\overline{c^2} = \sum_{i=1}^{N_c} C_i^2 \frac{V_{p_i}}{V_c}. \tag{4.24}$$

It is well-known that the IEM model introduces spurious fluxes that alter the estimation of the mean concentration field and more sophisticated models are usually implemented (e.g. IECM model, Sawford, 2004; Cassiani, Franzese, and Giostra, 2005a). However, this effect does not affect the VPA model since the mean concentration is computed through Eq. 4.23 (Cassiani, 2013).

We recall that the approximations introduced in the VPA model provide a satisfactory accuracy in computing the second-order statistics only, whereas the higher-order

C_0	σ_0	C_r	$\mu_{t,VPA}$
4.5	$\sqrt{2/3}d_s$	0.3	0.44

Table 4.1: Parameter values adopted in the SLAM simulations.

statistics are affected by significant errors (Cassiani, 2013; Marro et al., 2018); for this reason, it fails in describing the correct evolution of the PDF concentration.

The estimate of the scalar PDF can be provided by assuming a Gamma distribution as a reliable model for the concentration, as shown in Chapter 3 and in several previous works (Villermaux and Duplat, 2003; Yee and Skvortsov, 2011). Taking advantage by these results, we followed the approach, called VPΓ, proposed and tested by Marro et al. (2018): $\overline{c}$ and σ_c are evaluated by means of the VPA model (Eqs. 4.23 and 4.24) and the higher-order statistics are obtained by assuming a Gamma distribution.

The VPA model requires the tuning of some free parameters in order to get a suitable accuracy in the solutions (Postma, Wilson, and Yee, 2011): the Kolmogorov constant C_0, that influences the Lagrangian integral time scales, the Richardson-Obukhov constant C_r and the micro-mixing constant μ_t, that affect the micro-mixing time, the initial source distribution σ_0, that depends on the source diameter d_s.

We performed some preliminary numerical simulations to suitably set such parameters. Table 4.1 summarises the values adopted in the simulations in order to have a satisfactory agreement with the measurements.

In the VPA model the concentration at the source is approximated by a cylindrical top-hat distribution of size equal to $\sqrt{12}\sigma_0$ (Marro et al., 2018), as:

$$C_{src,VPA} = \frac{Q}{\frac{\pi}{4}(12\sigma_0^2)w_s}\,, \tag{4.25}$$

where Q is the source mass-flow and w_s is the emission velocity.

4.3.3 Results

First order moment

In this paragraph we compare the first order moment of the concentration and the plume centreline of the experiment with the ones provided by Ventjet and SLAM.

The Ventjet simulation is set on the real case scenario parameter reported in Table 3.2, with the vertical release of a gas mixture at the source with: 92.5% CO2, 6% air, 1.5% C_2H_6 of 42.94 molecular weight. The release rate is set at 47.85 kg/s with a temperature of 19.8°C. The source diameter and elevation are 1.2 m 7.6 m respectively, the ambient air temperature is 20.0°C and the wind velocity at $z_{ref} = 10m$ is 10.7 m/s, D stability class and surface roughness $z_0 = 0.0113\,m$.

The set-up parameters in the SLAM simulations are the same of the experimental configuration (Table 3.2). The particles number is of the order of magnitude of 10^9, sufficiently large to neglect the statistic error on the concentration and velocity

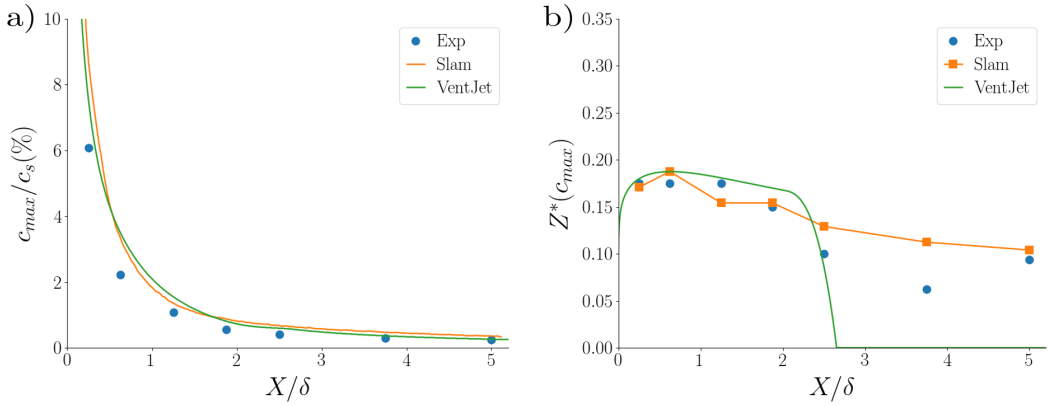

Figure 4.2: Longitunal profiles of a) the maximum concentration normalised over the concentration at the source c_{max}/c_s (in percentage) and b) its corresponding height $Z^*(c_{max})$ for the model SLAM and VentJet compared to the experimental results.

moments. The time step is 1000 time smaller than the macroscale Lagrangian times. The wind velocity profiles is considered uniform, interpolated with a power law function as described in Section 3.4.

The results concerning the maximum concentration c_{max} normalised over the source concentration c_s (Fig. 4.2.a) show that both Ventjet and SLAM succeed in reproducing the experimental longitudinal profile. It worth noting that the percentage of concentration decreases with an exponential-like trend and it drops at 6% at the first measurement section, corresponding in the real case scenario to 2 m from the source over 40 m of the total longitudinal section, meaning that the dispersion process is fast and effective. In Figure 4.2.b is reported the dimensionless height of the maximum concentration $Z^*(c_{max})$. In proximity of the source and in the middle field both models are in good agreement with the experimental data, indicating a reliable simulation of the mean concentration field of the heavy gas emission. When the lower bound of the plume touches the ground (around $X/\delta = 2.5$), Ventjet does not take into account the plume reflection and underestimates the height of the plume centreline, placing it on the ground. However, the estimate of the distance touchdown along X is quite precise. The SLAM model is consistent with the experimental results also in the far field. It differs from the measured $Z^*(c_{max})$ at $X/\delta = 3.75$, this point is probably affected by the local variability that characterise both the measurements and the particle model, otherwise the simulation is consistent. SLAM results allow us to compare for each measurement section the vertical profiles of $\overline{c^*}$ (Fig. 4.3), showing a general good agreement between the numerical and the wind tunnel data. Therefore, we interpolate these profiles with a Gaussian curve, estimating the height of the centre of mass (Eq. 3.9), obtaining similar values for both SLAM and experimental results (Fig. 4.4).

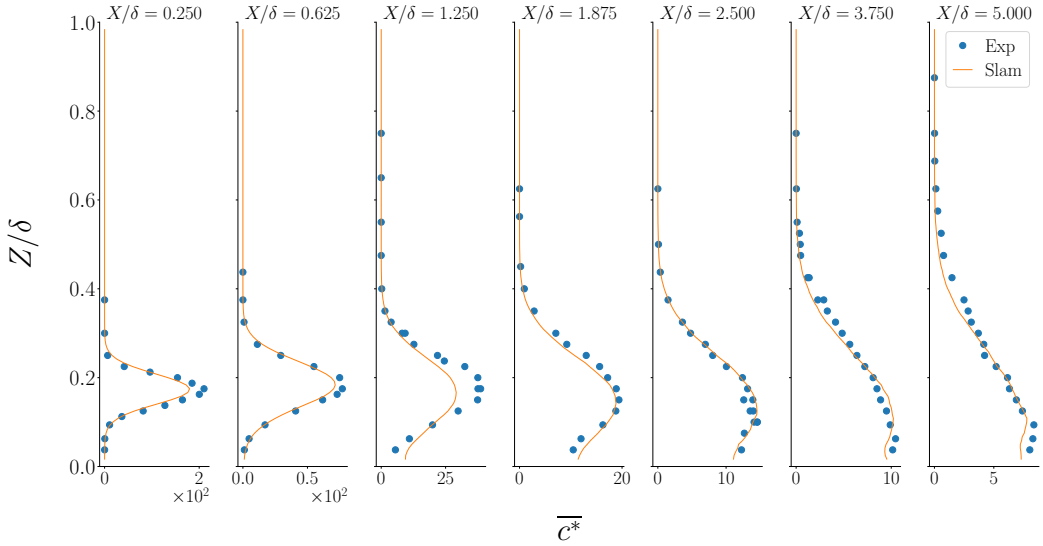

Figure 4.3: Vertical profiles of dimensionless mean concentration, experiment vs. SLAM model

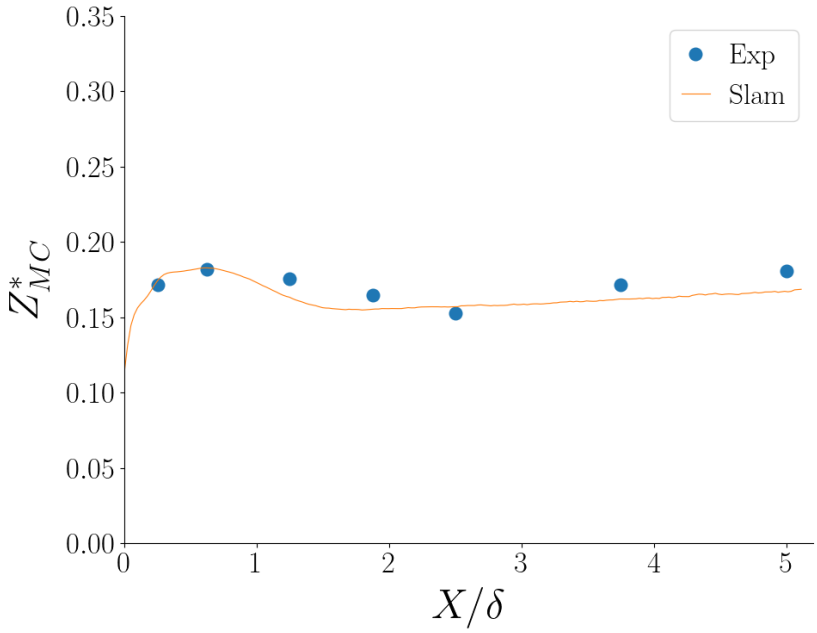

Figure 4.4: Longitudinal profiles of the dimensionless height of the centre of mass Z_{MC}, experiment vs. SLAM model

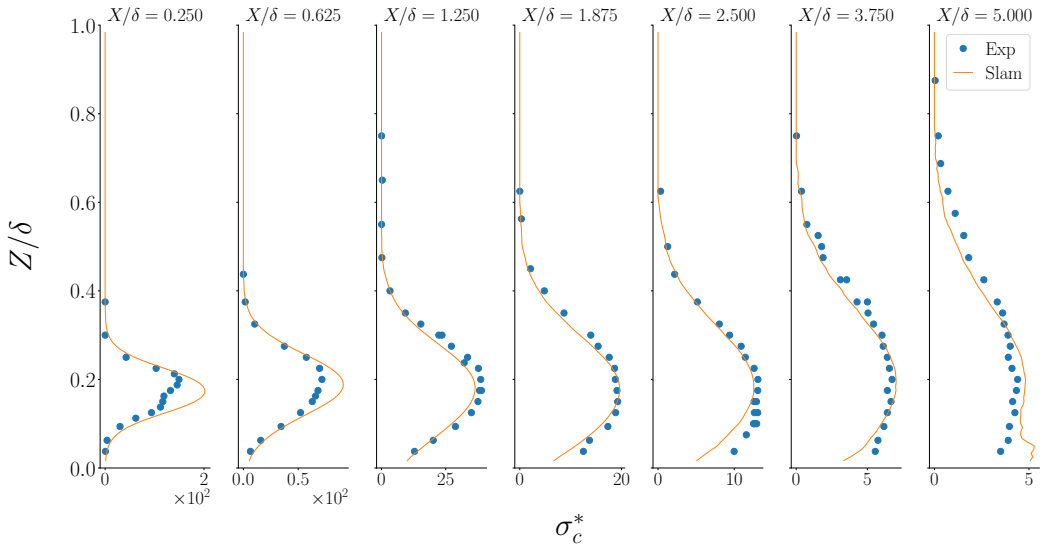

Figure 4.5: Vertical profiles of dimensionless concentration standard deviation, experiment vs. SLAM model

Higher order moments

The second order moment of the concentration is provided by SLAM simulation, only. Vertical profiles of σ_c^* are reported in Figure 4.5. In the first two sections, the maximum of the concentration standard deviation is slightly overestimated, whilst the fitting of the vertical distribution is acceptable. The SLAM model uncouples the concentration and the velocity field and it does not take into account the effect of the momentum emitted by the source on the velocity field. In the wind tunnel experiments, in proximity of the source, this effect is not negligible and reduces the concentration fluctuations. For this reason, in the first two sections, the value of σ_c^* estimated with SLAM is higher than that in the experiments.

The 3rd and 4th order moments of the concentration field are not directly evaluated by the Lagrangian model and they can be estimated knowing that the PDF of the concentration field can be described by a family of one parameter Gamma distribution (Eq. 3.15). The analysis of the 3rd and 4th order moment of the concentration field has been performed by comparing the experimental m_{3c}^* and m_{4c}^* (Eq. 3.7) with the corresponding moment of a Gamma distribution, defined as a function of the concentration mean and standard deviation (Eq. 3.16 and 3.17). In Figure 4.6 are reported vertical profiles of the 3rd and 4th order moment of the concentration near the source at $X/\delta = 0.0625$ (Fig. 4.6 a,b), in the middle field at $X/\delta = 1.875$ (Fig. 4.6 c,d) and in the far field at $X/\delta = 3.750$ (Fig. 4.6 e,f). As discussed in Section 3.5.2, the higher order moments estimated with the Gamma distribution form the experimental values of $\overline{c^*}$ and σ_c^* are in generally good agreement with the measured moments (reported in light blue, respectively round points and dotted line) in the middle and far field. The profiles of m_{3c}^* and m_{4c}^* obtained from the concentration and standard deviation of numerical simulation and the Gamma distribution model are highly

overestimated near the source, while they show good agreement in the middle and far field. As discussed before for σ_c^*, higher differences in proximity of the source are due to the uncoupling of the velocity and concentration field in SLAM, that leads to moments overestimation.

In order to study the global behaviour of the model, we focus on the longitudinal profiles of the first four moments of the concentration at the height of the centre of mass Z_{MC} (Fig. 4.7). The comparison between the measurements and the numerical results enlighten that the SLAM simulation is able to compute very accurate solutions for the mean concentration (Fig. 4.7.a). The agreement of the intensity of the fluctuation profiles is satisfactory in the middle and far field, while in the first two sections the evaluation of σ_c^* is overestimated and in the third $\overline{c^*}$ is underestimated, leading to higher values of i_c^* (Fig. 4.7.b). For the 3rd and 4th order moments (Fig. 4.7.c and Figure 4.7.d, respectively), the model significantly overestimates the experimental values near the source and in the middle field whilst it shows a good agreement in the far field, following a distribution similar to i_c^*. We estimate the concentration field skewness $Sk_c = \frac{m_{3c}^{*3}}{\sigma_c^{*3}}$ and kurtosis $Ku_c = \frac{m_{4c}^{*4}}{\sigma_c^{*4}}$ (Fig. 4.7.e and Figure 4.7.f, respectively). In this case, the differences observed before are amplified due to the raise a power of σ_c^* that increases the statistics values in all the domain.

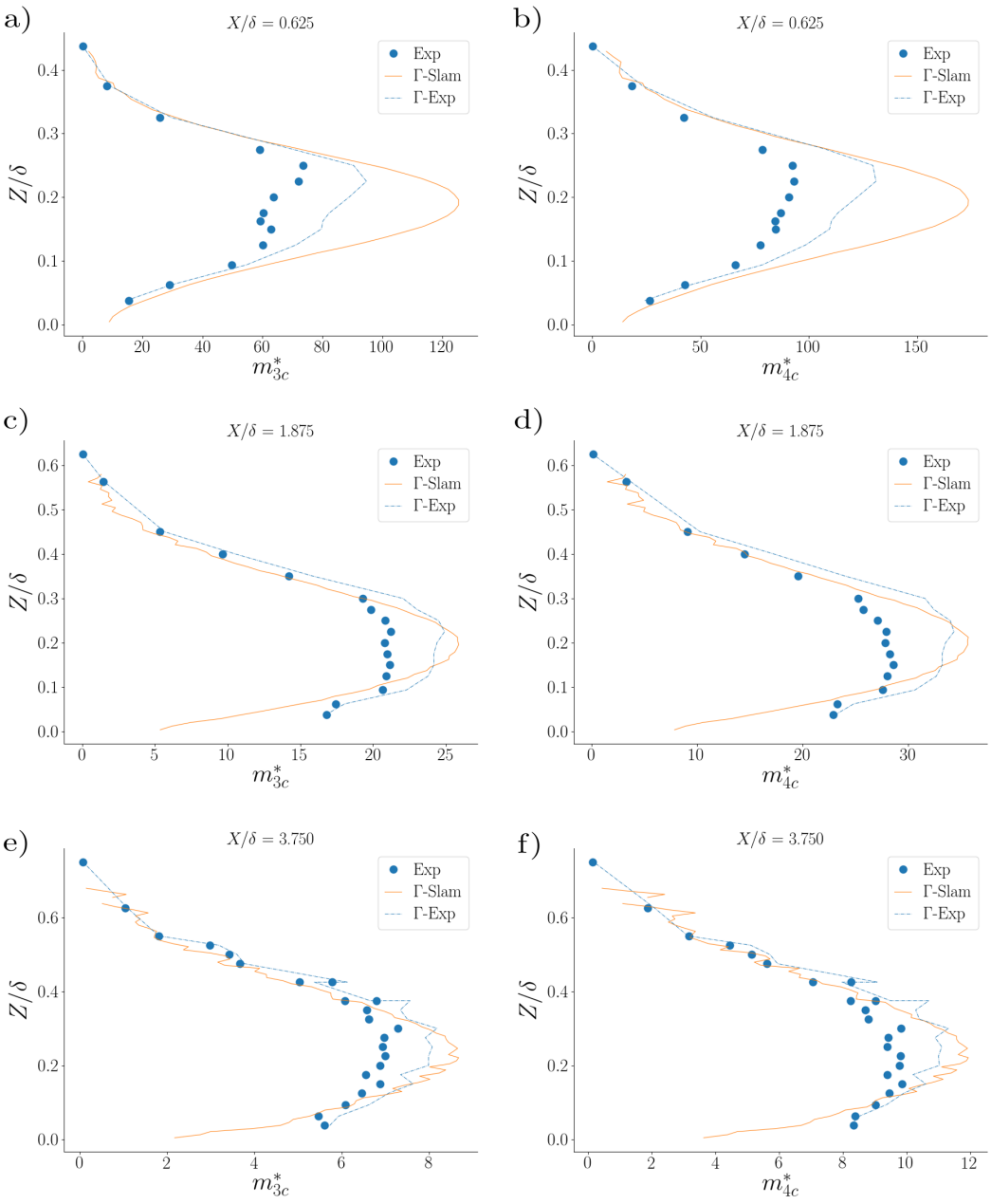

Figure 4.6: Vertical profiles of the dimensionless moment of 3rd and 4th order a), b) near the source c), d) in a middle section and e), f) in the far field. The experimental results are compared with the moment estimated as moment of a Gamma distribution in function of concentration mean and standard deviation obtained from model SLAM and experiment.

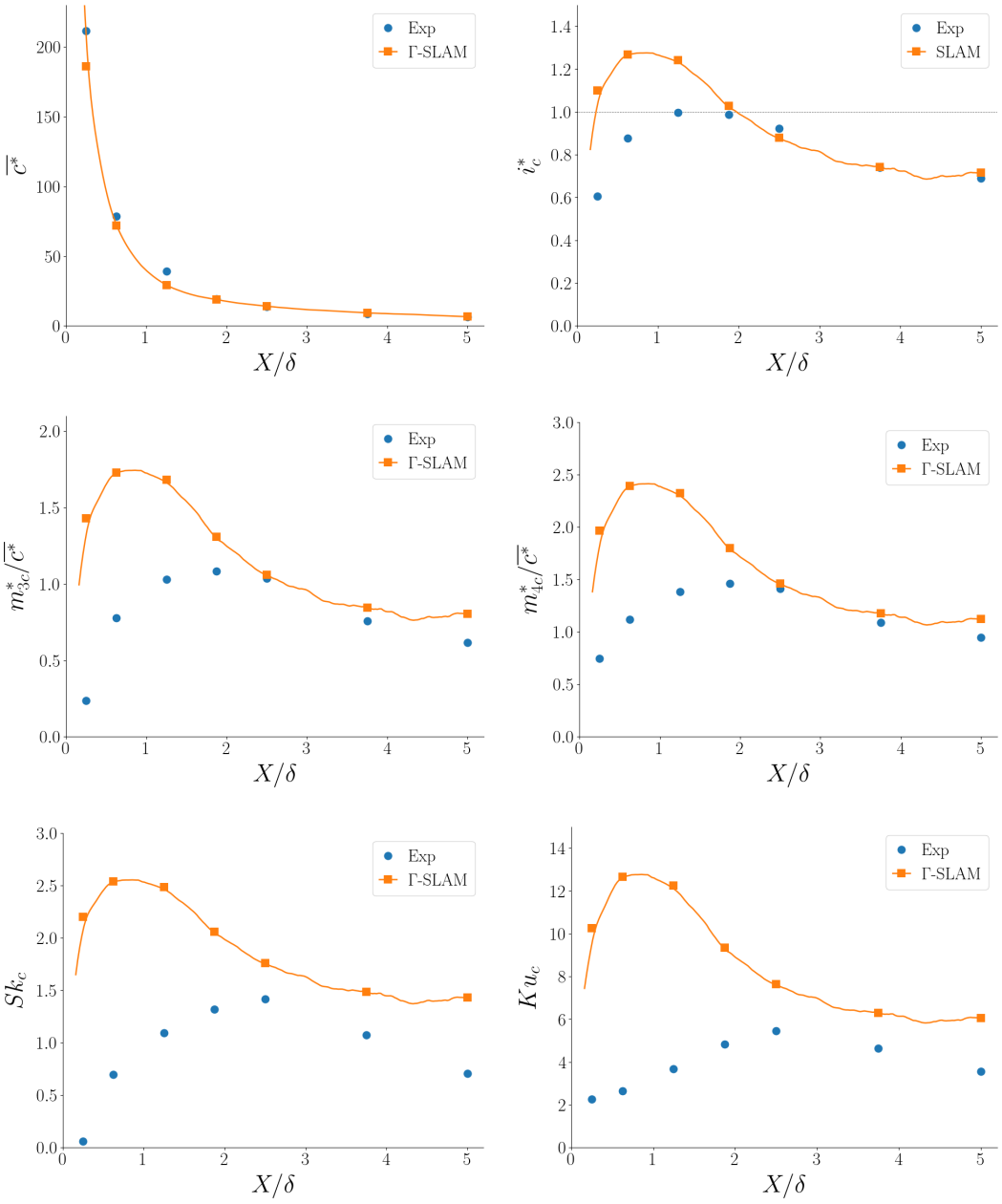

Figure 4.7: Longitudinal profiles of the experiment results vs. SLAM in the centre of mass of the dimensionless a) mean concentration $\overline{c^*}$, b) intensity of fluctuation i_c^*, concentration moment of c) 3rd order and d) 4th order normalised over the mean concentration, concentration e) Skweness and f) Kurtosis.

4.4 Concentration time series

In the risk assessment of atmospheric pollutant dispersion, the knowledge of the temporal dynamics of the concentration is important as well as the insight on the concentration statistics. The level crossing is particularly relevant in case of toxic, inflammable or explosive substance, in which case even a local excess of the concentration threshold limit can lead to fatal consequences. In case of toxic substances, the exposure time plays a crucial role in the risk management. Therefore, we consider the work of Bertagni et al. (2020) for the estimate of the level crossing time and rate. They provide a simple stochastic model for the concentration dynamics of a passive scalar emitted from a localised source in a neutral boundary layer. Through this model, they are able to estimate in close form for a given concentration level the crossing rate N_ϕ^+, defined as the mean frequency of passing the threshold, and the crossing time T_ϕ^+ which is the relative average time spent above it. Three concentration statistics are needed as model inputs: the mean, the standard deviation, and the integral time scale. We analyse the crossing rates and times based on the work of Bertagni et al. (2020), comparing the experiments with the model results, estimated using the experimental statistics and the ones obtained from the Lagrangian stochastic model.

4.4.1 Compound Poisson Process

Turbulent dispersion of a fluctuating plume is driven by two physical processes: the transport by turbulent eddies of the plume centre, called meandering, and the relative dispersion around it (Gifford, 1959). The first process is dominant near the source, where the size of the plume is small enough to be transported as a whole by turbulent eddies. In the far field, the plume spreads reaching dimension that are higher than these eddies, therefore the meandering is negligible compared to the relative dispersion and the plume is blended following concentration gradients. In the middle field, both process occur influencing the concentration dynamics. Bertagni et al. (2020) define a stochastic model for the concentration dynamics that takes into account the two physical processes and guarantees the Gamma distribution Eq. 3.15 as the steady-state PDF. This model is based on the Compound Poisson Process (CPP) with linear losses:

$$dc = -\frac{c}{\vartheta}dt + d\zeta, \tag{4.26}$$

where t is time, ϑ is the integral time scale and $d\zeta$ is a white shot noise, which represents the variation induced by turbulent eddies. The shot intensity and the time interval between subsequent shots are extracted from space-dependent exponential PDFs with mean values $\sigma_c^2/\bar{c}$ and $\vartheta\sigma_c^2/\bar{c}^2$, respectively (Laio et al., 2001). The shot can be interpreted as effect of meandering, while the deterministic part of Eq. 4.26 recalls the relative dispersion models or micro-mixing (Section 3.9) but without the relaxation of the concentration towards a mean value.

From the CPP model, Bertagni et al. (2020) propose to estimate in closed form the upcrossing time T_ϕ^+, which is the time average concentration stays above a certain threshold level ϕ:

$$T_\phi^+ = \vartheta e^{\phi\, k/\bar{c}} E\left[1-k, k\,\phi/\bar{c}\right], \tag{4.27}$$

where $k = i_c^{-2} = (\bar{c}/\sigma_c)^2$ is the parameter of the Gamma distribution, $E[n,m] = \int_1^\infty exp[-ms]/s^n ds$ is the exponential integral function (Abramowitz and Stegun, 1964). Likewise, it is possible to determine the crossing rate N_ϕ^+, defined as the mean frequency of crossing the threshold level ϕ:

$$N_\phi^+ = \frac{P_\phi^+}{T_\phi^+} = \frac{(k\phi/\bar{c})^k\ e^{-k\,\phi/\bar{c}}}{\vartheta\,\Gamma[k]}, \tag{4.28}$$

where P_ϕ^+ is the probability of $C > \phi$, knowing from the PDF distribution equation (Eq. 3.15). Observing Eq. 4.27 and 4.28, it is clear that we need only the concentration mean and standard deviation and the integral time scale to evaluate upcrossing times and rates.

The integral time scale

The integral time scale ϑ is defined as the integral of the autocorrelation function of c and can be interpreted as the temporal memory of the one-point concentration dynamics (Ridolfi, D'Odorico, and Laio, 2011). This Eulerian time-scale is usually defined through an empirical relationship that links it to the plume size and the mean velocity $\overline{u}$ (Iacono and Reynolds, 2008; Cassiani, Franzese, and Albertson, 2009; Wilson, 2010). The temporal correlation of the concentration signal is related to the plume spread. As a general behaviour, where the meandering motion dominates, the correlation of the concentration time series is very low. As the plume spreads and the relative dispersion become the main mechanisms, the temporal correlation increases. We estimate the integral time scale ϑ with a model that takes into account the vertical anisotropy of the turbulent field and the presence of the ground as lower boundary, adopting the vertical spread of the plume σ_z as the spatial scale of references. The relationship proposed by Bertagni et al. (2020) is:

$$\vartheta = \alpha_3 \frac{\sigma_z}{\overline{u}_{MC}}(1 + r_\vartheta), \tag{4.29}$$

where $\alpha_3 = 0.4$, $\overline{u}_{MC}$ is the mean velocity at height of the centre of mass and the term $r_\vartheta = \sigma_z/z$ stands for the reflection induced by the ground, which smooths the concentration fluctuations and increases the concentration autocorrelation.

4.4.2 Results

We analyse the one-point concentration signal of the heavy gas experiment to estimate the upcrossing time and rate of a certain threshold ϕ. Referring to Figure 4.8, we

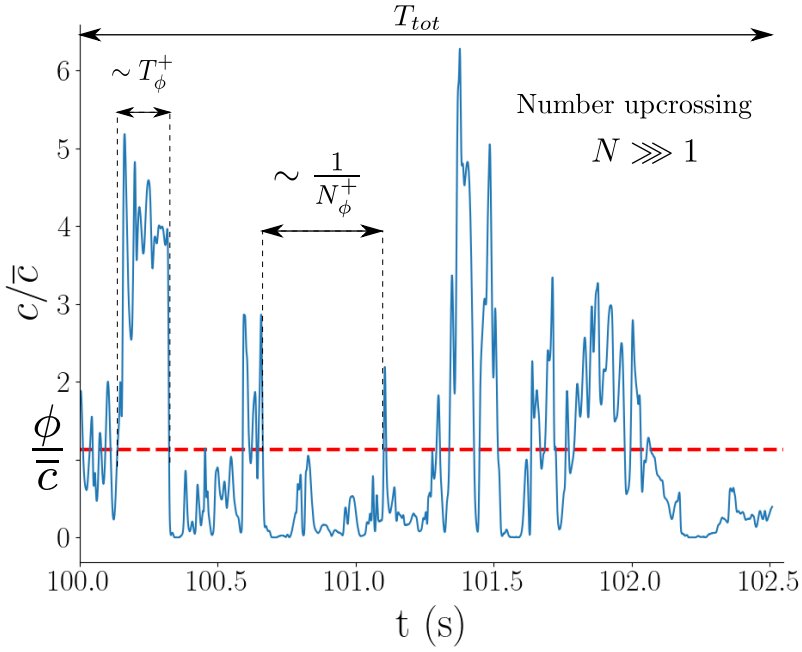

Figure 4.8: Schematic representation of the concentration signal, the threshold level ϕ, the upcrossing time T_ϕ^+, the upcrossing frequency N_ϕ^+, the signal duration T_{tot}, when the number of the upcrossing concentration is $N \ggg 1$.

evaluate:

$$T_\phi^+ = \sum_{i=1}^{N} \frac{T_i}{N}, \tag{4.30}$$

$$P_\phi^+ = \sum_{i=1}^{N} \frac{T_i}{T_{tot}}, \tag{4.31}$$

$$N_\phi^+ = \frac{P_\phi^+}{T_\phi^+} = \frac{N}{T_{tot}}, \tag{4.32}$$

where T_i and N are the interval of time and the number of the upcrossing concentration, respectively, and T_{tot} is the signal duration.

Furthermore, we estimate T_ϕ^+ and N_ϕ^+ from Eq. 4.27 and 4.28 respectively, using two set of parameters $\bar{c}$, σ_c and ϑ (Eq. 4.29): the first with the experimental results and the second with the values obtained from the SLAM simulation. We compared the validity of Eq. 4.27 and 4.28 with the wind tunnel data taken at the centre of mass of the plume (Fig. 4.9) for a section close the source ($X/\delta = 0.625$), in the middle ($X/\delta = 1.875$) and in the far field ($X/\delta = 3.75$). The upcrossing time (Fig. 4.9.a,c,d) and rate (Fig. 4.9.b,d,e) are estimated at different concentration level ϕ, normalised by $\bar{c}$. For what we showed in Section 3.5.2 close the source ($X/\delta = 0.625$) the PDF on the one-point concentration is not suitably modelled by a Gamma distribution. We would therefore not expect the prediction of the CPP process, even when fed by parameters directly estimated by experimental data series, to be accurate both for upcrossing time and rate. As shown by Figure 4.9.a and 4.9.b this lack of accuracy

is slight for T_ϕ^+ and much more evident for N_ϕ^+. Surprisingly, when adopting model parameters computed by the output of the Lagrangian model SLAM, the prediction of T_ϕ^+ fits better the experimental data. This good accuracy has however to be interpreted as the effect of two independent errors: the first related to the model for the shape of the concentration PDF, the second to the estimate of the concentration variance (which is overestimated by SLAM in the very near field). Instead, in case of the average frequency N_ϕ^+, the combined effects of these two sources of error further deteriorate the model predictions. Indeed, as shown in Figure 4.9.b, estimates of N_ϕ^+ provided by Eq. 4.28 fed by SLAM output, tend to systematically overestimate N_ϕ^+ for concentration level $\phi/\bar{c} > 2.5$. Further away from the source the difference between the CPP process with the experimental and SLAM parameters decrease for both T_ϕ^+ and N_ϕ^+. Observing Figure 4.9.c,d,e and f is necessary to pay attention to the logarithmic scale of the ordinate axis, the difference between the curves decreases, even if the distance between them is higher. We observe an overall good agreement between the CPP process and the experimental results.

Considering that the integral time scale is also estimated from an analytical model, the CPP process is a robust model to estimate T_ϕ^+ and N_ϕ^+. At high value of $\phi/\bar{c}$ the wind tunnel data show some discontinuity, it is possible to reduce this effect by performing one-point measurement for longer time, that has not be planned as a part of this work.

4.5 Conclusions

In this study we compare our experimental data to an integral model, Ventjet, and a Lagrangian particle model, SLAM. Both models, requiring small computational costs, give insight on the first order statistics that are in good agreement with experimental results. The trajectory of the plume is better described by SLAM, that takes into account the reflection on the ground. From the SLAM simulation it is possible to evaluate the higher order moments: σ_c^* is directly estimated by the micro-mixing module and the 3rd and 4th order moments are obtained with the assumption that the PDF is a Gamma distribution. This last assumption has been proven in Chapter 3 to be in good agreement with the wind tunnel data of a heavy gas release sufficiently further from the source. The higher order moments are consistent with the experimental results, with the exception of the first two sections close to the source. In this region, not only the Gamma distribution does not describe the concentration PDF (making unreliable the estimation of m_3^* and m_4^*) but, furthermore, the maximum of the σ_c^* is overestimated. The reason is that in the wind tunnel experiment, in proximity of the source, the momentum emitted by the source affects the velocity field and reduces the concentration fluctuations, while the SLAM model does not take into account this effect, uncoupling the concentration and the velocity fields. Taking into account the significant small running time of the numerical simulation with SLAM and the good agreement with the experimental results, the Lagrangian stochastic model is a reliable

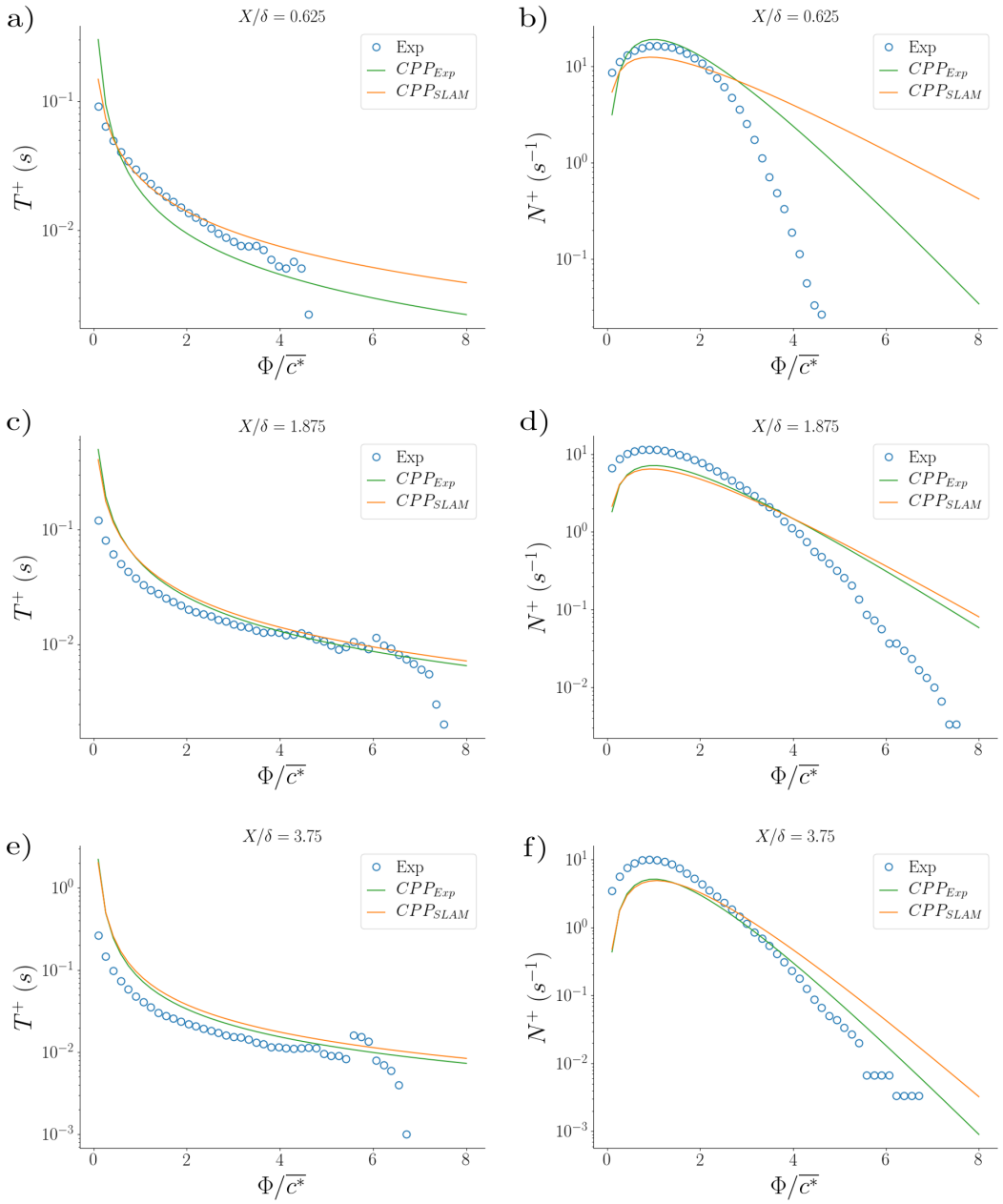

Figure 4.9: a) c) e) Upcrossing times and b), d), f) rates in function of the threshold ϕ (normalised over the mean concentration) in proximity of the source ($X/\delta = 0.0625$), in the middle field ($X/\delta = 1.875$) and in the far field ($X/\delta = 3.75$). Experimental results are compared to the ones of the CPP model, obtained with the experimental value of $\overline{c^*}$ and σ_c^* (CPP_{Exp}) and with the mean concentration and standard deviation estimated by SLAM (CPP_{SLAM}).

option for the estimation of the dispersion dynamic of a heavy gas plume emitted from an elevated source. To complete the model information with the structure of concentration time series, we estimate the crossing time T_ϕ^+ and frequency N_ϕ^+ of a concentration threshold and we compared it with the results obtained from the model of Bertagni et al. (2020). The latter applies the CPP process and estimates T_ϕ^+ and N_ϕ^+ using three parameters, the mean, the standard deviation and the integral time scale of the concentration signal. Comparison with the experimental results are in good agreement with the model, fed by both experimental and SLAM simulation $\overline{c^*}$ and σ_c^*, proving to be a robust method to estimate T_ϕ^+ and N_ϕ^+. Further analysis can be made by validating the model for the integral time scale ϑ, comparing it to the one estimated as the auto-correlation of the experimental concentration signal, that has not been included in this work.

Chapter 5

Conclusions

To fulfill the requirements for the risk assessment of heavy gas releases in industrial environment it is necessary to understand the physics of the atmospheric dispersion of gas heavier than air. The aims of this work were to investigate the turbulent dispersion dynamics of an elevated heavy gas emission by means of wind tunnel experiments and to test the ability of operational dispersion models in simulating these phenomena. In particular, we focused on three main issues:

- the metrological aspect related to the measurements within plumes that have density other than air;
- the analysis of the results of an experimental campaign simulating a heavy and a passive gas release, highlighting their main differences;
- the simulation of these releases by means of operational models.

The scenario of interest has been defined with the industrial partner Air Liquide as the emission from an Air Separation Unit (ASU) that releases O_2 at a temperature of -40°C in the atmospheric boundary layer. We simulated it in a reduced scale model in the wind tunnel facilities of the LMFA, where the inflow condition has been set to reproduce a fully developed turbulent BL over a rough surface in neutral condition. From an elevated source we released a mixture of CO_2 and ethane, the latter used as a tracer in concentration measurements, with density $\rho_s \approx 1.5\rho_a$. To reproduce a passive scalar release, a mixture of air and ethane has been released under the same flow and emission set-up, obtaining a dataset to compare with the results of the heavy gas plume.

The risk assessment of heavy gas release required to correctly estimate the intensity of the concentration fluctuations and their interactions with the velocity fluctuations. For this reason, we employed a coupled system HWA-FID to characterise the pollutant plumes downwind the source by measuring simultaneously the concentration and the velocity field. Since this experimental technique is sensitive to the density gradients within the plume, a specific calibration procedure had to be defined. We analysed the FID response in function of the density of the mixture and $r = C_{CO_2}/C_{C_2H_6}$, identifying a critical density that correspond to $\Delta\rho = 30\%\rho_a$. For a density of the mixture below this value, we could define a one-to-one function to calibrate the FID. The HWA response depended on both the flow control velocity and the density of the

gas mixture. We defined a calibration procedure aiming at estimating a calibration surface, to take into account the dependence on both quantities. We tested the reliability of our measurements by evaluating the total mass fluxes in the cross-flow section. The results verified the mass conservation for both passive and heavy gas plumes, proving that the calibration procedure for heavy gas did not increase the uncertainty of the coupled measurements.

Analysing the results, the focus was set on the mean concentration field and its higher-order moments, the concentration PDFs and the turbulent mass fluxes, characterising the spectra, the turbulent kinetic energy exchange, the mixing on large and small scale, as well as the temporal structure of the signal.

The mean concentration vertical profiles showed how the plume of gas heavier than air developed closer to the ground. Comparing σ_c with $\overline{c}$, we identified the border of the plume as the region where entrainment of air into the plume was predominant for both passive scalar and heavy gas. From the Gaussian interpolation of the mean concentration profiles, we estimated the height of the centre of mass and the vertical and transverse spread. The longitudinal profiles of Z_{MC} highlighted the vertical displacement of the heavy gas plume compared to the passive scalar plume, whereas the values of σ_z and σ_y were similar in both cases, suggesting that the vertical dispersion was not influenced by buoyancy effects.

We analysed the correspondence between the fluctuation intensity i_c, defined as the ratio of σ_c and $\overline{c}$, to the concentration PDFs, verifying that it was possible to model the concentration distributions by a family of one parameter Gamma distribution. In this way, we related i_c and the concentration PDFs to understand if the dispersion dynamics of the plume centre was driven by the meandering motion or the relative dispersion. Furthermore, knowing the mean and the standard deviation of the concentration field, we were able to estimate the higher order moments. The comparison between m_3^* and m_4^* directly measured in the wind tunnel and those obtained from the Gamma distribution model, showed a general good agreement in the middle and far field. In proximity of the source, instead, the Gamma distribution model did not fit the measured moments, due to the effect of the momentum and buoyancy emitted by the source on the concentration field.

Simultaneous measurements of concentration and velocity allowed us to obtain vertical profiles of vertical and longitudinal turbulent mass fluxes. Near the source, the dispersion dynamic was significantly influenced by the plume emission velocities, with sharper profile of $\overline{w'c'}$ and $\overline{u'c'}$. Observing the mean concentration profiles, we noticed that $\overline{w'c'}$ has counter gradient vertical evolution, hence, by applying a standard closure hypothesis, we were able to estimate the turbulent dispersion coefficient for each profile, and evidence its enhancement for increasing distance from the source. The longitudinal profile of D_t were similar for the heavy gas and the passive scalar release, therefore, they were not influenced by buoyancy effects, in agreement with the vertical and transverse spread results.

The analysis of the mean TKE equation allowed us to verify the balance between

production and dissipation away from the source, with no significant difference for a plume of gas heavier than air. Moreover, for the heavy gas emission case, we estimated the flux Richardson number, identifying a stable condition in the upper part of the plume and an unstable condition near the ground, and the bulk Richardson number, relating it to the critical value of the Richardson gradient number $R_{ig} \approx 0.2 - 0.25$. We observed that $R_{ib} \ll 0.2$, meaning that the negative buoyancy did not affect the dynamics of the turbulence within the plume.

We analysed the dissipation, transport and production terms of the concentration variance equation and we identified two robust methods to estimate $\varepsilon_{\sigma_c^2}$: the first by assuming the Taylor's hypothesis of frozen turbulent and the isotropic approximation, and the second by fitting the one-dimensional spectra of the concentration in the inertial subrange. The results of the two methods showed a general good agreement, except close to the source, where the homogeneity and isotropy conditions were affected by the momentum emitted by the source.

The micro-mixing time scale of the plume was estimated applying the IEM and the IECM models and compared to the turbulent time scale. The values of τ_m obtained with the two models showed a general good agreement in all the domain and asymptotically tended to a typical turbulent scale $\tau = k/\varepsilon$ in the far field, where the relative dispersion drove the mixing mechanisms.

The data collected during the experiments on the heavy gas release was used to test and validate two operational dispersion models: Ventjet, an integral model developed by Air Product and Air Liquide, and SLAM, a Lagrangian particle dispersion model developed by the team AIR of the École Centrale de Lyon. Both models have small running time and computational costs, making them suitable tools for the risk assessment of pollutant dispersion in the industrial domain. The mean concentration and the trajectory of the plume, estimated by the models, were in very good agreement with the experimental results. The trajectory of the plume was better simulated by SLAM, that takes into account the reflection on the ground.

The evaluation of the higher order moments was possible from the results of SLAM: σ_c was directly estimated during the simulation and the 3rd and 4th order moments were obtained with the assumption that the PDF was a Gamma distribution, which was verified in the middle and far field during the analysis of the wind tunnel results of a heavy gas release. The higher order moments were consistent with the experimental results, with the exception of the first two sections close to the source. In this region, not only the Gamma distribution does not describe the concentration PDF making unreliable the estimate of m_3 and m_4, but, furthermore, the maximum of the σ_c was overestimated. The reason was that in the wind tunnel experiment, in proximity of the source, the momentum emitted by the source affected the velocity field and reduced the concentration fluctuations, while the SLAM model did not take into account this effect.

We completed the study by investigating the structure of the concentration time series, estimating the level crossing time T_ϕ^+ and frequency N_ϕ^+ of a concentration

threshold ϕ. The results were compared with the ones obtained from the model of Bertagni et al. (2020), who applied the CPP process and estimated T_ϕ^+ and N_ϕ^+ using three parameters, the mean, the standard deviation and the integral time scale of the concentration signal. The integral time scale ϑ was evaluated from an analytical model as a function of the vertical spread of the plume σ_z, considered the spatial scale of references. Therefore, the model took into account the vertical anisotropy of the turbulent field and the presence of the ground as lower boundary. Comparison with the experimental results were in good agreement with the model, fed by both wind tunnel and SLAM simulation $\overline{c}$ and σ_c, proving to be a robust method to estimate T_ϕ^+ and N_ϕ^+.

Further analysis can be made on the concentration PDFs, estimating them with the SLAM mean and the standard deviation and comparing them with the experimental PDFs. Moreover, comparing the integral time scale ϑ estimated with the presented model and the experiments results, obtained as the auto-correlation of the experimental concentration signal, is a useful information for the model validation, and will be included in future studies.

The wind tunnel experiments proved that the trajectory of the heavy gas plume, emitted from an elevated source, was affected by buoyancy effects, whereas its turbulent dispersion was unaltered compared to the passive scalar. For this reason, operational models, validated to simulate passive scalar release, were employed with success to model the heavy gas releases from an elevated source. These models considered the gravitational effect on the vertical displacement on the plume centreline, reproducing with good agreement the trajectory, the mean concentration and the higher order moments of the wind tunnel experiments.

The configuration of an elevated source has been chosen as a typical industrial scenario that is widely employed for the validation of atmospheric dispersion models. Further studies are needed to investigate the concentration and velocity fields in case of a ground level source of heavy gas. In this case, we expect the plume to be characterised by larger density differences, with more relevant effects of buoyancy on the velocity field and the turbulent mass fluxes. These larger buoyancy effects may imply a higher complexity in modelling these release, since it may not be possible (as we did for the case studied here) assume that the velocity field driving the dispersion is not affected by the presence of the heavy plume, i.e. no feedbacks between plume and atmospheric flow. The modelling of these releases will then necessarily have to be simulated with CFD codes, that are able to reproduce the fluctuations of the concentration on the velocity field and their interactions. Other studies that still need to be performed concern the effects of obstacles on the turbulent dispersion of heavy gas plumes, aspects that have been so far rarely investigated in the literature. (i.e. Robins, Hayden, and Wingstedt, 2016; Merlier, Jacob, and Sagaut, 2019)

Appendix A

Signal treatment

The recirculation of the air in wind tunnel leads to increasing value of concentration of the gas release in the flow, generating a time varying background concentration. As on example, in Figure A.1a is reported the FID raw signal E_c (Volt), with a zoom at low values. During the experiment campaign for each point of measurement, we determine the background noise (BG) at the beginning and at the end of the 5 minutes sampling. In order to do so, the emission at the source is stopped for $10s$ and then the FID measure the concentration for other $10s$. The initial and final background noises are linearly interpolate over time.

During the post-processing, we notice that in the first hours of measurements in the wind tunnel, the background noise is often lower than the measured concentration (Fig. A.1b). Observing the signal, we individuate a band of noise probably linked to the instrumentation noise. To take it into account we evaluate the noise upper bound, we calibrate as described in Chapter 2 and then we subtract it to the signal of concentration in Volt. Furthermore, we clipped the signal at zero in correspondence of the upper bound, resulting signal is reported in Figure A.2.

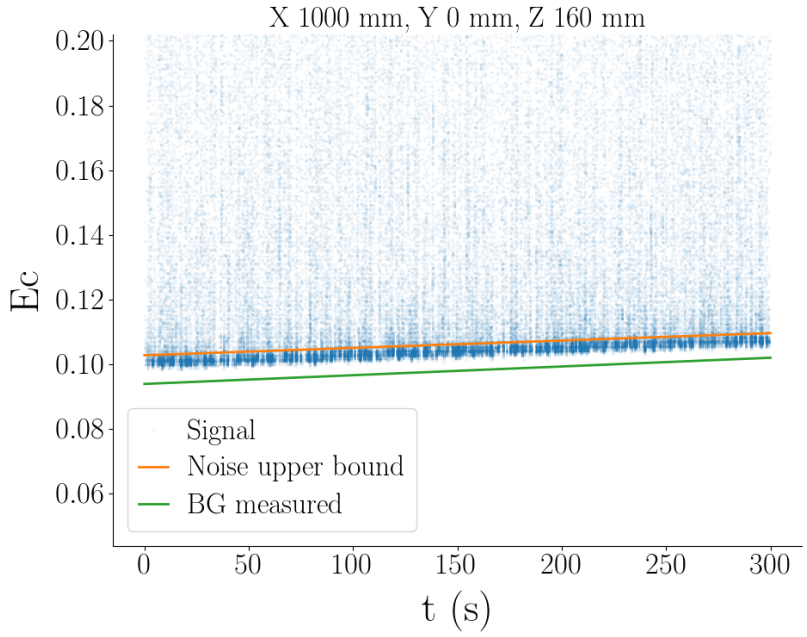

Figure A.1: FID raw signal (E_c) in Volt with background noise (BG) measured and upper bound noise estimated in post-processing.

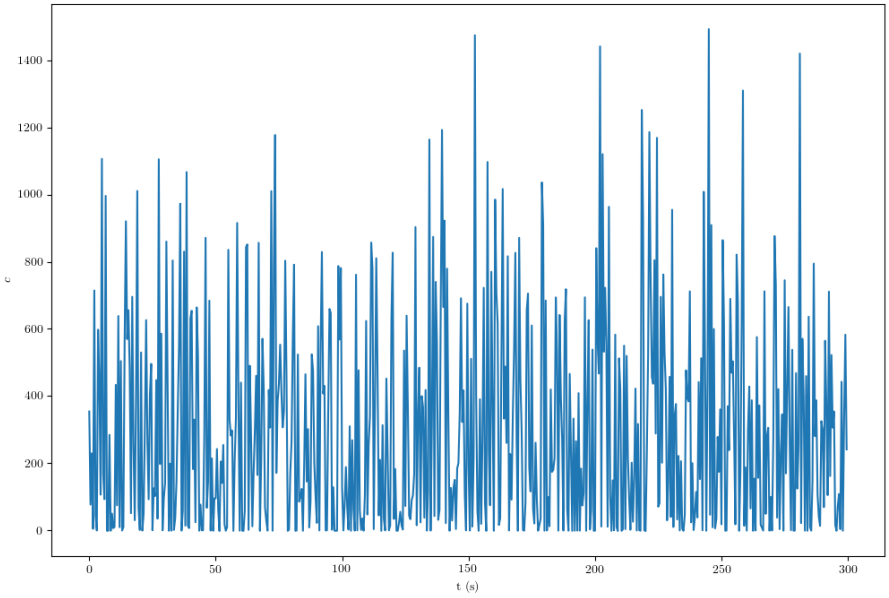

Figure A.2: Concentration signal in ppm after calibration and background noise substraction.

Appendix B

Dissipation evaluation through spectra analysis

The power spectral density PSD_k provides the distribution of energy in the wave number space. The measured function is decomposed into waves of different wavelength and the power spectrum is computed as the Fourier transform of the autocorrelation of the time series. If the autocorrelation is expressed in function of the spatial separation, the transform variable is the wave number k. In this study, the one-dimensional wave number spectra is evaluated with the Welch's method (Welch, 1967), that computes and estimates the PSD_k by dividing the data into overlapping segments (Hamming window), computing a modified periodogram for each segment and averaging the periodograms. In Figure B.1 are reported the power spectral density of the concentration and the velocity fluctuations in function of the wave number $k = 2\pi f/\overline{u}$, expressed in $(rad \cdot m^{-1})$ as a function of the frequency f and the local mean velocity $\overline{u}$. In this section the subscript 'u' and 'c' refers to the velocity and the concentration, respectively.

The u-spectrum (Fig. B.1.a), according to the Kolmogorov theory of isotropic turbulence (Kolmogorov et al., 1941), is divided into three ranges: the production range, that corresponds to the large scale spectrum where the turbulent energy is extracted from the mean flow by buoyancy and shear; the inertial subrange, that is conservative, no energy is added or dissipated by viscous forces yet handed down to

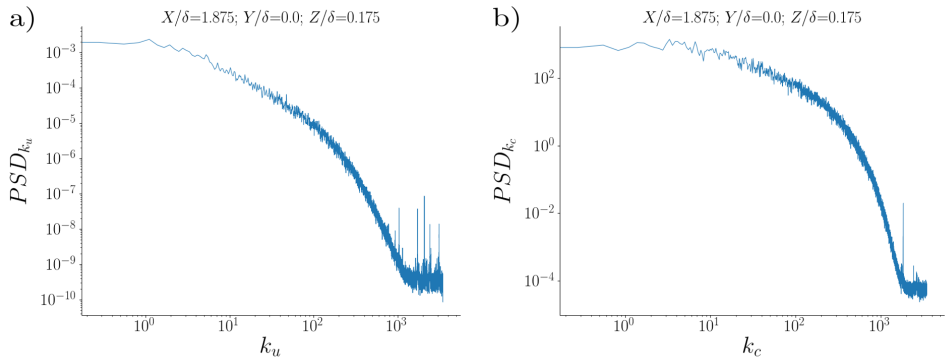

Figure B.1: Power spectral density in function of the wave number for a) velocity and b) concentration fluctuations.

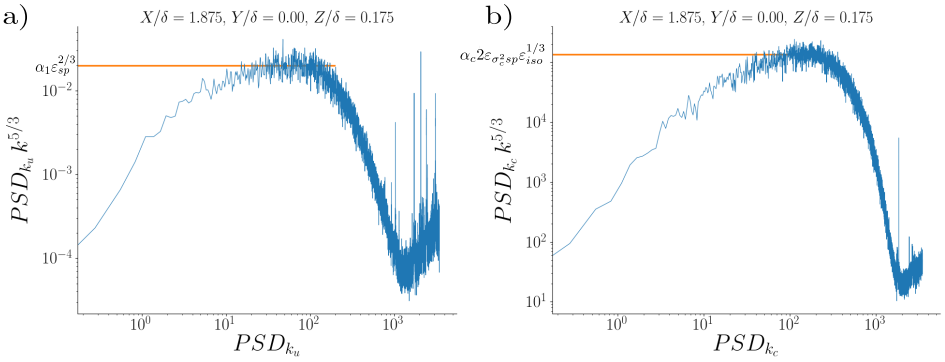

Figure B.2: PSD_k multiplied for $k^{-5/3}$ in function of PSD_k for a) velocity signal and b) concentration fluctuations.

smaller scales; the dissipation range, where kinetic energy is converted to internal energy. Since the inertial subrange is conservative and the dissipation correspond to the total amount of energy dissipated per unit mass and time (Tennekes and Lumley, 1972), it is possible to deduce the dissipation rate of the TKE by fitting the one-dimensional spectra of the velocity in this region, following the relation:

$$PSD_{k_u} = \alpha_1 \cdot \varepsilon_{sp}^{\frac{2}{3}} \cdot k^{-\frac{5}{3}}, \tag{B.1}$$

with $\alpha_1 = 0.5$ (Pope, 2000).

According to Tennekes and Lumley (1972), *"the scales of contaminant fluctuations range from the scale of the energy-containing eddies to a smallest scale that depends on the ratio of diffusivities"*. Therefore, for large Reynolds number, many of the concept applied to the PSD_k of velocity can be used for the spectra of the fluctuations of pollutant concentration (Fig. B.1.b). The dissipation rate of the concentration variance is estimated likewise ε_{sp}, by adopting the following relation with the one-dimensional spectra of the concentration:

$$PSD_{k_c} = \alpha_c \cdot 2\varepsilon_{\sigma_c^2 sp} \cdot \varepsilon_{iso}^{\frac{1}{3}} \cdot k^{-\frac{5}{3}}, \tag{B.2}$$

where $\alpha_c = 0.5$ is a constant (Warhaft, 2000). We employ the rate of dissipation obtained from Eq. 3.5 for the estimation of $\varepsilon_{\sigma_c^2 sp}$.

Eq. B.1 and Eq. B.2 follow the well know -5/3 power law, for which in the inertial subrange the u-spectrum should be proportional to $\varepsilon^{2/3} \cdot k^{-5/3}$ and, likewise, the c-spectrum proportional to $\varepsilon_{\sigma_c^2} \cdot \varepsilon^{\frac{1}{3}} \cdot k^{-\frac{5}{3}}$. To estimate the dissipation from the power spectra density, we plot the product between the spectra and the wave number elevated to the power of $-5/3$, as a function of the PSD_k, in this way we are able to evaluate the maximum of this function by averaging over a fixed interval, taking into account the noise. From the corresponding value, knowing Eq. B.1 and Eq.B.2, we obtain the estimate of ε_{sp} and $\varepsilon_{\sigma_c^2 sp}$.

Appendix C

Plume rise model

The plume rise model is based on an integral model that solves the mass, momentum and heat balance equations, as a Gaussian model ADMS (Atmospheric Dispersion Modelling System, Robins et al., 2009). Space and time averaging on the transverse sections of the plume are performed to estimate the variables of the plume dynamics. As customary, the entrainment mechanism is parametrised by an entrainment velocity, referred to as u_e. The velociy u_e linearly depends on the ambient turbulence and on the relative motion between the plume centre of mass and the external flow. Two more hypotheses are adopted: a) a circular section of the plume and b) the absence of feedback between the plume and the atmospheric turbulence. The latter assumption is acceptable if the plume dimensions are significantly lower than the BL height δ (Marro et al., 2013).

The integral plume rise model

The trajectory of the centre of mass of a plume emitted by an elevated source is computed by integrating:

$$\frac{d\mathbf{x}_p}{dt} = \mathbf{u}_p, \tag{C.1}$$

where $\mathbf{x}_p$ is the location of the plume centre of mass with respect to the source coordinates ($x = 0$, $y = 0$, $z = h_s$) and $\mathbf{u}_p$ is the velocity of the plume centroid. The subscript 'p' refers to the plume variables and 'a' to those of the ambient flow and the vectors are represented with bold characters. Defined b the plume radius and $u_\xi = |u_p|$ the plume velocity norm, we determine the global plume mass flux $F_m = \pi b^2 \rho_p u_\xi$, the mass flux of each species $F_{m,\Gamma} = \Gamma F_m$, the momentum flux $\mathbf{F}_M = F_m \mathbf{u}_p$, the buoyancy force $\mathbf{B} = \pi b^2 \mathbf{g} (\rho_p - \rho_a)$, and the aerodynamic drag force $\mathbf{D} = \rho_a 2\pi b \Delta\mathbf{u}_N |\Delta\mathbf{u}_N| C_D$, with the drag coefficient C_D assumed to be equal to 0.21 (Robins et al., 2009), and $\Delta\mathbf{u}_N$ the relative velocity of the plume perpendicular to the plume axis.

The plume density is related to the CO_2 concentration through:

$$\rho_p = c_{CO_2} \frac{\overline{M}}{M_{CO_2}} \rho_{CO_2} + (1 - c_{CO_2}) \frac{\overline{M}}{M_{air}} \rho_{air}, \tag{C.2}$$

$$\frac{1}{\overline{M}} = \frac{c_{CO_2}}{M_{CO_2}} + \frac{1 - c_{CO_2}}{M_{air}}, \tag{C.3}$$

where M_{air}, M_{CO_2} and $\overline{M}$ are the molecular weights (g/mol) of air, CO_2, and of the plume, respectively.

The value of u_p in Eq. C.1 is determined by solving the following balance equations of volume, buoyancy and momentum (along the three directions):

$$\frac{dF_m}{dt} = 2\pi b u_\xi \rho_a u_e, \tag{C.4}$$

$$\frac{dF_{m,c_{CO_2}}}{dt} = 0, \tag{C.5}$$

$$\frac{dF_{Mx}}{dt} = 2\pi b u_\xi \rho_a u_e u_x^a - u_\xi D_x, \tag{C.6}$$

$$\frac{dF_{My}}{dt} = 2\pi b u_\xi \rho_a u_e u_y^a - u_\xi D_y, \tag{C.7}$$

$$\frac{dF_{Mz}}{dt} = 2\pi b u_\xi \rho_a u_e u_z^a + u_\xi B_z - u_\xi D_z. \tag{C.8}$$

Adding the relation between c_{CO_2} and ρ_p (Eq. C.2) we obtain a linear system with 6 equations and 7 unknowns (ρ_p, c_{CO_2}, $\mathbf{u_p}$, b, u_e). To close the system we have to introduce a further equation modelling the entrainment velocity u_e which is assumed to be the sum of two process:

$$u_e = u_e^{rise} + u_e^{turb}. \tag{C.9}$$

The u_e^{rise} component depends on the relative motion between the plume and the external air and it is parameterised as follows:

$$u_e^{rise} = \alpha_1 |\Delta u_\xi| + \alpha_2 |\Delta u_N|, \tag{C.10}$$

where u_ξ is the relative velocity component along the plume axis. The u_e^{turb} component depends instead on the atmospheric turbulence and it is modelled as a function of the flight time t, turbulent kinetic energy dissipation rate ε (Eq. 3.5), vertical velocity fluctuation σ_w and Lagrangian temporal macro-scale T_{Lw} (Eq. 3.12):

$$u_e^{turb} = \alpha_3 \min\left((\varepsilon b)^{1/3}, \sigma_w \left(1 + \frac{t}{2T_{Lw}}\right)^{-1/2} \right). \tag{C.11}$$

Following (Robins et al., 2009), the values of the entrainment coefficients are set equal to $\alpha_1 = 0.057$, $\alpha_2 = 0.5$, and $\alpha_3 = 0.655$.

The linear system is discretised with an explicit Euler scheme and implemented with an adaptive algorithm that increases the accuracy of the solutions. This algorithm is based on the information provided by an error indicator that modifies the time step-length in order to control the error due to the time discretisation (Berrone and Marro, 2010). This plume rise model takes into account the drag force acting on the plume by the dynamic pressure, with good accuracy on the plume trajectory. However, it overestimates the dilution rate and plume spread. The model has been tested against an experimental data collected in neutral BL by Marro et al. (2013).

Bibliography

Abbiss, J.B., T.W. Chubb, and E.R. Pike (1974). "Laser Doppler anemometry". In: *Optics & Laser Technology* 6.6, pp. 249 –261. ISSN: 0030-3992. DOI: https://doi.org/10.1016/0030-3992(74)90006-1. URL: http://www.sciencedirect.com/science/article/pii/0030399274900061.

Abramowitz, Milton and Irene A Stegun (1964). *Handbook of mathematical functions with formulas, graphs, and mathematical tables*. Vol. 55. US Government printing office.

Aliyu, Abubakar Sadiq, Nikolaos Evangeliou, Timothy Alexander Mousseau, Junwen Wu, and Ahmad Termizi Ramli (2015). "An overview of current knowledge concerning the health and environmental consequences of the Fukushima Daiichi Nuclear Power Plant (FDNPP) accident". In: *Environment International* 85, pp. 213–228. ISSN: 0160-4120. DOI: https://doi.org/10.1016/j.envint.2015.09.020. URL: https://www.sciencedirect.com/science/article/pii/S016041201530060X.

Amicarelli, Andrea, Giovanni Leuzzi, and Paolo Monti (Dec. 2012). "Lagrangian Micromixing Models for Concentration Fluctuations: An Overview". In: *AJES* 8.6. URL: https://thescipub.com/abstract/ajessp.2012.577.590.

Anfossi, D., G. Tinarelli, S. Trini Castelli, M. Nibart, C. Olry, and J. Commanay (2010). "A new Lagrangian particle model for the simulation of dense gas dispersion". In: *Atmospheric Environment* 44.6, pp. 753 –762. ISSN: 1352-2310. DOI: https://doi.org/10.1016/j.atmosenv.2009.11.041. URL: http://www.sciencedirect.com/science/article/pii/S1352231009009959.

ARIA-Developpement-durable (2006). *Explosion in an oil depot*. URL: https://www.aria.developpement-durable.gouv.fr/fiche_detaillee/2914_en/?lang=en.

— (2008). *Explosion dans une raffineries*. URL: https://www.aria.developpement-durable.gouv.fr/fiche_detaillee/3969/.

Arya, S.P.S and J.F Lape (1990). "A comparative study of the different criteria for the physical modeling of buoyant plume rise in a neutral atmosphere". In: *Atmospheric Environment. Part A. General Topics* 24.2, pp. 289 –295. ISSN: 0960-1686. DOI: https://doi.org/10.1016/0960-1686(90)90109-Z. URL: http://www.sciencedirect.com/science/article/pii/096016869090109Z.

Ayrault, Michel, Jean-Louis Balint, and Robert Morel (1991). "An experimental study on the evolution and dispersion of a cloud of gas heavier than air". In: *Journal of Hazardous Materials* 26.1, pp. 1 –26. ISSN: 0304-3894. DOI: http://dx.doi.

org/10.1016/0304-3894(91)85002-5. URL: http://www.sciencedirect.com/science/article/pii/0304389491850025.

Ayrault, Michel, Serge Simoëns, and Patrick Méjean (1998). "Negative buoyancy effects on the dispersion of continuous gas plumes downwind solid obstacles". In: *Journal of Hazardous Materials* 57.1–3, pp. 79 –103. ISSN: 0304-3894. DOI: http://dx.doi.org/10.1016/S0304-3894(97)00075-7. URL: http://www.sciencedirect.com/science/article/pii/S0304389497000757.

Banerjee, Arindam and Malcolm J. Andrews (Apr. 2007). "A Convection Heat Transfer Correlation for a Binary Air-Helium Mixture at Low Reynolds Number". In: *Journal of Heat Transfer* 129.11, pp. 1494–1505. ISSN: 0022-1481. DOI: 10.1115/1.2764086. eprint: https://asmedigitalcollection.asme.org/heattransfer/article-pdf/129/11/1494/5559690/1494_1.pdf. URL: https://doi.org/10.1115/1.2764086.

Batchelor, G. K. (1959). "Small-scale variation of convected quantities like temperature in turbulent fluid Part 1. General discussion and the case of small conductivity". In: *Journal of Fluid Mechanics* 5.1, 113–133. DOI: 10.1017/S002211205900009X.

Berrone, S. and M. Marro (2010). "Numerical investigation of effectivity indices of space-time error indicators for Navier–Stokes equations". In: *Computer Methods in Applied Mechanics and Engineering* 199.25, pp. 1764 –1782. ISSN: 0045-7825. DOI: https://doi.org/10.1016/j.cma.2010.02.004. URL: http://www.sciencedirect.com/science/article/pii/S0045782510000629.

Bertagni, Matteo B., Massimo Marro, Pietro Salizzoni, and Carlo Camporeale (2019). "Solution for the statistical moments of scalar turbulence". In: *Phys. Rev. Fluids* 4 (12), p. 124701. DOI: 10.1103/PhysRevFluids.4.124701. URL: https://link.aps.org/doi/10.1103/PhysRevFluids.4.124701.

— (2020). "Level-crossing statistics of a passive scalar dispersed in a neutral boundary layer". In: *Atmospheric Environment* 230, p. 117518. ISSN: 1352-2310. DOI: https://doi.org/10.1016/j.atmosenv.2020.117518. URL: http://www.sciencedirect.com/science/article/pii/S1352231020302545.

Blocken, B., T. Stathopoulos, P. Saathoff, and X. Wang (2008). "Numerical evaluation of pollutant dispersion in the built environment: Comparisons between models and experiments". In: *Journal of Wind Engineering and Industrial Aerodynamics* 96.10. 4th International Symposium on Computational Wind Engineering (CWE2006), pp. 1817–1831. ISSN: 0167-6105. DOI: https://doi.org/10.1016/j.jweia.2008.02.049. URL: https://www.sciencedirect.com/science/article/pii/S0167610508000494.

Briggs, G., R. E. Britter, S. R. Hanna, J. Havens, S. B. King, A. G. Robins, W. H. Snyder, and K. W. Steinberg (1998). "Advances in Dense Gas Dispersion Modeling of Accidental Releases over Rough Surfaces during Stable Conditions". In: *Air Pollution Modeling and Its Application XII*. Ed. by Sven-Erik Gryning and Nadine Chaumerliac. Boston, MA: Springer US, pp. 509–516. ISBN: 978-1-4757-9128-0.

DOI: 10.1007/978-1-4757-9128-0_52. URL: https://doi.org/10.1007/978-1-4757-9128-0_52.

Briggs, G.A., R.E. Britter, S.R. Hanna, J.A. Havens, A.G. Robins, and W.H. Snyder (2001). "Dense gas vertical diffusion over rough surfaces and results of wind-tunnel studies". In: *Atmospheric Environment* 35. DOI: https://doi.org/10.1016/S1352-2310(00)00360-5. URL: http://www.sciencedirect.com/science/article/pii/S1352231000003605#aep-bibliography-id24.

Britter, R E (1989). "Atmospheric Dispersion of Dense Gases". In: *Annual Review of Fluid Mechanics* 21.1, pp. 317–344. DOI: 10.1146/annurev.fl.21.010189.001533. eprint: http://dx.doi.org/10.1146/annurev.fl.21.010189.001533. URL: http://dx.doi.org/10.1146/annurev.fl.21.010189.001533.

Britter, R.E. and R.F. Griffiths (1982). "The role of dense gases in the assessment of industrial hazards". In: *Journal of Hazardous Materials* 6.1–2. Dense Gas Disperation, pp. 3 –12. ISSN: 0304-3894. DOI: http://dx.doi.org/10.1016/0304-3894(82)80032-0. URL: http://www.sciencedirect.com/science/article/pii/0304389482800320.

Britter, Rex E. and William H. Snyder (1988). "Fluid modeling of dense gas dispersion over a ramp". In: *Journal of Hazardous Materials* 18.1, pp. 37 –67. ISSN: 0304-3894. DOI: http://dx.doi.org/10.1016/0304-3894(88)85058-1. URL: http://www.sciencedirect.com/science/article/pii/0304389488850581.

Broughton, Edward (2005). "The Bhopal disaster and its aftermath: a review". In: *Environmental Health* 4.1, p. 6. ISSN: 1476-069X. URL: https://doi.org/10.1186/1476-069X-4-6.

Bruun, H H (1996). "Hot-Wire Anemometry: Principles and Signal Analysis". In: *Measurement Science and Technology* 7.10. DOI: 10.1088/0957-0233/7/10/024. URL: https://doi.org/10.1088%2F0957-0233%2F7%2F10%2F024.

Carpenter, R.J., R.P. Cleaver, P.J. Waite, and M.A. English (1987). "The calibration of a simple model for dense gas dispersion using the Thorney Island Phase I trials data". In: *Journal of Hazardous Materials* 16, pp. 293 –313. ISSN: 0304-3894. DOI: https://doi.org/10.1016/0304-3894(87)80039-0. URL: http://www.sciencedirect.com/science/article/pii/0304389487800390.

Carpentieri, Matteo, Paul Hayden, and Alan G. Robins (2012). "Wind tunnel measurements of pollutant turbulent fluxes in urban intersections". In: *Atmospheric Environment* 46, pp. 669 –674. ISSN: 1352-2310. DOI: https://doi.org/10.1016/j.atmosenv.2011.09.083. URL: http://www.sciencedirect.com/science/article/pii/S1352231011010909.

Carpentieri, Matteo and Alan G. Robins (2010). "Tracer Flux Balance at an Urban Canyon Intersection". In: *Boundary-Layer Meteorology* 135.2, pp. 229–242. ISSN: 1573-1472. URL: https://doi.org/10.1007/s10546-010-9471-6.

Carvalho, J. C., Gervasio Annes Degrazia, Domenico Anfossi, and S. Trini Castelli (1999). "SIMULATION OF COPENHAGEN TRACER DIFFUSION EXPERIMENT BY MEANS OF A LAGRANGIAN PARTICLE MODEL". In: *Hybrid Methods in Engineering* 1.4. ISSN: 1099-2391.

Cassiani, M., P. Franzese, and J. D. Albertson (2009). "A coupled Eulerian and Lagrangian mixing model for intermittent concentration time series". In: *Physics of Fluids* 21.8, p. 085105. DOI: 10.1063/1.3202534. eprint: https://doi.org/10.1063/1.3202534. URL: https://doi.org/10.1063/1.3202534.

Cassiani, M., P. Franzese, and U. Giostra (2005a). "A PDF micromixing model of dispersion for atmospheric flow. Part I: development of the model, application to homogeneous turbulence and to neutral boundary layer". In: *Atmospheric Environment* 39.8, pp. 1457 –1469. ISSN: 1352-2310. DOI: https://doi.org/10.1016/j.atmosenv.2004.11.020. URL: http://www.sciencedirect.com/science/article/pii/S1352231004010994.

— (2005b). "A PDF micromixing model of dispersion for atmospheric flow. Part II: application to convective boundary layer". In: *Atmospheric Environment* 39.8, pp. 1471 –1479. ISSN: 1352-2310. DOI: https://doi.org/10.1016/j.atmosenv.2004.11.019. URL: http://www.sciencedirect.com/science/article/pii/S1352231004011008.

Cassiani, Massimo (2013). "The Volumetric Particle Approach for Concentration Fluctuations and Chemical Reactions in Lagrangian Particle and Particle-grid Models". In: *Boundary-Layer Meteorology* 146.2, pp. 207–233. ISSN: 1573-1472. DOI: https://doi.org/10.1007/s10546-012-9752-3. URL: https://doi.org/10.1007/s10546-012-9752-3.

Cassiani, Massimo, Matteo B. Bertagni, Massimo Marro, and Pietro Salizzoni (2020). "Concentration Fluctuations from Localized Atmospheric Releases". In: *Boundary-Layer Meteorology* 177.2, pp. 461–510. ISSN: 1573-1472. URL: https://doi.org/10.1007/s10546-020-00547-4.

Chernov, Dmitry Chernov and Didier Sornette (2016). *Man-made Catastrophes and Risk Information Concealment. Case Studies of Major Disasters and Human Fallibility*. Springer International Publishing. DOI: https://10.1007/978-3-319-24301-6.

Comte-Bellot, G (1976). "Hot-Wire Anemometry". In: *Annual Review of Fluid Mechanics* 8.1, pp. 209–231. DOI: 10.1146/annurev.fl.08.010176.001233. eprint: https://doi.org/10.1146/annurev.fl.08.010176.001233. URL: https://doi.org/10.1146/annurev.fl.08.010176.001233.

Contini, Daniele, Paul Hayden, and Alan Robins (2006). "Concentration field and turbulent fluxes during the mixing of two buoyant plumes". In: *Atmospheric Environment* 40.40, pp. 7842 –7857. ISSN: 1352-2310. DOI: https://doi.org/10.1016/j.atmosenv.2006.07.024. URL: http://www.sciencedirect.com/science/article/pii/S1352231006007850.

Corrsin, Stanley (1947). "Extended Applications of the Hot-Wire Anemometer". In: *Review of Scientific Instruments* 18.7, pp. 469–471. DOI: 10.1063/1.1740981. eprint: https://doi.org/10.1063/1.1740981. URL: https://doi.org/10.1063/1.1740981.

Crimaldi, John P, Megan B Wiley, and Jeffrey R Koseff (2002). "The relationship between mean and instantaneous structure in turbulent passive scalar plumes". In: *Journal of Turbulence* 3, N14. DOI: 10.1088/1468-5248/3/1/014. eprint: https://doi.org/10.1088/1468-5248/3/1/014. URL: https://doi.org/10.1088/1468-5248/3/1/014.

Csanady, GT (1967). "Concentration fluctuations in turbulent diffusion". In: *Journal of Atmospheric Sciences* 24.1, pp. 21–28.

Di Bernardino, Annalisa, Paolo Monti, Giovanni Leuzzi, and Giorgio Querzoli (2019). "Turbulent Schmidt Number Measurements Over Three-Dimensional Cubic Arrays". In: *Boundary-Layer Meteorology*. ISSN: 1573-1472. URL: https://doi.org/10.1007/s10546-019-00482-z.

Donat, Jochen and Michael Schatzmann (Nov. 1999). "Wind tunnel experiments of single-phase heavy gas jets released under various angles into turbulent cross flows". In: *Journal of Wind Engineering and Industrial Aerodynamics - J WIND ENG IND AERODYN* 83, pp. 361–370. DOI: 10.1016/S0167-6105(99)00085-9.

Duplat, J. and E. Villermaux (2008). "Mixing by random stirring in confined mixtures". In: *Journal of Fluid Mechanics* 617, 51–86. DOI: 10.1017/S0022112008003789.

European-Commission (2017). *Major accident hazards*. URL: https://ec.europa.eu/environment/seveso/.

F. T. Bodurtha, Jr (1961). "The Behavior of Dense Stack Gases". In: *Journal of the Air Pollution Control Association* 11.9, pp. 431–437. DOI: 10.1080/00022470.1961.10468023. eprint: https://doi.org/10.1080/00022470.1961.10468023. URL: https://doi.org/10.1080/00022470.1961.10468023.

Fackrell, J E (1980). "A flame ionisation detector for measuring fluctuating concentration". In: *Journal of Physics E: Scientific Instruments* 13.8, p. 888. URL: http://stacks.iop.org/0022-3735/13/i=8/a=021.

Fackrell, J. E. and A. G. Robins (1982). "Concentration fluctuations and fluxes in plumes from point sources in a turbulent boundary layer". In: *Journal of Fluid Mechanics* 117, 1–26. DOI: 10.1017/S0022112082001499.

Fannelöp, Torstein K. (1994). "Fluid Mechanics for Industrial Safety and Environmental Protection". In: *Industrial Safety Series*. Vol. 3.

Gamel, H. (2015). "Caractérisation expérimentale de l'écoulement et de la dispersion autour d'un obstacle bidimensionnel". PhD thesis. École Centrale de Lyon.

Gardiner, C. W. (2004). *Handbook of stochastic methods for physics, chemistry and the natural sciences*. Third. Vol. 13. Springer Series in Synergetics. Berlin: Springer-Verlag, pp. xviii+415. ISBN: 3-540-20882-8.

Gavelli, Filippo, Edward Bullister, and Harri Kytomaa (2008). "Application of {CFD} (Fluent) to {LNG} spills into geometrically complex environments". In: *Journal*

of Hazardous Materials 159.1. Papers Presented at the 2006 Annual Symposium of the Mary Kay O'Connor Process Safety Center, pp. 158 –168. ISSN: 0304-3894. DOI: http://dx.doi.org/10.1016/j.jhazmat.2008.02.037. URL: http://www.sciencedirect.com/science/article/pii/S0304389408002380.

Gifford, Frank (1959). "Statistical Properties of A Fluctuating Plume Dispersion Model". In: ed. by H.E. Landsberg and J. Van Mieghem. Vol. 6. Advances in Geophysics. Elsevier, pp. 117 –137. DOI: https://doi.org/10.1016/S0065-2687(08)60099-0. URL: http://www.sciencedirect.com/science/article/pii/S0065268708600990.

Gousseau, P., B. Blocken, T. Stathopoulos, and G.J.F. van Heijst (2011). "CFD simulation of near-field pollutant dispersion on a high-resolution grid: A case study by LES and RANS for a building group in downtown Montreal". In: *Atmospheric Environment* 45.2, pp. 428–438. ISSN: 1352-2310. DOI: https://doi.org/10.1016/j.atmosenv.2010.09.065. URL: https://www.sciencedirect.com/science/article/pii/S1352231010008514.

Hall, D.J. and R.A. Waters (1985). "Wind tunnel model comparisons with the thorney island dense gas release field trials". In: *Journal of Hazardous Materials* 11, pp. 209 –235. ISSN: 0304-3894. DOI: https://doi.org/10.1016/0304-3894(85)85039-1. URL: http://www.sciencedirect.com/science/article/pii/0304389485850391.

Hanna, S.R. and K.W. Steinberg (2001). "Overview of Petroleum Environmental Research Forum (PERF) dense gas dispersion modeling project". In: *Atmospheric Environment* 35.13, pp. 2223 –2229. ISSN: 1352-2310. DOI: https://doi.org/10.1016/S1352-2310(00)00284-3. URL: http://www.sciencedirect.com/science/article/pii/S1352231000002843.

Hanna, Steven, Rex Britter, Edward Argenta, and Joseph Chang (2012). "The Jack Rabbit chlorine release experiments: implications of dense gas removal from a depression and downwind concentrations." eng. In: *Journal of hazardous materials* 213-214, pp. 406–12.

Hanna, Steven R and Joseph C Chang (2001). "Use of the Kit Fox field data to analyze dense gas dispersion modeling issues". In: *Atmospheric Environment* 35.13, pp. 2231 –2242. ISSN: 1352-2310. DOI: http://dx.doi.org/10.1016/S1352-2310(00)00481-7. URL: http://www.sciencedirect.com/science/article/pii/S1352231000004817.

Havens, JA and T Spicer (1988). "A dispersion model for elevated dense gas jet chemical releases". In: *Volumes I and II, US Environmental Protection Agency, Office of Air and Radiation, Office of Air Quality Planning and Standards, Research Triangle Park, North Carolina* 27711.

Hay, J.S. and F. Pasquill (1959). "Diffusion from a Continuous Source in Relation to the Spectrum and Scale of Turbulence". In: ed. by H.E. Landsberg and J. Van Mieghem. Vol. 6. Advances in Geophysics. Elsevier, pp. 345–365. DOI: https://doi.

org/10.1016/S0065-2687(08)60122-3. URL: https://www.sciencedirect.com/science/article/pii/S0065268708601223.

Heidorn, K.C., M.C. Murphy, P.A. Irwin, H. Sahota, P.K. Misra, and R. Bloxam (1992). "Effects of obstacles on the spread of a heavy gas—Wind tunnel simulations". In: *Journal of Hazardous Materials* 30.2. Heavy Gas Dispersion, pp. 151 –194. ISSN: 0304-3894. DOI: http://dx.doi.org/10.1016/0304-3894(92)85077-E. URL: http://www.sciencedirect.com/science/article/pii/030438949285077E.

HGSYSTEM (1990). "HGSYSTEM Technical Reference Manual. Chapter 5. Plume or jet models in HGSYSTEM". In: DOI: www.HGSYSTEM.com.

Hilderman, Trevor and David J. Wilson (2007). "Predicting plume meandering and averaging time effects on mean and fluctuating concentrations in atmospheric dispersion simulated in a water channel". In: *Boundary-Layer Meteorology* 122.3, pp. 535–575. ISSN: 1573-1472. URL: https://doi.org/10.1007/s10546-006-9125-x.

Hinze, J.O. (1975). "Turbulence." In: *McGraw-Hill, New York*, 799 pp.

Homberger, E., G. Reggiani, J. Sambeth, and H. K. Wipf (Nov. 1979). "The Seveso accident: its nature, extent and consequences". In: *The Annals of Occupational Hygiene* 22.4, pp. 327–370. ISSN: 0003-4878. DOI: 10.1093/annhyg/22.4.327. eprint: https://academic.oup.com/annweh/article-pdf/22/4/327/7290567/22-4-327.pdf. URL: https://doi.org/10.1093/annhyg/22.4.327.

Hoot, TG, RN Meroney, and JA Peterka (1973). "Wind tunnel tests of negatively bouyant plumes[Final Report]". In.

Hsieh, Kun-Jung, Fue-Sang Lien, and Eugene Yee (2007). "Numerical modeling of passive scalar dispersion in an urban canopy layer". In: *Journal of Wind Engineering and Industrial Aerodynamics* 95.12, pp. 1611 –1636. ISSN: 0167-6105. DOI: https://doi.org/10.1016/j.jweia.2007.02.028. URL: http://www.sciencedirect.com/science/article/pii/S0167610507000761.

Iacobello, G., M. Marro, L. Ridolfi, P. Salizzoni, and S. Scarsoglio (2019). "Experimental investigation of vertical turbulent transport of a passive scalar in a boundary layer: Statistics and visibility graph analysis". In: *Phys. Rev. Fluids* 4 (10), p. 104501. DOI: 10.1103/PhysRevFluids.4.104501. URL: https://link.aps.org/doi/10.1103/PhysRevFluids.4.104501.

Iacono, Giovanni Lo and Andy M Reynolds (2008). "Modelling of concentrations along a moving observer in an inhomogeneous plume. Biological application: model of odour-mediated insect flights". In: *Environmental Fluid Mechanics* 8.2, pp. 147–168.

Irwin, H.P.A.H. (1981). "The design of spires for wind simulation". In: *Journal of Wind Engineering and Industrial Aerodynamics* 7.3, pp. 361 –366. ISSN: 0167-6105. DOI: https://doi.org/10.1016/0167-6105(81)90058-1. URL: http://www.sciencedirect.com/science/article/pii/0167610581900581.

Jørgensen, Finn E. (2002). *How to measure turbulence with hot-wire anemometers - a practical guide*. Ed. by Dantec Dynamics.

Koeltzsch, Konrad (2000). "The height dependence of the turbulent Schmidt number within the boundary layer". In: *Atmospheric Environment* 34.7, pp. 1147 –1151. ISSN: 1352-2310. DOI: https://doi.org/10.1016/S1352-2310(99)00369-6. URL: http://www.sciencedirect.com/science/article/pii/S1352231099003696.

Kolmogorov, Andrei Nikolaevich, V. Levin, Julian Charles Roland Hunt, Owen Martin Phillips, and David Williams (1941). "The local structure of turbulence in incompressible viscous fluid for very large Reynolds numbers". In: *Proceedings of the Royal Society of London. Series A: Mathematical and Physical Sciences* 434.1890, pp. 9–13. DOI: 10.1098/rspa.1991.0075. eprint: https://royalsocietypublishing.org/doi/pdf/10.1098/rspa.1991.0075. URL: https://royalsocietypublishing.org/doi/abs/10.1098/rspa.1991.0075.

König-Langlo, G. and M. Schatzmann (1991). "Wind tunnel modeling of heavy gas dispersion". In: *Atmospheric Environment. Part A. General Topics* 25.7, pp. 1189 –1198. ISSN: 0960-1686. DOI: https://doi.org/10.1016/0960-1686(91)90230-5. URL: http://www.sciencedirect.com/science/article/pii/0960168691902305.

Laio, F., A. Porporato, L. Ridolfi, and I. Rodriguez-Iturbe (2001). "Mean first passage times of processes driven by white shot noise". In: *Phys. Rev. E* 63 (3), p. 036105. DOI: 10.1103/PhysRevE.63.036105. URL: https://link.aps.org/doi/10.1103/PhysRevE.63.036105.

Landucci, Gabriele, Alessandro Tugnoli, Valentina Busini, Marco Derudi, Renato Rota, and Valerio Cozzani (2011). "The Viareggio LPG accident: Lessons learnt". In: *Journal of Loss Prevention in the Process Industries* 24.4, pp. 466–476. ISSN: 0950-4230. DOI: https://doi.org/10.1016/j.jlp.2011.04.001. URL: https://www.sciencedirect.com/science/article/pii/S0950423011000362.

Marro, M., H. Gamel, P. Méjean, H. Correia, L. Soulhac, and P. Salizzoni (2020). "High-frequency simultaneous measurements of velocity and concentration within turbulent flows in wind-tunnel experiments". In: *Experiments in Fluids* 61.12, p. 245. ISSN: 1432-1114. DOI: https://doi.org/10.1007/s00348-020-03074-7. URL: https://doi.org/10.1007/s00348-020-03074-7.

Marro, Massimo, Pietro Salizzoni, Cierco François-Xavier, Irène Korsakissok, Enrico Danzi, and Lionel Soulhac (Aug. 2013). "Plume rise and spread in buoyant releases from elevated sources in the lower atmosphere". In: *Environmental Fluid Mechanics* 14. DOI: 10.1007/s10652-013-9300-9.

Marro, Massimo, Pietro Salizzoni, Lionel Soulhac, and Massimo Cassiani (2018). "Dispersion of a Passive Scalar Fluctuating Plume in a Turbulent Boundary Layer. Part III: Stochastic Modelling". In: *Boundary-Layer Meteorology* 167.3, pp. 349–369. ISSN: 1573-1472. DOI: 10.1007/s10546-017-0330-6. URL: https://doi.org/10.1007/s10546-017-0330-6.

McCall, Chris (Apr. 2016). "Chernobyl disaster 30 years on: lessons not learned". In: *The Lancet* 387.10029, pp. 1707–1708. ISSN: 0140-6736. DOI: 10.1016/s0140-6736(16)30304-x. URL: https://doi.org/10.1016/S0140-6736(16)30304-X.

McQuaid, J. (1985). "Objectives and design of the phase I heavy gas dispersion trials". In: *Journal of Hazardous Materials* 11, pp. 1 –33. ISSN: 0304-3894. DOI: http://dx.doi.org/10.1016/0304-3894(85)85031-7. URL: http://www.sciencedirect.com/science/article/pii/0304389485850317.

McQuaid, J. and W. Wright (1973). "The response of a hot-wire anemometer in flows of gas mixtures". In: *International Journal of Heat and Mass Transfer* 16.4, pp. 819 –828. ISSN: 0017-9310. DOI: https://doi.org/10.1016/0017-9310(73)90093-8. URL: http://www.sciencedirect.com/science/article/pii/0017931073900938.

Merlier, Lucie, Jérôme Jacob, and Pierre Sagaut (2019). "Lattice-Boltzmann large-eddy simulation of pollutant dispersion in complex urban environment with dense gas effect: Model evaluation and flow analysis". In: *Building and Environment* 148, pp. 634–652. ISSN: 0360-1323. DOI: https://doi.org/10.1016/j.buildenv.2018.11.009. URL: https://www.sciencedirect.com/science/article/pii/S0360132318307042.

Meroney, Robert N. (1982). "Wind-tunnel experiments on dense gas dispersion". In: *Journal of Hazardous Materials* 6.1. Dense Gas Disperation, pp. 85 –106. ISSN: 0304-3894. DOI: https://doi.org/10.1016/0304-3894(82)80035-6. URL: http://www.sciencedirect.com/science/article/pii/0304389482800356.

— (1987). "Guidelines for fluid modeling of dense gas cloud dispersion". In: *Journal of Hazardous Materials* 17.1, pp. 23 –46. ISSN: 0304-3894. DOI: https://doi.org/10.1016/0304-3894(87)85040-9. URL: http://www.sciencedirect.com/science/article/pii/0304389487850409.

Meroney, Robert N. and Achim Lohmeyer (1984). "Statistical characteristics of instantaneous dense gas clouds released in an atmospheric boundary-layer wind tunnel". In: *Boundary-Layer Meteorology* 28.1, pp. 1–22. ISSN: 1573-1472. DOI: https://doi.org/10.1007/BF00119454. URL: https://doi.org/10.1007/BF00119454.

Metzger, M M and J C Klewicki (2003). "Development and characterization of a probe to measure scalar transport". In: *Measurement Science and Technology* 14.8, pp. 1437–1448. DOI: 10.1088/0957-0233/14/8/333. URL: https://doi.org/10.1088%2F0957-0233%2F14%2F8%2F333.

Miles, John W. (1961). "On the stability of heterogeneous shear flows". In: *Journal of Fluid Mechanics* 10.4, 496–508. DOI: 10.1017/S0022112061000305.

Miller, D, E Vyazmina, A Chen, and E Lutostansky (2021). "Gone with the wind : Ventjet is a new engineering model for atmospheric dispersion". In: *Spring Meeting & 17th Global Congress on Process Safety*.

Morton, B. R., Geoffrey Ingram Taylor, and John Stewart Turner (1956). "Turbulent gravitational convection from maintained and instantaneous sources". In: *Proceedings of the Royal Society of London. Series A. Mathematical and Physical Sciences* 234.1196, pp. 1–23. DOI: doi:10.1098/rspa.1956.0011. eprint: https://royalsocietypublishing.org/doi/pdf/10.1098/rspa.1956.0011. URL: https://royalsocietypublishing.org/doi/abs/10.1098/rspa.1956.0011.

Negre, Elsa (2021). "Crisis management and distrust: Study of an industrial accident in France". In: *Proceedings of the 54th Hawaii International Conference on System Sciences*, p. 2235.

Nironi, Chiara, Pietro Salizzoni, Massimo Marro, Patrick Mejean, Nathalie Grosjean, and Lionel Soulhac (2015). "Dispersion of a Passive Scalar Fluctuating Plume in a Turbulent Boundary Layer. Part I: Velocity and Concentration Measurements". In: *Boundary-Layer Meteorology* 156.3, pp. 415–446. ISSN: 1573-1472. DOI: 10.1007/s10546-015-0040-x. URL: https://doi.org/10.1007/s10546-015-0040-x.

Ooms, G. (1972). "A new method for the calculation of the plume path of gases emitted by a stack". In: *Atmospheric Environment (1967)* 6.12, pp. 899 –909. ISSN: 0004-6981. DOI: https://doi.org/10.1016/0004-6981(72)90098-4. URL: http://www.sciencedirect.com/science/article/pii/0004698172900984.

Perry, A. E. and G. L. Morrison (1971). "A study of the constant-temperature hot-wire anemometer". In: *Journal of Fluid Mechanics* 47.3, 577–599. DOI: 10.1017/S0022112071001241.

Pitts, William M. and Bernard J. McCaffrey (1986). "Response behaviour of hot wires and films to flows of different gases". In: *Journal of Fluid Mechanics* 169, 465–512. DOI: 10.1017/S0022112086000721.

Pontiggia, Marco, Gabriele Landucci, Valentina Busini, Marco Derudi, Mario Alba, Marco Scaioni, Sarah Bonvicini, Valerio Cozzani, and Renato Rota (2011). "{CFD} model simulation of {LPG} dispersion in urban areas". In: *Atmospheric Environment* 45.24, pp. 3913 –3923. ISSN: 1352-2310. DOI: http://dx.doi.org/10.1016/j.atmosenv.2011.04.071. URL: http://www.sciencedirect.com/science/article/pii/S1352231011004602.

Pope, S.B. (1998). "The vanishing effect of molecular diffusivity on turbulent dispersion: implications for turbulent mixing and the scalar flux". In: *Journal of Fluid Mechanics* 359, 299–312. DOI: 10.1017/S0022112097008380.

Pope, Stephen B. (2000). *Turbulent Flows*. Cambridge University Press. DOI: 10.1017/CBO9780511840531.

Postma, John V., John D. Wilson, and Eugene Yee (2011). "Comparing Two Implementations of a Micromixing Model. Part I: Wall Shear-Layer Flow". In: *Boundary-Layer Meteorology* 140.2, pp. 207–224. ISSN: 1573-1472. URL: https://doi.org/10.1007/s10546-011-9605-5.

Pritchard, D. T. and J. A. Currie (1982). "Diffusion of coefficients of carbon dioxide, nitrous oxide, ethylene and ethane in air and their measurement". In: *Journal of Soil Science* 33.2, pp. 175–184. ISSN: 1365-2389. DOI: 10.1111/j.1365-2389.1982.tb01757.x. URL: http://dx.doi.org/10.1111/j.1365-2389.1982.tb01757.x.

Raupach, M. R. and B. J. Legg (1983). "Turbulent dispersion from an elevated line source: measurements of wind-concentration moments and budgets". In: *Journal of Fluid Mechanics* 136, 111–137. DOI: 10.1017/S0022112083002086.

Raupach, M. R., A. S. Thom, and I. Edwards (1980). "A wind-tunnel study of turbulent flow close to regularly arrayed rough surfaces". In: *Boundary-Layer Meteorology* 18.4, pp. 373–397. ISSN: 1573-1472. URL: https://doi.org/10.1007/BF00119495.

Reeuwijk, Maarten van and John Craske (2015). "Energy-consistent entrainment relations for jets and plumes". In: *Journal of Fluid Mechanics* 782, 333–355. DOI: 10.1017/jfm.2015.534.

Ridolfi, Luca, Paolo D'Odorico, and Francesco Laio (2011). *Noise-induced phenomena in the environmental sciences*. Cambridge University Press.

Roberts, P.T. and D.J. Hall (1994). "Wind-tunnel simulation. Boundary layer effects in dense gas dispersion experiments". In: *Journal of Loss Prevention in the Process Industries* 7.2, pp. 106–117. ISSN: 0950-4230. DOI: https://doi.org/10.1016/0950-4230(94)80026-X. URL: https://www.sciencedirect.com/science/article/pii/095042309480026X.

Robins, A, P Hayden, and EMM Wingstedt (2016). *MODITIC wind tunnel experiments*. Tech. rep. FFI-RAPPORT 16/01483. Norwegian Defence Research Establishment (FFI). DOI: http://hdl.handle.net/20.500.12242/1258.

Robins, AG, DD Apsley, DJ Carruthers, CA McHugh, and SJ Dyster (2009). *Plume rise model specification. Technical report.* Tech. rep. University of Surrey, National Power and CERC.

Robins, Alan, Ian Castro, Paul Hayden, Nathan Steggel, Daniele Contini, and David Heist (2001a). "A wind tunnel study of dense gas dispersion in a neutral boundary layer over a rough surface". In: *Atmospheric Environment* 35.13, pp. 2243 –2252. ISSN: 1352-2310. DOI: https://doi.org/10.1016/S1352-2310(01)00072-3. URL: http://www.sciencedirect.com/science/article/pii/S1352231001000723.

Robins, Alan, Ian Castro, Paul Hayden, Nathan Steggel, Daniele Contini, David Heist, and T. John Taylor (2001b). "A wind tunnel study of dense gas dispersion in a stable boundary layer over a rough surface". In: *Atmospheric Environment* 35.13, pp. 2253 –2263. ISSN: 1352-2310. DOI: http://dx.doi.org/10.1016/S1352-2310(01)00073-5. URL: http://www.sciencedirect.com/science/article/pii/S1352231001000735.

Sawford, B. L. (2004). "Micro-Mixing Modelling of Scalar Fluctuations for Plumes in Homogeneous Turbulence". In: *Flow, Turbulence and Combustion* 72.2, pp. 133–160. ISSN: 1573-1987. URL: https://doi.org/10.1023/B:APPL.0000044409.74300.db.

Sawford, B. L. and H. Stapountzis (1986). "Concentration fluctuations according to fluctuating plume models in one and two dimensions". In: *Boundary-Layer Meteorology* 37.1, pp. 89–105. ISSN: 1573-1472. URL: https://doi.org/10.1007/BF00122758.

Schatzmann, M., William H. Snyder, and Robert E. Lawson (1993). "Experiments with heavy gas jets in laminar and turbulent cross-flows". In: *Atmospheric Environment. Part A. General Topics* 27.7, pp. 1105 –1116. ISSN: 0960-1686. DOI: https://doi.

org/10.1016/0960-1686(93)90145-O. URL: http://www.sciencedirect.com/science/article/pii/096016869390145O.

Simpson, J.E. (1999). *Gravity Currents: In the Environment and the Laboratory*. In the Environment and the Laboratory. Cambridge University Press. ISBN: 9780521664011. URL: https://books.google.it/books?id=2HhBMYBZe-oC.

Simpson, R L and W G Wyatt (1973). "The behaviour of hot-film anemometers in gas mixtures". In: *Journal of Physics E: Scientific Instruments* 6.10, pp. 981–987. DOI: 10.1088/0022-3735/6/10/012. URL: https://doi.org/10.1088%2F0022-3735%2F6%2F10%2F012.

Snyder, William H (2001). "Wind-tunnel study of entrainment in two-dimensional dense-gas plumes at the EPA's fluid modeling facility". In: *Atmospheric Environment* 35.13, pp. 2285 –2304. ISSN: 1352-2310. DOI: http://dx.doi.org/10.1016/S1352-2310(00)00214-4. URL: http://www.sciencedirect.com/science/article/pii/S1352231000002144.

Stapountzis, H., B. L. Sawford, J. C. R. Hunt, and R. E. Britter (1986). "Structure of the temperature field downwind of a line source in grid turbulence". In: *Journal of Fluid Mechanics* 165, 401–424. DOI: 10.1017/S0022112086003154.

Talbot, Benoît, Nicolas Mazellier, Bruno Renou, Luminita Danaila, and Mourad Abdelkrim Boukhalfa (2009). "Time-resolved velocity and concentration measurements in variable-viscosity turbulent jet flow". In: *Experiments in Fluids* 47.4, p. 769. ISSN: 1432-1114. DOI: 10.1007/s00348-009-0729-z. URL: https://doi.org/10.1007/s00348-009-0729-z.

Talluru, K M, C Hernandez-Silva, J Philip, and K A Chauhan (2017). "Measurements of scalar released from point sources in a turbulent boundary layer". In: *Measurement Science and Technology* 28.5, p. 055801. DOI: 10.1088/1361-6501/aa614a. URL: https://doi.org/10.1088%2F1361-6501%2Faa614a.

Talluru, K. M., J. Philip, and K. A. Chauhan (2018). "Local transport of passive scalar released from a point source in a turbulent boundary layer". In: *Journal of Fluid Mechanics* 846, 292–317. DOI: 10.1017/jfm.2018.280.

Taylor, G. I. (1922). "Diffusion by Continuous Movements". In: *Proceedings of the London Mathematical Society* s2-20.1, pp. 196–212. DOI: 10.1112/plms/s2-20.1.196. eprint: https://londmathsoc.onlinelibrary.wiley.com/doi/pdf/10.1112/plms/s2-20.1.196. URL: https://londmathsoc.onlinelibrary.wiley.com/doi/abs/10.1112/plms/s2-20.1.196.

Tennekes, Hendrik and John L Lumley (1972). *A first course in turbulence*. MIT press.

Thomson, D. J. (1987). "Criteria for the selection of stochastic models of particle trajectories in turbulent flows". In: *Journal of Fluid Mechanics* 180, 529–556. DOI: 10.1017/S0022112087001940.

Tinarelli, G., D. Anfossi, S. Trini Castelli, M. Bider, and E. Ferrero (2000). "A New High Performance Version of the Lagrangian Particle Dispersion Model Spray, Some Case Studies". In: *Air Pollution Modeling and Its Application XIII*. Ed. by Sven-Erik Gryning and Ekaterina Batchvarova. Boston, MA: Springer US,

pp. 499–507. ISBN: 978-1-4615-4153-0. DOI: 10.1007/978-1-4615-4153-0_51. URL: https://doi.org/10.1007/978-1-4615-4153-0_51.

Trini Castelli, Silvia, D. Anfossi, and Sandro Finardi (Jan. 2010). "Simulations of the dispersion from a waste incinerator in the Turin area in three different meteorological scenarios". In: *INTERNATIONAL JOURNAL OF ENVIRONMENT AND POLLUTION* 40, pp. 10–25. DOI: 10.1504/IJEP.2010.030879.

Turner, J. S. (1973). *Buoyancy Effects in Fluids*. Cambridge Monographs on Mechanics. Cambridge University Press. DOI: 10.1017/CBO9780511608827.

Vendel, F, L Soulhac, P Mejean, L Donnat, and O Duclaux (2011). "Validation of the Safety Lagrangian Atmospheric Model (SLAM) against a wind tunnel experiment over an industrial complex area". In: *14th conference on harmonisation within atmospheric dispersion modelling for regulatory purposes, Kos*.

Vendel, Florian (Apr. 2011). "Modélisation de la dispersion atmosphérique en présence d'obstacles complexes : application à l'étude de sites industriels". Theses. Ecole Centrale de Lyon. URL: https://tel.archives-ouvertes.fr/tel-00601470.

Villermaux, E. and J. Duplat (2003). "Mixing as an Aggregation Process". In: *Phys. Rev. Lett.* 91 (18), p. 184501. DOI: 10.1103/PhysRevLett.91.184501. URL: https://link.aps.org/doi/10.1103/PhysRevLett.91.184501.

Warhaft, Z. (2000). "Passive Scalars in Turbulent Flows". In: *Annual Review of Fluid Mechanics* 32.1, pp. 203–240. DOI: 10.1146/annurev.fluid.32.1.203. eprint: https://doi.org/10.1146/annurev.fluid.32.1.203. URL: https://doi.org/10.1146/annurev.fluid.32.1.203.

Wasan, D. T. and K. M. Baid (1971). "Measurement of velocity in gas mixtures: Hot-wire and hot-film anemometry". In: *AIChE Journal* 17.3, pp. 729–731. DOI: 10.1002/aic.690170342. eprint: https://aiche.onlinelibrary.wiley.com/doi/pdf/10.1002/aic.690170342. URL: https://aiche.onlinelibrary.wiley.com/doi/abs/10.1002/aic.690170342.

Way, Jhon and Paul A. Libby (1970). "Hot-wire probes for measuring velocity and concentration in helium-air mixtures". In: *AIAA Journal* 8.5, pp. 976–978. DOI: 10.2514/3.5814. eprint: https://doi.org/10.2514/3.5814. URL: https://doi.org/10.2514/3.5814.

Webster, H.N. and D.J. Thomson (2002). "Validation of a Lagrangian model plume rise scheme using the Kincaid data set". In: *Atmospheric Environment* 36.32, pp. 5031 –5042. ISSN: 1352-2310. DOI: https://doi.org/10.1016/S1352-2310(02)00559-9. URL: http://www.sciencedirect.com/science/article/pii/S1352231002005599.

Welch, P. (1967). "The use of fast Fourier transform for the estimation of power spectra: A method based on time averaging over short, modified periodograms". In: *IEEE Transactions on Audio and Electroacoustics* 15.2, pp. 70–73. ISSN: 1558-2582. DOI: 10.1109/TAU.1967.1161901.

Wilson, David J (2010). *Concentration fluctuations and averaging time in vapor clouds*. John Wiley & Sons.

Wilson, John D and Thomas K Flesch (1993). "Flow boundaries in random-flight dispersion models: enforcing the well-mixed condition". In: *Journal of Applied Meteorology and Climatology* 32.11, pp. 1695–1707. DOI: https://doi.org/10.1175/1520-0450(1993)032<1695:FBIRFD>2.0.CO;2.

Wilson, John D. and Brian L. Sawford (1996). "Review of Lagrangian stochastic models for trajectories in the turbulent atmosphere". In: *Boundary-Layer Meteorology* 78.1, pp. 191–210. ISSN: 1573-1472. URL: https://doi.org/10.1007/BF00122492.

Witlox, H.W.M. and A. Holt (1999). "A unified model for jet, heavy and passive dispersion including droplet rainout and re-evaporation -". In: *CCPS 1999 UDM paper*.

Yee, Eugene and Christopher A. Biltoft (2004). "Concentration Fluctuation Measurements in a Plume Dispersing Through a Regular Array of Obstacles". In: *Boundary-Layer Meteorology* 111.3, pp. 363–415. ISSN: 1573-1472. URL: https://doi.org/10.1023/B:BOUN.0000016496.83909.ee.

Yee, Eugene, Ralph M. Gailis, Alexander Hill, Trevor Hilderman, and Darwin Kiel (2006). "Comparison of Wind-tunnel and Water-channel Simulations of Plume Dispersion through a Large Array of Obstacles with a Scaled Field Experiment". In: *Boundary-Layer Meteorology* 121.3, pp. 389–432. ISSN: 1573-1472. URL: https://doi.org/10.1007/s10546-006-9084-2.

Yee, Eugene and Alex Skvortsov (2011). "Scalar fluctuations from a point source in a turbulent boundary layer". In: *Phys. Rev. E* 84 (3), p. 036306. DOI: 10.1103/PhysRevE.84.036306. URL: https://link.aps.org/doi/10.1103/PhysRevE.84.036306.

Zannetti, Paolo (1990). *Gaussian Models. In: Air Pollution Modeling*. Springer, Boston, MA. DOI: https://doi.org/10.1007/978-1-4757-4465-1_7.

Zhu, Guwei, S.Pal Arya, and William H. Snyder (1998). "An experimental study of the flow structure within a dense gas plume". In: *Journal of Hazardous Materials* 62.2, pp. 161 –186. ISSN: 0304-3894. DOI: http://dx.doi.org/10.1016/S0304-3894(98)00162-9. URL: http://www.sciencedirect.com/science/article/pii/S0304389498001629.

dernière page de la thèse

AUTORISATION DE SOUTENANCE

Vu les dispositions de l'arrêté du 25 mai 2016,

Vu la demande du directeur de thèse

Monsieur P. SALIZZONI

et les rapports de

M. M. CARPENTIERI
Professeur - University of Surrey - Royaume-Uni

et de

M. T. BONOMETTI
Maître de Conférences HDR - Institut de Mécanique des Fluides de Toulouse (UMR 5502 IMFT) - Toulouse

Madame VIDALI Cristina

est autorisée à soutenir une thèse pour l'obtention du grade de **DOCTEUR**

Ecole doctorale Mécanique, Energétique, Génie Civil et Acoustique

Fait à Ecully, le 7 mai 2021

P/Le directeur de l'E.C.L.
Le directeur des Etudes

Grégory VIAL